REMOVAL OF HEAVY METAL IONS FROM AQUATIC ENVIRONMENT USING GAMMA-IRRADIATION-MODIFIED CARBOXYMETHYL CELLULOSE HYDROGELS

トラン, トウ, ホン

REMOVAL OF HEAVY METAL IONS FROM AQUATIC ENVIRONMENT USING GAMMA-IRRADIATION-MODIFIED CARBOXYMETHYL CELLULOSE HYDROGELS

By

Tran Thu Hong

Submitted in Partial Fulfilment of the Requirements

For the Degree

Doctor of Engineering

Supervised by

Professor Kazuhiro Hara

Department of Applied Quantum Physics and Nuclear Engineering

Graduate School of Engineering

Kyushu University

2019

CONTENTS

ABSTRACT IV

ACKNOWLEDGEMENTS VI

LIST OF FIGURES VII

LIST OF TABLES IX

LIST OF ABBREVIATIONS X

CHAPTER 1 1

I. Introduction 1

1. *Heavy metal pollutants in water* 1

2. *Treatment technologies of heavy metals in water* 3

3. *Polymeric materials for heavy metals elimination in polluted water* 3

II. Literature review 5

1. *Hydrogels as polymeric adsorbents* 5

2. *^{60}Co gamma irradiation synthesis of hydrogels* 9

3. *Carboxymethyl cellulose (CMC) based hydrogel* 9

4. *Adsorption process* 13

III. Objectives of this study 20

CHAPTER 2 21

I. Starting materials 21

II. Synthesis of samples 23

1. *Gamma-ray-induced grafting of the active monomer SSS onto CMC structure (abbreviated as CS hydrogel)* 23

2. *Establishing cross-linked networks from CMC, SSS and BMEP (abbreviated as CSB hydrogel)* 23

3. *Preparation of interpenetrating network adsorbent from CMC and CMCts polymers containing simultaneously SSS (abbreviated as CCS hydrogel)* 23

III. Gamma irradiation 25

IV. Characterization of samples 27

1. *Gel fraction and swelling ability* 27

2. *Fourier transforms infrared spectroscopy (FTIR) analysis* 29

3. *The Carbon-13 Nuclear Magnetic Resonance (^{13}C-NMR) spectroscopy analysis* 31

4. *Thermos-physical analysis* 33

5. *Surface characteristics by SEM and EDS measurements* 33
6. *Compressive tests* 34
V. Experiments for metal adsorption 36
VI. Desorption and reuse 36
CHAPTER 3 38
I. Synthesis of grafted CMC hydrogel (abbreviated as CS hydrogel) 38
II. Identification of prepared hydrogel structure 40
1. *FT-IR analysis of prepared hydrogel* 40
2. *^{13}C-NMR recorded spectroscopy* 42
3. *EDS and SEM* 44
4. *Other characteristics of prepared hydrogels* 47
III. Metal ion adsorption performance of CS hydrogel 51
1. *Effect of hydrogel composition* 51
2. *Effect of adsorbate solution pH* 53
3. *Kinetic study* 55
4. *Equilibrium isotherms* 58
5. *Desorption metal ions from CS adsorbent and reusability* 61
IV. Conclusion 63
CHAPTER 4 64
I. Reinforcing of SSS-grafted-CMC hydrogel network (abbreviated as CSB hydrogel) 64
II. Characterization of CSB hydrogel 66
1. *FT-IR spectra analysis* 66
2. *^{13}C-NMR Nuclear magnetic resonance spectroscopy* 68
3. *EDS and SEM* 70
4. *Other characteristics of prepared hydrogels* 74
III. Metal adsorption performance 81
1. Metal adsorption in competitive condition 81
2. Metal adsorption in non-competitive condition 85
3. Effect of pH 90
4. Adsorption kinetics 92
5. Adsorbent re-use 95

IV. Conclusion 98

CHAPTER 5 99

I. Composing of selective IPN CMC-based hydrogel (abbreviated CCS hydrogel) 101

II. Recognization of CCS hydrogel 103

1. FT-IR spectrum 103

2. ^{13}C-NMR Nuclear magnetic resonance spectroscopy 105

3. EDS and SEM analysis 107

4. Swelling ability 117

III. Metal adsorption behaviors 119

1. *Metal adsorption selectivity* 120

2. *Effect of weight ratios of (CMC+CMCts) to SSS on Ag^+ adsorption* 125

3. *Effect of adsorbent weight* 127

4. *pH solution effect on selective adsorption for Ag^+* 129

5. *Adsorption kinetics of Ag^+ metal ion system* 131

6. *Adsorption activate energy* 137

7. *Adsorption isotherms* 137

8. *Adsorption thermodynamics* 141

9. *Desorption and reusability of CCS hydrogel* 147

IV. Conclusion 149

CHAPTER 6 150

I. Research achievement 150

II. Limitations of current work and corresponding recommendations for future work 151

REFERENCES 152

ABSTRACT

Heavy metal contamination in water has caused unending concern for environment and human health. Upon entering the human body, the metallic ions discharged from the industrial processes can cause many serious complications such as brain damage, shrinkage of muscle bundles, death, and hereditary deformities and teratogenicity. The treatments of these toxic elements have become the objectives of many studies for decades. Under these circumstances, the author has been developing new organic-hydrogel adsorbents by utilizing the gamma irradiation method.

Among the technologies adopted to eliminate the toxic elements, the adsorption method utilizing organic hydrogels has been considered an effective and user-friendly approach from the viewpoints of high cost performance and availability, which are attributed to their light-element(C, H, O, N, etc.) polymer network made from inexpensive and common natural substances, such as green plants and crab/shrimp shells, massively disposed as wastes in daily life. As for the method producing organic hydrogels from these easily obtainable materials, the gamma irradiation method is the most suitable one due to unnecessity of toxic reaction-initiator and cross-linker agents, which are generally used in the ordinary chemical-reaction methods for forming gel-network and for grafting functional-groups to the network.

In the present study, the author has newly developed organic-hydrogel adsorbents derived from readily obtainable cellulose-based materials by utilizing Cobalt-60 gamma radiation, and has evaluated their capabilities as recyclable metal-ion adsorbents by performing repetitive adsorption-and-desorption experiments. The thesis compiles these author's investigations and is composed of 6 chapters.

Chapter 1 provides overviews of heavy metal pollutants in waste water and available removal techniques, including the previous studies on the utilization of organic hydrogels as adsorbents with emphasis on Carboxymethyl-Cellulose(CMC)-based hydrogels.

Chapter 2 explains on the fabrication of the CMC-based hydrogels by utilizing the gamma irradiation, and on the experimental methods to characterize the hydrogels. In the present study, three types of CMC-based hydrogels have been newly synthesized: (1) the CMC-hydrogels grafted with sodium sulfonate styrene (SSS) monomer, (2) the SSS-grafted CMC-hydrogels reinforced by Bis[2-(Methacryloyloxy) Ethyl] Phosphate (BMEP) monomer, and (3) the CMC-based hydrogel with an interpenetrating network produced by gamma irradiation after infusing carboxymethyl chitosan (CMCts) polymer into the SSS-grafted CMC-hydrogels.

Chapter 3 reports on the SSS-grafted CMC-hydrogels' capabilities of extracting metal ions from their aqueous mixture (Cr, Mn, Mo, Ni, Cu, Zn, Fe, U, Cd, Pb). In the experiments, the SSS-grafted CMC-hydrogels were demonstrated to adsorb all kinds of the metal ions in the

solution around twice the amounts by the CMC-hydrogel without showing significant difference by the elements. It was also noticed that the SSS-grafted CMC-hydrogel with CMC:SSS=1:2 of weight-ratio shows the highest removal efficiency for all of the metal ions in the solution, indicating strong electrostatic interaction between SSS and the metal ions: the adsorbed metal-ion weight per that of the adsorbent were 40.7 and 15.0 μg/g for Fe and Cr, respectively, and 7.00 μg/g for both of Cu and Zn. However, it was also revealed that the capturing ability of CMC:SSS=1:2-hydrogel after 2 cycles decreased to a half by the disintegration of the surface parts resulted from the large volume change caused by the SSS's strong electrostatic force, which indicated the necessity of reinforcement of the hydrogel's structure.

Chapter 4 describes an attempt to improve the reusability of the SSS-grafted CMC-hydrogel by introducing a network reinforcer, Bis[2-(Methacryloyloxy)Ethyl] Phosphate (BMEP). In the simultaneous multi-ion capturing experiments in the above-mentioned conditions, the reinforced SSS-grafted CMC-hydrogels (CSB hydrogels) revealed different capturing-efficiencies for the coexisting metal ions in the order of Mo < V < Zn < Cr < Cu < Mn < Cd < Co < Ag < Ni. As for the mechanical strength, the CSB hydrogels showed higher elasticities {in a range from 5.75 kPa of Young's Modulus (*E*) with the addition of 12.9 mM of BMEP to *E*: 3.41 kPa with 2.6 mM of BMEP} than that without the reinforcement (*E*: 2.76 kPa). Though the adsorption capacity decreased with the BMEP addition increment, the CSB hydrogel with 2.6 mM of BMEP (CSB2.6 hydrogel) showed a high adsorption capability comparable to the hydrogel without the reinforcement as well as showing no disintegration in the repetitive adsorption-and-desorption experiments. In addition, the CSB2.6 hydrogel also demonstrated a high desorption capacity, even for Ni (~81 % after the 4th iteration) exhibiting the highest affinity to the CSB hydrogels, which indicated a possibility as a recyclable adsorbent.

Chapter 5 gives the investigations on the SSS-grafted CMC-hydrogel modified to have an interpenetrated network composed of CMC and CMCts. By the modification, the SSS-grafted CMC-hydrogel was found to show a high selectivity for Ag^{+} among the 10 metal ions described previously: the modified-hydrogel{(CMC+CMCts):SSS=4:2}'s adsorption capacity for Ag is 4 times higher (>40 μg/g) than those for other metal ions. Besides, it was also found that decrease in the Ag-capturing efficiency is less than 15 % after the 4th repetition of the adsorption-and-desorption cycle, indicating the possibility as an element-selective resource-recycling material.

Chapter 6 summarizes the results obtained in the present study and discusses the subjects to be solved in future investigations.

ACKNOWLEDGEMENTS

Special thanks to my beloved family: my parents, younger brother and son for their love, support and patience. Thanks my son for tolerating my absence from home for long stay in Japan.

I would like to express my deepest gratitude to my supervisor Prof. Kazuhiro HARA and Prof. Hirotaka OKABE for dedicated supervision, insight into this research topic, useful ideas and advice for nearly 6 years. I am extremely grateful to Profs. Further, I would like to thank Prof. Yoshiki HIDAKA, Mr. KAWANO and all the faculty members in the Department of Applied Quantum Physics and Nuclear Engineering for their guidance and critical comments that have helped during this study.

I would also like to express my acknowledgement to Rotary Yoneyama Memorial Foundation and Kyushu University Scholarship for 3-year-financial support and for giving me an opportunity to study here in Japan. My sincere thanks and appreciation to Fukuoka Higashi Rotary Club, Vietnam Atomic Energy Institute (VINATOM) and Nuclear Research Institute (NRI), thank you very much for your support and advice.

Many thanks sent to Brian, for his guidance in ICP-MS, FT-IR, SEM and willing to solve my technique problems and numerous discussions on research work. I would also like to thank all my friends at the Hara Lab. their direct and indirect help.

I am thankful to Ms. Ishihara, Mr. Koyanagi, Mr. Yoshida and his family in Fukuoka Higashi Rotary Club for their encouragement.

I would also like to thank all of the friends that I have met in Kyushu University, teachers and classmates, managers of Harmony House for making my living run smoothly in Japan.

LIST OF FIGURES

Figure 1. Main sources of heavy metal emissions. 2

Figure 2. Dried and swollen hydrogel in response to stimuli external environment conditions. 6

Figure 3. Hydrogels for removal of metal ions from aqueous solution. 7

Figure 4. Chemical structures of main materials in current study. 22

Figure 5. Samples irradiated at ^{60}Co gamma ray point source at Kyushu University center for accelerator and beam applied science. 26

Figure 6. Calculation process of gel content of gelation and swelling ability. 28

Figure 7. Typical chemical shifts of organic compound in ^{13}C NMR..... 32

Figure 8. Experiment for determination of hydrogel adsorption capacity. 37

Figure 9. FT-IR of CMC, SSS and CS grafted hydrogel 41

Figure 10. ^{13}C-NMR spectral characterization of CS hydrogel 43

Figure 11. EDS spectroscopy of CMC and CMC/SSS (CS)..... 44

Figure 12. SEM observations of (a) CMC, (b) CMC:SSS=2:1, (c) CMC:SSS=1:1 and (d) CMC:SSS=1:2 hydrogels..... 46

Figure 13. Gel fraction and swelling ratio versus SSS concentration. 48

Figure 14. TGA profile of CMC and CS..... 50

Figure 15. Dependance of the removal percentage for various metals 52

Figure 16. pH solution effect on the adsorption capacity of CS hydrogel for multi-elements..... 54

Figure 17. Kinetic studies for adsorption capacity of CS hydrogels..... 56

Figure 18. Freundlich and Langmuir isotherm fitting curves for metal ions adsorption by CS hydrogel. 60

Figure 19. Regeneration of CS hydrogel..... 62

Figure 20. FT-IR spectra records of pure materials (CMC, SSS, BMEP) and CMC/SSS/BMEP (CSB) hydrogel. 67

Figure 21. ^{13}C-NMR analysis of CSB hydrogel..... 69

Figure 22. EDS map of CSB before and after phosphonation. 71

Figure 23. SEM surface morphology photos of CSB hydrogels: (a) without BMEP and (b) – (e) with different BMEP contents (Mag. ×5000). 73

Figure 24. The (a) gelled part percentage and (b) equilibrium swelling abitlity of CSB hydrogels. ... 75

Figure 25. Visible compression tests demonstrate the CSB hydrogel recovers their original shape. . 77

Figure 26 a. σ vs. $\varepsilon_{long.}$ fitting plots at σ = 0.00 – 1.21 (kPa) for the CSB hydrogels..... 78

Figure 27. Multi-element capturing in solution by CSB hydrogels. 83

Figure 28. Ni and Ag adsorption in non-competitive conditions. 88

Figure 29. pH dependent adsorption capacity of CSB hydrogel for multi-elements in solution. 91

Figure 30. Time dependent adsorption of CSB hydrogel for multi elements in aquatic environment. 93

Figure 31. Simple recycle process of Ni-absorbed hydrogel. 96

Figure 32. Ni-removal recycles by CSB hydrogels..... 97

Figure 33. Some possible associations of hydrophilic polysaccharides used to synthesis IPN hydrogels [97][98][99]. 100

Figure 34. FT-IR records of CMC, CMCts, SSS and CCS interpenetrating polymeric hydrogel. 104

Figure 35. ^{13}C-NMR record of CCS hydrogel. 106

Figure 36. EDS spectra of CMC/CMCts and CMC/CMCts/SSS (CCS). 108

Figure 37. The surface morphology SEM of CMC, CMCts, CMC/CMCts and CCS (Mag. ×2000). 110

Figure 38. 2D-FFT analysis of hydrogels: (a) Original SEM photos; (b) 2D-FFT power spectrum results; (c) 3D-images of power spectra. 112

Figure 39. Intensity plots against the angle of acquisition of 2D-FFT power spectra. 114

Figure 40. The radial distribution of intensity against wavenumber..... 116

Figure 41. SSS content influence on water-uptake capacity of the CCS (irradiation dose 60 kGy).. 118

Figure 42. Interaction between metal ion (Ag, Cu, Cr, Ni ions) and CCS hydrogel before (a) and after (b) adsorption. 120

Figure 43. Selective adsorption capacity for Ag^+ by CCS hydrogels in non-competitive (a) and competitive (b and c) condition. 122

Figure 44. Weight ratio of (CMC/CMCts) to SSS effect on Ag^+ adsorption performance..... 126

Figure 45. Influence of CCS adsorbent weight on Ag^+ uptake. 128

Figure 46. Effect of solution pH on Ag^+ adsorption capacity of CCS hydrogel. 130

Figure 47. Dependence of Ag^+ adsorption capacity of CCS hydrogel on contacting time. 132

Figure 48. The graphs of q_t vs. $t^{1/2}$ for Ag^+ adsorption. 135

Figure 49. Adsorption isotherms of Ag^+ adsorbed onto CCS hydrogel 140

Figure 50. Langmuir fitting curves for Ag adsorption on CCS hydrogel at 298, 323 and 343 K. 143

Figure 51. Graph for ΔG vs. T of the Ag adsorption by CCS hydrogel. 145

Figure 52. Adsorption and desorption recycles..... 148

LIST OF TABLES

Table 1. Major heavy metal ions discharged by major industries. 2

Table 2. Polymeric adsorbents for heavy metals capturing in aqueous solution. 4

Table 3. Classification of hydrogels based on the different properties [19]. 8

Table 4. Applications of CMC in major field of industry [23]. 10

Table 5. Physical adsorption and chemical adsorption. 14

Table 6. Isotherm models for analyzing experimental data. 17

Table 7. Different ratios of CMC and SSS for CS hydrogel synthesis 24

Table 8. Initial composition for synthesized CSB hydrogel 24

Table 9. Material combinations for preparation of CCS hydrogel synthesis 24

Table 10. Some FTIR peaks of the hydrogel functional groups [54][55]. 30

Table 11. Initial concentration of metal ions (μg/L). 52

Table 12. Calculated kinetic results of metal adsorption by CS hydrogel adsorbent. 57

Table 13. Caculated Langmuir and Freundlich parameters for metal adsorption by CS hydrogels. 59

Table 14. The calculated values of Poisson's ratio and Young's moduli for the CSB hydrogels. 80

Table 15. Adsorption capacities of CSB hydrogels for multi-elements. 84

Table 16. Parameters of single metal adsorption experiments. 86

Table 17. Results on the adsorption performance of CSB hydrogel for Ni and Ag single ion metal solutions. 89

Table 18. Overview of ionic radius of hydrated metal ions in aqueous solution [92] and the pseudo-2nd-order kinetic model analysis of CSB hydrogel adsorption behavior for multi-element. 94

Table 19. Summarized batch mode experimental conditions. 119

Table 20. Competitive binding behaviors of CCS hydrogel for Ag^+ over other ions. 124

Table 21. Calculated kinetic results of Ag^+ adsorption process by CCS adsorbent. 133

Table 22. Parameters for intra-particle diffusion. 136

Table 23. Isotherm models for analyzing experimental data. 139

Table 24. Calculation of thermos-dynamic data for Ag^+ adsorption of Ag^+ by CCS hydrogel. 146

LIST OF ABBREVIATIONS

2D-FFT	Two-dimensional fast Fourier transform
BMEP	Bis[2-(Methacryloyloxy)Ethyl] Phosphate
CCS	Hydrogel composed of CMC, CMCts and SSS
CMC	Carboxymethyl Cellulose
CMCts	Carboxymethyl Chitosan
CS	Hydrogel composed of CMC and SSS
CSB	Hydrogel composed of CMC, SSS and BMEP
DW	Deionized water
EDS	Energy-dispersive X-ray spectroscopy
FTIR	Fourier Transform Infrared
ICP-MS	Inductively coupled plasma mass spectrometry
IPN	Interpenetrating polymeric network
NMR	Nuclear Magnetic Resonance
SEM	Scanning Electron Microscope
SSS	Styrene Sulfonate Sodium
TGA	Thermal Gravimetric Analysis

CHAPTER 1

INTRODUCTION AND OVERVIEW

I. Introduction

1. *Heavy metal pollutants in water*

Heavy metals or metallic elements, with high atomic number (>20) and with specific density 5 times higher than that of water (5 g/cm^3), occur naturally and abundantly on the Earth's crust. It is divided into 3 kinds: hazardous metals (As, Cr, Cu, Co, Cd, Hg, Ni, Pb, Sn, Zn, etc.), noble metals (Ag, Au, Pd, Pt, Ru, etc.) and radioactive metals (Am, Ra, Th, U, etc.). In the periodic table, so-called heavy metals includes Group V, VI, VII elements and the transition metals [1]. Inspite of not being harmful in the metal states, almost of the heavy metals in ionic states are toxic and fatal on plants, living things and humans; such a situation becomes worse by their property not being degraded or destroyed by themselves.

Heavy metals come from a variety of sources, but most are generated by industrial production. Heavy metals exist in soil, water and air and can enter to human bodies through eating, drinking and breathing. In the right concentrations, some heavy metals, e.g, copper (Cu), selenium (Se) or zinc (Zn) are micro-nutrients which necessary for maintaining the human-body metabolism. In excess of the allowed level, by contrast, they will be a danger to human health in the long run. If the body accumulates a large amount of heavy metal, it will lead to many serious complications, brain damage, shrinkage of muscle bundles. Heavy metals may contact the cell membrane, affect the process of dividing DNA, leading to fetal death, deformity, teratogenicity of later generations. The use of water containing heavy metal impurities is the cause of cancers: cervical cavity, throat ring and stomach: ... When heavy metals get into the water, it loses the natural components of the water, instead producing more harmful toxins. When we use water containing heavy metals that will hinder the metabolism of the body, the absorption of nutrients and excretion process becomes more difficult and restrain growth and development. Causes digestive disorders, cardiovascular disorders, nervous system dysfunctions ... Heavy metals in water also cause skin irritation, accumulation in the long term will cause dermatitis, skin diseases ... Some metals will benefit the body, but some of the metals mentioned above do not participate in the biochemical processes of the body, but accumulate and are toxic to our bodies [2]. In the scope of this article, we only mention readers of the unpredictable harmful effects of heavy metals in daily water.

Daily water is mainly obtained from surface water and underground water. These sources are easily polluted by wastewater containing heavy metals (As, Cd, Cu, Cr, Ni, Fe, Pb, V, etc.) from transportation, mines, agriculture, factories or industrial areas, … which directly discharge to environment with no treatment or unsatisfied treatment, as illustrated in **Figure 1** and **Table 1**. Every two years since 1997, the Agency for Toxic Substances and Disease Registry has been updated “Top 20 Hazardous Substances”, in which these metals are listed [3].

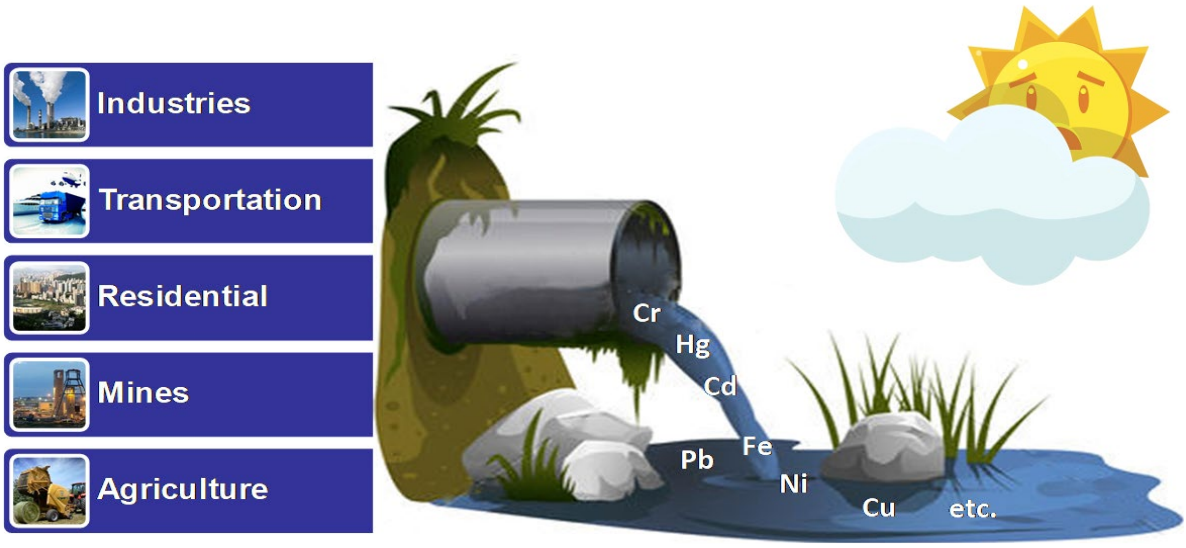

Figure 1. Main sources of heavy metal emissions.

Table 1. Major heavy metal ions discharged by major industries.

Industry	Cd	Cr	Cu	Pb	Hg	As	Ni	Zn	Ag
Textile mill		✓	✓						
Leather processing		✓			✓	✓		✓	
Organic chemicals	✓	✓		✓	✓		✓		
Inorganic chemicals	✓	✓	✓	✓	✓	✓	✓	✓	✓
Paint pigment and ink	✓	✓	✓	✓	✓	✓	✓	✓	✓
Glass industry				✓	✓	✓			✓
Petroleum refining	✓	✓	✓	✓	✓	✓	✓	✓	✓
Steam-generation power plants		✓	✓					✓	
Electroplating	✓	✓	✓	✓			✓	✓	✓
Pulp and paper industries		✓	✓	✓	✓		✓		
Rubber manufactory		✓		✓					
Machinery products	✓	✓	✓	✓	✓	✓	✓	✓	✓
Coal burning	✓	✓	✓	✓	✓	✓	✓		
Mining industry	✓	✓	✓	✓	✓	✓	✓	✓	✓

2. *Treatment technologies of heavy metals in water*

The heavy metal hazards in daily water are undesirable. The urgent mission now is how heavy metal ions must be thoroughly eliminated. Currently, many new/improved techniques are being utilized to reduce amount of heavy metal ions until meeting technology-based treatment standards in water such as membrane filtration, electro-chemical treatment, reverse osmosis, solvent extraction, chemical precipitation and biological-system utilization [4][5]. These methods are clasified into three categories: chemical, biological and, in addtion, physical treatments. However, the main disadvantages of these methods are no selectivity toward metal ions (ion-exchange); requirement of special pre-treatments before heavy metal ions precipitation (chemical precipitation); the high operational cost or loss of material through phase disengagement (membrane filtration), and disposal of large amount of extractant (solvent extraction) [5]. They are not also efficient in the case of metal ions in trace concentration. Adsorption technique is one of the important alternatives available for such case because adsorption is able to lower the metal-ion concentrations to below 10^{-9} levels [6]. In additions, adsorption has been considered to be superior compared with the other methods in regards to simplicity and flexibility of designing the operating system, ease of operation and initial cost. Moreover, the materials used as adsorbents can often be regenerated [7].

The most popular adsorbent with usefulness, activated carbon (AC), which derives mainly from the high surface area but the source of commercial coal-based AC now becomes depleted and results in increasing cost. This, together with AC loss during the regeneration process, restricts its applications therefore searching less expensive alternatives is of great concern. To date, many findings on the use of less expensive adsorbents have been presented. By making use of natural substances (mainly carbohydrates), these adsorbents have been fabricated on a low-cost base taking into consideration of the wastes and byproducts in the processes of agricultural and industrial activities, which also seems attractive for the practical and economic applications [8][9][10]. However, for the broader utilization, further improvement for other properties such as mechanical strength seems necessary as well as the adsorption capacities. In the preceding years, polymeric adsorbents have gained attention as a possible choice due to their chemical-physical properties and capabilities of the regeneration in gentle conditions and numerous publications are available on the topic[11].

3. *Polymeric materials for heavy metals elimination in polluted water*

The polymeric adsorbents (PA) were first introduced since the 1960s [12]. They can be classified into two kinds by their origins. In general, PA prepared from petroleum-based polymers are hydrophobic and with higher strength compared with those naturally produced. However, PAs synthesized from synthetic polymers have limitations due to high production costs and negative environment impacts. The PAs which are derived from nature-sourced materials are cheaper and biodegradable. These naturally-derived PAs or organic PAs, have gotten much attention in wastewater treatments because they can make complexes with a wide range of pollutants in solution in the processes of flocculation, chelation separate and adsorb. Some examples on PAs applied for heavy metals capturing are summarized in **Table 2** with the metal adsorption capacity of a PA is calculated by milligram (mg) of absorbed metal ion per gram (g) of adsorbent.

Table 2. Polymeric adsorbents for heavy metals capturing in aqueous solution.

Polymeric adsorbents	Metal adsorption capacities (mg/g)					References
	Pb^{2+}	Cd^{2+}	Ni^{2+}	Cu^{2+}	Cr^{6+}	
Graphene oxide/poly amido amine dendrimers					200.5	[13]
Clay/poly (methoxyethyl) acrylamide	81.0		80.8	29.8		[14]
Poly (4- styrene sulfonate sodium-co-acid acrylic)	40.0	2.6				[15]
Poly (methyl methacrylate-2-hydroxyethyl methacrylate)	31.4			31.1		[16]
Poly(styrene-*alt*-maleic anhydride)		81.3	76.9			[17]

II. Literature review

1. *Hydrogels as polymeric adsorbents*

The term "Hydrogel" contain "hydro" and "gel" parts. "Hydro" means "water" and "gel" stands for the material in the phase of "jelly-like" that can have properties ranging from soft (weak) to hard (tough). It might be said a "hydrogel" is a solid that absorbs water. Hydrogels are usually made from synthetic or natural polymeric materials. Synthetic polymer based hydrogels which are the most common, were first synthesized by Wycherley and Lim in 1960 [12]. The principal characteristics of hydrogel include water saturation, insolubility, viscoelasticity, porosity and stimuli responsiveness. Hydrogel is important in the adsorption process by providing sites for immobilization of adsorbate, acting as molecular sieves for size exclusion during adsorption while also increasing the surface area of adsorption. Insolubility, coming from the polymer-chain cross-linking, facilitates hydrogel's stability when applied in liquid environments; whereas viscoelasticity ensures that hydrogel shapes are flexible and that stress/strain levels are satisfactory. Water uptake or swelling is a special property of hydrogels unlike other adsorbents, which is generated by the presence of hydrophilic groups like the amide (–CONH), amine ($–NH_2$), the carboxylic (–COOH), hydroxyl (–OH) and sulfonic ($–SO_3H$) groups [18] on the three-dimensional 3D polymer chain network of hydrogel. This property enables these materials to absorb hundreds of times over their own weight in water, as demonstrated in **Figure 2**.

Due to swell-ability, hydrogels have been found an extremely large range of utilizations in the fields of biotechnology, medicine and pharmacy as controlled release of drugs, etc. Especially, hydrogels used for the treatments of toxic elements have become the objectives of many studies for decades. It has been found that by swelling, hydrogels can adsorb metal ions in solution by forming stable complexes with functional groups as shown in **Figure 3** and increase their capacity to uptake more adsorbate on their structure.

Swelling and de-swelling is a characteristic distinguishing property of hydrogels when immersed in water. The swelling degree is respond to the environmental stimuli such as temperature, pH, light, electric signal among others. In addition to structural features, hydrogels functional groups have also been very significant in their final properties. Functional groups from the natural polymers or synthetic monomers building units provide the valuable characteristic for hydrogels that is high selectivity adsorption. Depending on the targeted pollutants, these groups can also be customized during synthesis for the adsorption of such materials through various chemical interaction methods. The ability to synthesize hydrogels with customized properties and functional groups for targeted pollutants makes it stand out as a special adsorbent. This therefore requires careful choice of the synthetic monomers. Hydrogels can be classified using various criteria depending on their preparation methods, physical and/or chemical properties, origin, sources, nature of swelling, ionic charges, etc. and some of them are displayed in **Table 3**.

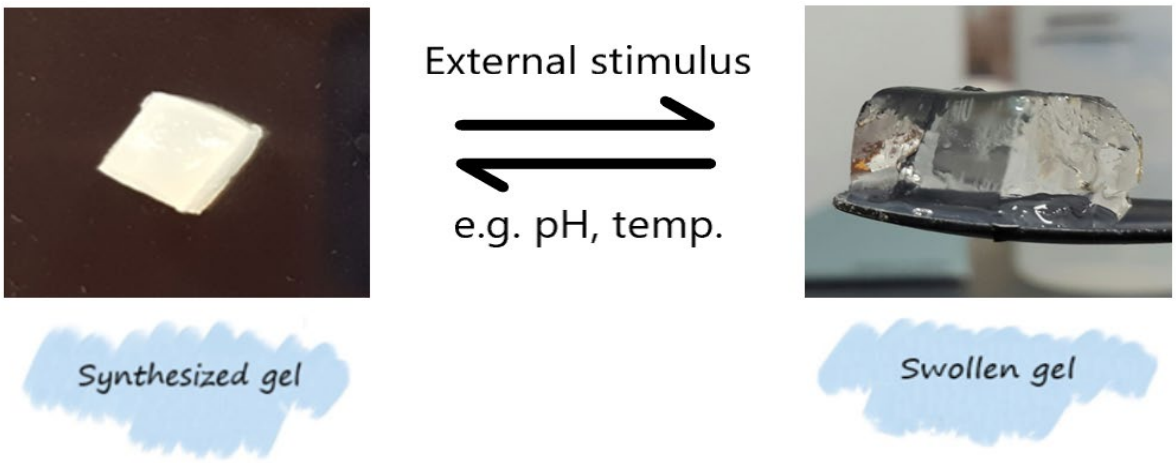

Figure 2. Dried and swollen hydrogel in response to stimuli external environment conditions.

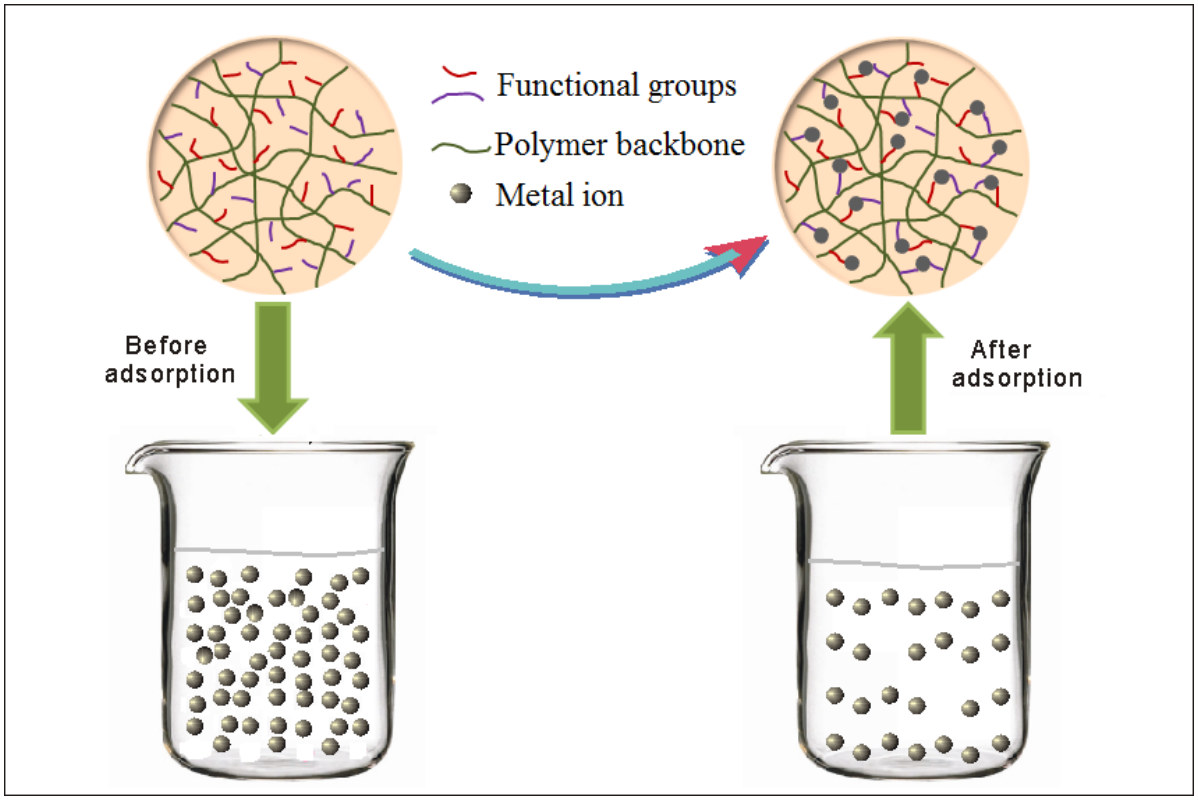

Figure 3. Hydrogels for removal of metal ions from aqueous solution.

Table 3. Classification of hydrogels based on the different properties [19].

Properties of hydrogel	Classified hydrogels
Source	- Natural - Synthetic - Hybrid
Degradability	- Biodegradable - Non-biodegradable
Cross-link nature	- Chemical bondage (Covalent bond) - Physical interaction
Response	- Biochemically responsive - Chemically responsive - Physically responsive
Physical properties	- Conventional hydrogels - Smart hydrogels
Preparation	- Co-polymeric hydrogels - Homo-polymeric hydrogels - Interpenetrating-network hydrogel
Ionic charge	- Anionic hydrogels - Cationic hydrogels - Ampholytic hydrogels

In the present study, according to term of preparation methods, hydrogel is classified as (i) Homo-polymeric hydrogel, (ii) Co-polymeric hydrogel and (iii) Interpenetrating network hydrogel

- Homo-polymeric hydrogels: They are synthesized from one type of hydrophilic monomer and/or polymer unit to form cross-linked networks.

- Co-polymeric hydrogels: They are generally ionically or covalently cross-linked networks from two or more different monomer and/or polymer components with at least one hydrophilic component along the polymer network chain.

- Interpenetrating network hydrogels: They are compsed of two independently cross-linked synthetic and/or natural polymer-network.

However, the commercial application of hydrogel has been slightly diminished in some applications for lack of mechanical strength, which has evoked a subject to put more stable hydrogels into practice by constructing strong network backbone in addition to high functionally.

2. ^{60}*Co gamma irradiation synthesis of hydrogels*

For many decades, hydrogel synthesized by the irradiation methods utilizing ultraviolet, electron beam and ɤ-rays has been considered as "clean". This is because it is a chemical-free synthetic technique, utilizing only the monomers and/or polymers and water under radiation environment to attain form gelation [20]. It does not require any additional reagents, such as polymerization initiator, cross-linking agent nor reaction accelerator to form cross-linked polymer hydrogel, and thus the final hydrogel can be easily characterized based on the type of starting monomers/ polymers. Moreover, the syntheis of hydrogel by irradiation technique, compared with the ordinal chemical methods, is capable of easy and easy control. So hydrogel synthesis by radiation technique is one of not bad options to improve the quality of materials made of polymers, which promotes their low-cost production and wide applications.

3. *Carboxymethyl cellulose (CMC) based hydrogel*

Carboxymethyl Cellulose (CMC) is a most popular derivative of cellulose with carboxymethyl groups (–CH_2COOH) linked to some hydroxyl groups of glucose-pyranose monomers to form the cellulose back-bone [21]. CMC is often used in sodium form called sodium carboxymethyl cellulose and has an immense importance to our life. Due to its non-allergenic, non-toxic and safety, CMC acts as a binder or thickener in pharmacy, cosmetic and food industry. Moreover, CMC has also water-solubility, biodegradability, high viscosity and availability at low cost [22]. It is utilized in cosmetics, textiles and print, etc., as shown in **Table 4**. Germany found CMC first in 1918 and it was patented 1921. The initial products of CMC were only used as an adhesive. From 1936 to 1941, the application of the sodium carboxymethyl cellulose industry was quite active and broad and it becomes popular in the world until now.

Table 4. Applications of CMC in major field of industry [23].

Kinds of industry	Utilizing form	Utilized function
Paper production	Internal additive	Binder, improve dry-strength
Detergent production	Laundry	Aiding soil-anti-re-deposition
Cosmetics production	Toothpaste	Thickener, suspension aid
Textiles production	Printing paste, dye	Water binder, thickener
Food production	Frozen desserts	Inhibitor of ice crystal growth
Wastewater treatment	Reduction of toxic pollutants	Organic flocculants
Ceramics production	Glazers, slips, welding rods	Binder, thickener, lubricant
Adhesive production	Wallpaper paste	Adhesion promoter, water-binder

The commercial production of CMC is in 2 stages: mercerization stage and etherification stage. In the mercerization step, by dissolving NaOH into the mixture of water and alcohol, the hydroxyl groups of cellulose are changed so as to form alkali celluloses: NaOH solvates -OH groups on cellulose structure by breaking the hydrogen bonds for the next etherification step. In the etherification stage, the alkali cellulose reacts with mono-chloro-acetic acid (MCA) or with its salt sodium mono-chloro-acetate (NaMCA) to form carboxymethyl cellulose ethers. In addition, NaOH reacts with MCA to form two by-products at the same time: NaCl and $C_2H_3NaO_3$. This process of CMC production by etherification is presented briefly according to the following reaction (**Scheme 1**).

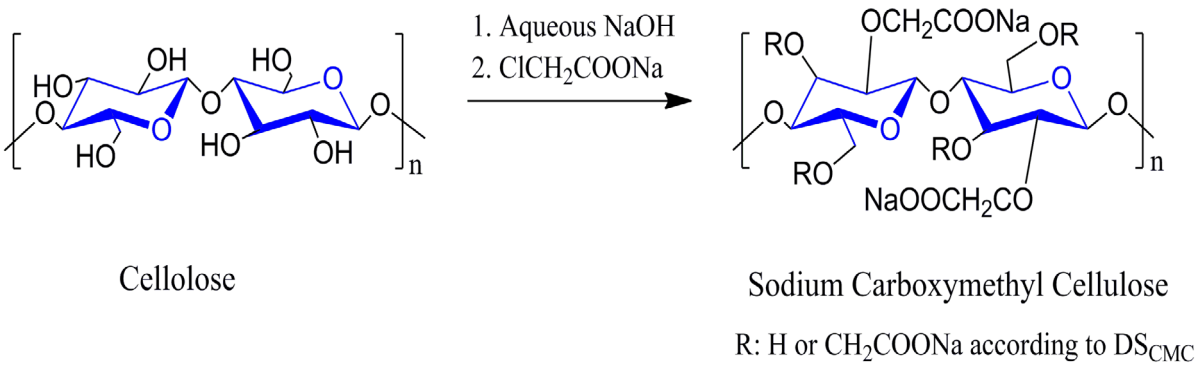

Cellolose

Sodium Carboxymethyl Cellulose

R: H or CH_2COONa according to DS_{CMC}

Scheme 1. Reaction scheme of carboxymethylation of cellulose [24].

It has been found that CMC hydrogel is a high-efficiency adsorbent for capturing of a large scale of heavy metal ion hazards such as Ag (I), Cr (III), Cu (II) [14], Fe (III), Ni (II) U (II) [13] and Zn (II) [15]. Wang et al. [16] proved reactive carboxymethyl group (–CH_2COOH) in CMC backbone render it water-soluble, chemically reactive and strongly chelating. This makes the application of CMC in adsorbent fields more promising and attractive. Nevertheless, the original CMC-backbone is weaker and more easily-broken than other cellulose-derived hydrogels with simpler structures. Therefore, the addition of more ingredients to CMC hydrogel systems can raise the mechanical strength and reactive property of CMC-based hydrogels. For instance, several vinyl monomers such as acrylic acid (AA) [17], acryl amide (AAm) [18], acrylonitrile [19] and acrylate [20] could be grafted onto CMC network in order to reinforece the hydrogel's structure as well as adsorption performance of CMC-based hydrogels. CMC-g-Poly (AA) gels have shown higher flocculation capability than simple CMC which is the main role of poly (AA) in river water clarification [21]. Hydrogel prepared from CMC and AAm is an efficient flocculant . Only 10 ppm of the CMC/AAm flocculant dosage in 400 ml, 0.25% (w/v) portion of kaolin-suspension reduced to 80.3 % in turbidity, whereas the simple CMC hydrogels reduces 13.8 % of turbidity in the same experimental conditions [25]. Another vinyl monomer containing hydrophilic group not so much recognized is styrene sodium sulfonate (SSS) group. The advantages of SSS compared with other monomers are highly reactive, less toxic and thermally higher stability [23]. SSS is also known as a promising vinyl monomer for synthesizing the polysaccharide hydrogels containing polyelectrolytes [24].

Several other studies of modification of CMC backbone to obtain high metal adsorption ability as well as dyes were reported:

- Heinze et al. [26] used CMC (H-form) for metal ion treatment in wastewater. Adsorption batch experiments for Ni^{2+}, Co^{2+}, Cu^{2+}, Cd^{2+}, Pb^{2+}, Fe^{3+}, and Al^{3+} indicated a high adsorption capacity of up to 0.32 mM Ni^{2+}/g with a very high absorption rate. About 90% of Ni-capturing process is accomplished within 1 hr by using 1.1 g CMC gel beads in 100 ml water containing 0.02 mol/L of Ni. The filtration method is used to optimize CMC beads for metal separation. As a results, the spherical shape is not destroyed and hence it can be regenerated and reused.

- K. Hara et al. [27] explored Cu^{2+} absorption property of CMC hydrogel that was cross-linked by ɤ-irradiation without toxic cross-linker. The CMC gel captured Cu^{2+} ions by chelating process.

- Hongzhu Ma et al. [28] conducted a study of sorption cationic and anionic dyes by crosslinking CMC grafting Dimethyl-diallyl-ammonium chloride. The study proved that such CMC-g-PDMDAAC microspheres became pH-sensitive and could adsorb effectively anionic dye orange II (OR II) or cationic dye methylene blue (MB), at acidic (pH < 3) or near neutral (pH > 4) condition, respectively.

- Nuri Astrini et al. [29] investigated the adsorption capacities of CMC-graft-poly (acrylic acid)/montmorillonite (CMC-g-PAA/MT) hydrogels for the Zn^{2+} and Pb^{2+} ions. The results showed the Zn^{2+} and Pb^{2+} ion adsorption capacities (the weight ratio of absorbed metal [mg] to adsorbent [g]) were 286.67 mg/g and 146.19 mg/g, respectively.

- Genlin Zhang et al. [30] carried out batch experiments for dyes adsorption in the 100 mL of dyes solutions (Methyl Orange MO and Malachite Green chloride MG 30 mg/L, Disperse Blue DB 200 mg/L) using 20mg of synthetic CMC-acrylic acid adsorbent for 60 min at 25-50°C. The removal ratio

of adsorbent to MO, DB and MG reached to 84.2%, 79.6% and 99.9%, respectively.

- Samaneh Saber-Samandari et al. [31] synthesized a nano-composite membrane CMC-graft-poly(acrylic acid) together with silica gel and used it for adsorbing crystal violet (CV) and cadmium (Cd (II)) ion. The membrane's maximum CV- and Cd (II)-adsorption capacities were 546 and 781 mg/g, respectively.

- Aiqin Wang et al. [32] experimented with several CMC-g-poly (acrylic acid)/attapulgite (CMC-g-PAA/APT) hydrogel composites for examining Pb(II)-adsorption capacity from aqueous solution, which demonstrated a fast Pb(II)-adsorption rate.

- El. Nagger et al. [33] prepared the hydrogel films with the different ratios of CMC/polyethylene oxide (PEO) by using the solution-cast method, the hydrogel cast-films showed capabilities of high absorption and releasing functionalities of metal ions which is preferable for the agricultural usage.

- A. Hiroki et al. [34] found that CMC/carboxymethyl chitosan (CMCts) blend hydrogel highly adsorbs Pb and Au, of which the functionality can be controlled by amino groups in the network.

4. *Adsorption process*

Adsorption process takes place when one or more components (adsorbate) are attracted and bonded to the surface of a solid (adsorbent) with which they are in contact. According the type of adsorbent-adsorbate forces formed, adsorption is classified into two forms: physical adsorption or chemical adsorption.

- Physical adsorption (physisorption) is adsorption in which the forces involved are weak Van der Waal forces. It is also known as Van der Waal's adsorption. The physisorption process mostly reversible, i.e., the adsorption bonds are easily formed and broken, due to the low energy of adsorption that characterizes such systems.

- Chemical adsorption (chemisorption) is adsorption in which the forces involved are valence forces, i.e., chemical bonds exist between adsorbate and adsorbent. It is also known as Langmuir adsorption. This process is usually irreversible as the bonds formed are semi-permanent; thus for desorption to occur, the adsorbate undergoes a chemical change. Comparison between physisorption and chemisorption is shown in **Table 5**.

In order to properly understand the adsorption process of metal ions, it is necessary to understand basic ingredients: adsorbate-adsorbent interaction, adsorption selectivity process, equilibrium and kinetics. An adsorption isotherm represents the relationship between the equilibrium metal adsorption capacity of the adsorbent and the equilibrium concentration of metal ions in solution. Kinetics deals with changes of adsorption in time and is concerned especially with rates od adsorption. Hence isotherm and kinetic models are often used to understand the mechanism of heavy metal adsorption by the adsorbent. The selectivity is a measure of the competitiveness of adsorption between the components of a metal ion mixture in solution while adsorbate-adsorbent interaction can reflect the nature of adsorption.

Table 5. Physical adorption and chemical adsorption.

	Physical adsorption	Chemical adsorption
1. Heat emission on adsorption	Low, 20 – 40 kJ/mol	High, 40 – 400 kJ/mol
2. Attraction Force	Van der Waals' forces	Chemical bond forces
3. Features	- Strong at low temperature and weaker at higher temperature - Reversible - Related to the liquefaction of the gas - Not very specific - Forms multi-molecular layers - Not require any activation energy	- Takes place at high temperature - Irreversible - Generally, not related to liquefaction of the gas - Highly specific - Forms mono-molecular layers - Requires activation energy

a. *Adsorption selectivity*

Generally, various components are often present in industrial effluents. Hence, selective adsorption is necessary for all techniques attempting wastewater pollutants remediation. The adsorption selectivity of a given material is the ability of the material to adsorb one component preferably to the others. The selectivity of an adsorbent is often measured from the distribution coefficient K_d (mL/g) and selectivity coefficient α (dimensionless), which is defined by **Eq. 1** and **Eq. 2**.

$$K_d = \frac{C_0 - C_f}{C_f} \times \frac{V}{m}, \qquad \textbf{Eq. 1}$$

$$\alpha = \frac{K_d(T)}{K_d(I)}, \qquad \textbf{Eq. 2}$$

where C_0 and C_f (µg/L) are the initial and equilibrium concentrations, respectively, of the adsorbate during adsorption process; V (mL) is the testing adsorption volume; m (g) is the amount of adsorbent. K_d (T) and K_d (I) are the distribution coefficient values of the target adsorbate, and the other adsorbates, respectively, in the experimental solution. The term K_d indicates the adsorption affinity for a particular adsorbate in the presence of other interfering-adsorbates, while α, the superiority degree of selectivity for a particular adsorbate compared with the other adsorbates [35].

b. *Interaction between adsorbates and adsorbents*

The interaction between a metal ion and a ligand on adsorbent can be explained in terms of the Ralph Pearson's concept of Hard and Soft Acids and Bases (HSAB). According this definition, the hard Lewis bases prefer binding to hard Lewis acids to give ionic complexes, whereas soft Lewis bases prefer binding to the soft Lewis acids to give covalent complexes [36].

- **Hard Lewis acids** are defined by small ionic radii (<90 pm), high positive charge, strongly solvated, empty orbitals in the valence shell, low electronegativity (0.7 – 1.6) and low electron affinity.
- **Soft Lewis acids** are defined by large ionic radii (>90 pm), low positive charge, completely filled atomic orbitals and intermediate electronegativities (1.9 – 2.5).
- **Hard Lewis bases** are defined by small ionic radii (around 120pm), strongly solvated, electronegative atomic centres (3.0 – 4.0), weakly polarizable
- **Soft Lewis bases** are defined by large ionic radii (>170 pm), intermediate electronegativity (2.5 – 3.0), highly polarizable.
- The **Border line** Lewis acids and bases have intermediate properties.

Because the electronegativity differs so large between the hard acid and the hard base, there occurs strong ionic interactions. On the other hand, the soft acid and the soft base show almost the same electronegativity, therefore the interaction between them is less ionic and has a characteristic of covalency. The interactions between other pairs such as between the hard acid and the soft base and/or between the soft acid and the hard base are intermediate ones being unstable and reactive; which are easily transform into either ionic ineraction or covalent bond if there are stimula to react.

Also base on the HSAB concept, many previous studies devided the interaction between binding sites of hydrogel adsorbent and metal ions in aqueous solution into 3 dissimilar kinds i.e., crystallization, electrostatic attraction/ion exchange or chelation/complexation , as described by following equilibrium reaction [18]:

$$\text{R–active site} \rightleftharpoons \text{R–active site}^- + H^+$$

$$n\text{R–active site}^- + M^{n+} \rightleftharpoons (\text{R – active site})_n M$$

$$M^{n+} + nOH^- \rightleftharpoons M(OH)_n$$

With M is the metal ions and R represents for "hydrocarbon chain" in adsorbent structure.

c. *Modeling of metal adsorption isotherms*

The adsorption process is usually studied through graphs, known as adsorption isotherm, between the total adsorbed amount adsorbed on the surface of adsorbent and pressure at constant temperature. Up to now, there is no isotherm that fully describes all adsorption experimental results without increasing the accuracy or changing the condition assumption.

In order to correlate experimental data, several two-parameter-equations such as Langmuir, Freundlich, and Temkin have been proposed in the literature in **Table 6**. These models utilized for analyzing the adsorption process are based on some assumptions which limit the scope capable of applying them [37].

✓ In 1916, Irving **Langmuir** primarily built an adsorption model with following assumptions to evaluate a gas-solid phase adsorption process on glass, mica and platinum [38]. Recently, Langmuir isotherm was developed using the following assumptions[39]:

- Adsorption process takes place at defined locations on the adsorbent surface.
- All adsorption positions on the adsorbent surface are the same.
- The surface of the adsorbent is covered with a single layer of adsorbates.
- There is no interaction between adsorbates and adsorbents.

The Langmuir isotherm is used to evaluate the adsorption capacity of an adsorbent with the non-linear form of this isotherm can be written as **Eq. 3**:

$$q_e = \frac{q_{max} . K_L C_e}{1 + K_L C_e} \quad , \qquad \textbf{Eq. 3}$$

where

q_e (µg/g) : adsorbed metal-ion amount per gram of adsorbent at equilibrium,

C_e (µg/L) : equilibrium metal-ion concentration in the solution,

q_{max} (µg/g) : maximum monolayer coverage capacity,

K_L (L/µg) : equilibrium constant related to the magnitude of interaction between adsorbate and the adsorbent's surface (adsorption energy).

A large K_L value indicates the existence of strong interaction between adsorbate and adsorbent while smaller value, a weak interaction.

✓ **The Freundlich isothermal model** is another method used to describe multi-layer adsorption and the inhomogeneous surface of adsorbent materials [40]. However, this model can not describe either the (arithmetic) linearity range at very low concentrations or the saturation effect at very high concentrations. Hence, the Freundlich isotherm does not describe the saturation behavior of an adsorbent [41]. This model is shown in nonlinear form by the **Eq. 4** :

$$q_e = K_F C_e^{\frac{1}{n}}, \qquad \textbf{Eq. 4}$$

where

K_F (µg/g) : Freundlich constant used for predicting adsorption capacity of a adsorbent,

n : adsorption intensity which indicates the surface heterogeneity,

C_e (µg/L): the equilibrium concentration of metal ions

The number of active sites n in the hydrogels for all investigated adsorbates was greater than unit indicates that the sorption by adsorbent is favorable [42].

✓ **Temkin model** takes into account the effects of indirect adsorbing species–adsorbate interactions on the adsorption process; it is also assumed that the heat of adsorption of all molecules in the layer decreases linearly as a result of increase surface coverage [43]. The derivation form of Temkin isotherm model is given by the following [44]:

$$q_e = \frac{RT}{b}\ln(K_T C_e) \qquad \textbf{Eq. 5}$$

C_e (µg/L) : equilibrium metal-ion concentration in the solution,

T and R in Temkin equation: 298 K and universal gas constant (8.314 J/mol K), respectively,

K_T (L/µg) : isotherm equilibrium binding constant,

b (J/mol) : constant related to heat of adsorption.

Table 6. Isotherm models for analyzing experimental data.

Model	**Langmuir** [39]	**Freundlich** [41]	**Temkin** [44]
Equation	$q_e = \frac{q_{max}.K_L C_e}{1 + K_L C_e}$	$q_e = K_F C_e^{\frac{1}{n}}$	$q_e = \frac{RT}{b}\ln(K_T C_e)$
Describes	Monolayer adsorption	Heterogeneous surface	Indirect interaction

d. *Modeling of metal adsorption kinetics*

Although diffusion models are widely accepted as appropriate models to describe adsorption kinetics for porous adsorbents, a number of papers published recently have described the adsorption kinetics using simple models based on chemical reaction kinetics. These papers relate to the adsorption of different adsorbates including not only organic substances but also heavy metals. The works reported were mainly onto alternative adsorbents (bio-sorbents, low-cost adsorbents) and activated carbon. Under the assumption that the adsorbate uptake follows the Lagergren equation (**Eq. 6**) or the equation describing the second-order kinetics (**Eq.7**) [45].

$$\frac{\mathrm{d}q_t}{\mathrm{d}t} = k_1(q_e - q_t)\,, \qquad \textbf{Eq. 6}$$

$$\frac{\mathrm{d}q_t}{\mathrm{d}t} = k_2(q_e - q_t)^2\,, \qquad \textbf{Eq. 7}$$

where k_1, k_2 are the rate constants of adsorption, q_t and q_e (μg/g) are the adsorbed-metal weights (μg) per those of adsorbent (g) at a time t and at equilibrium time (min.), respectively.

Both of kinetic models assume that:

- The adsorption process only occurs at binding sites on the surface of the adsorbent.
- The adsorption energy does not depend on the formation of adsorption layer on the surface of adsorbent.
- No interaction appears between adsorbates and surface of adsorbents.

The first-order model (Lagergren equation) determines the speed of the adsorption process whereas the second-order model considers the speed limit step when forming chemical bonds involving the sharing or exchange of electrons between metal ions and adsorbents. Although the reaction kinetic models are widely applied, they need to be reviewed critically.

In the assessment for selecting more suitable kinetics from the 1st- and 2nd-order-model fitting of the experimental data, the author adopted three criteria:

(a) Adsorption capacity estimated from the fitting (q_{cal}) by the more suitable model should be closer to that obtained in the experiments (q_{ex}).

(b) Correlation coefficient (R^2) derived from the better fitting with more suitable model should be large than that of the other one.

(c) Chi-squared value (χ^2) should be smaller for the fitting with more suitable model.

The χ^2 was calculated as the following **Eq. 8** [46]:

$$\chi^2 = \sum \frac{\left(q_{\mathrm{e,exp.}} - q_{\mathrm{e,cal.}}\right)^2}{q_{\mathrm{e,cal.}}}\,. \qquad \textbf{Eq. 8}$$

Though the kinetic models such as pseudo-1st and pseudo- 2nd order kinetic models are useful from the viewpoint of controlling the adsorption reaction by a few parameters, they might not make reference

to the discussion on temporal phase-changes in the adsorption process resulting from the alteration of rate-determining mechanisms in response to the expansion and/or displacement of metal-ion diffusion area. In the present section, the discussions on the microscopic process are described from this point of view.

Normally, the metal ions can penetrate to hydrogel network through three main steps [47]:

(i) Initial adsorption on the adsorbent surface facing external phase,
(ii) Gradual adsorption controlled by intra-particle diffusion into the adsorbent in the next stage,
(iii) Final adsorption limited by the low adsorbate concentration resulted from the preceding adsorptions and at the stage almost reaching the adsorption equilibrium.

To predict which step is the rate-determining step, the intra-particle diffusion model [46] was applied and expressed as **Eq. 9** below:

$$q_t = k_{\mathrm{id}} t^{0.5} + C \ , \qquad \textbf{Eq. 9}$$

where q_t (μg/g) is adsorbed-metal-ion amount after t hrs. from the initiation of the adsorption; k_{id} (μg/[g·hr$^{0.5}$]), the intra-particle diffusion rate constant; and C (μg/g), a constant related to thickness of the boundary layer formed between metal-ion solution and adsorbent surface [48]. These parameters can be derived from the slope of linear portion in the graph of q_t versus $t^{0.5}$. If C is negligibly small, the gradual adsorption (intra-particle diffusion) can be solely the rate-controlling step in the diffusion process [48].

e. *Adsorption activate energy*

Activation energy E_a (kJ/mol) is the minimum amount of energy that adsorbates need to have for separating from the adsorbent, which is calculated according to the Arrhenius equation **Eq. 10** [49]:

$$E_a = RT(\ln A - \ln k) \ , \qquad \textbf{Eq. 10}$$

where

T : Temperature (K),

R : Gas constant = 8.314 (J/[mol K]),

A : Initial adsorption rate = $k \cdot q^2$ (mg/[g hr]),

k : Rate constant of adsorption (g/[mg hr]),

q : Adsorption capacity (μg/g).

The value of E_a in the adsorption process is generally utilized for distinguishing between chemical and physical adsorption. In the case of physical sorption, because the combination between adsorbates and adsorbent is caused by Van der Waal's interactions, the activation energies are less than 40 kJ/mol, therefore the bonds can be easily formed and broken at room temperature. On the other hand, the activation energy for the chemisorption is considerably higher than physical adsorption, from 40 up to 800 kJ/mol, because the adsorption is caused by the formation of covalent bond [50].

III. Objectives of this study

The foregoing overview presented in the previous sections has shown that the treatment of industrial effluents rich in heavy toxic metal ions before discharge is necessary. Moreover, adsorption by organic hydrogels are now considered as an effective, user-friendly purification and separation method for the removal of heavy metals from industrial wastewater with the advantages of specific affinity, low cost and simple design. Selective adsorption is also necessary for all techniques attempting wastewater pollutants remediation.

Hydrogel prepared from carboxymethyl cellulose (CMC) possesses reactive carboxymethyl group (–CH_2–COOH). This functional group can chelate with most of metal ions in solution and makes the application of CMC in metal adsorbent fields more attractive and promising. However, the active sites distributed in CMC hydrogel is not plentiful and strong enough. CMC molecules crosslink toghether to form the network by covalent bonds which cause CMC hydrogel structure be quite fraigile and then its reusability be decreased. So the modification of CMC is required to improve not only physical but also its chemical properties.

In view of these shortcomings, the objectives of this dissertation attempted to address those gaps. Hydrogel from modified-CMC will be used as the candidate adsorbents for this research works and fabrication of the hydrogel adsorbents will be via one-step irradiation using gamma rays. This method is an easily controlable and environment friendly process in hydrogel synthesis and also in grafting functional-groups to the hydrogel network because the achieved products are very sterile and pure [51].

The present study was carried out through the following stages:

1. The first approach focuses on the modification of CMC hydrogel to increase binding sites by synthesis of the CMC-hydrogel grafted with strong active monomer, sodium sulfonate styrene (SSS), for metal ion adsorption purposes.

2. The research attempts to improve the reusability modifed CMC-hydrogel by introducing a network reinforcer; then monitors some factors having clear and featured effect to adsorption capacity and kinetics to understand adsorption behavior.

3. Finally, potential applications and future perspectives of adsorbents are in selective adsorption by designing a CMC based hydrogel having functional groups that are geared towards specific properties of the target pollutant substrates instead of general properties.

CHAPTER 2

EXPERIMENTAL

I. Starting materials

The main used natural polymer in the thesis, Carboxymethyl cellulose sodium [CMC-Na: average weight of molecular M_w ~7×10^5 (Dalton), degree of substitution (DS) ~0.90] was purchased from Alfa Aesar (England). The another natural polymer and 2 vinyl monomers applied for modification of CMC hydrogel were Carboxymethyl chitosan (CMCts: M_w ~450,000, DS ~0.95), Sodium Styrene sulfonate monomer (SSS) and Bis[2-(Methacryloyloxy)Ethyl] Phosphate (BMEP), respectively. Their chemical formulas are displayed in **Figure 4**. Three of them were bought from Sigma Aldrich (Switzerland and Japan). Stock solution of varying metal ion *Trace*CERT® in metal adsorption experiments was obtained from Fluka, Sigma-Aldrich (Switzerland). All adding chemical reagents were purchased from Sigma Aldrich (Japan). In all the experiments, used was the deionized water (DW) from Puric ω Organo System (Japan), of which the concentrations of K, Na, Mg, Ca, Fe, Cu, Zn, Cd, Ni, Pb, Mn, Al, Co, Cr were less than 0.1 ppt (ppt = 10^{-12}) and, less than 1 ppt for B.

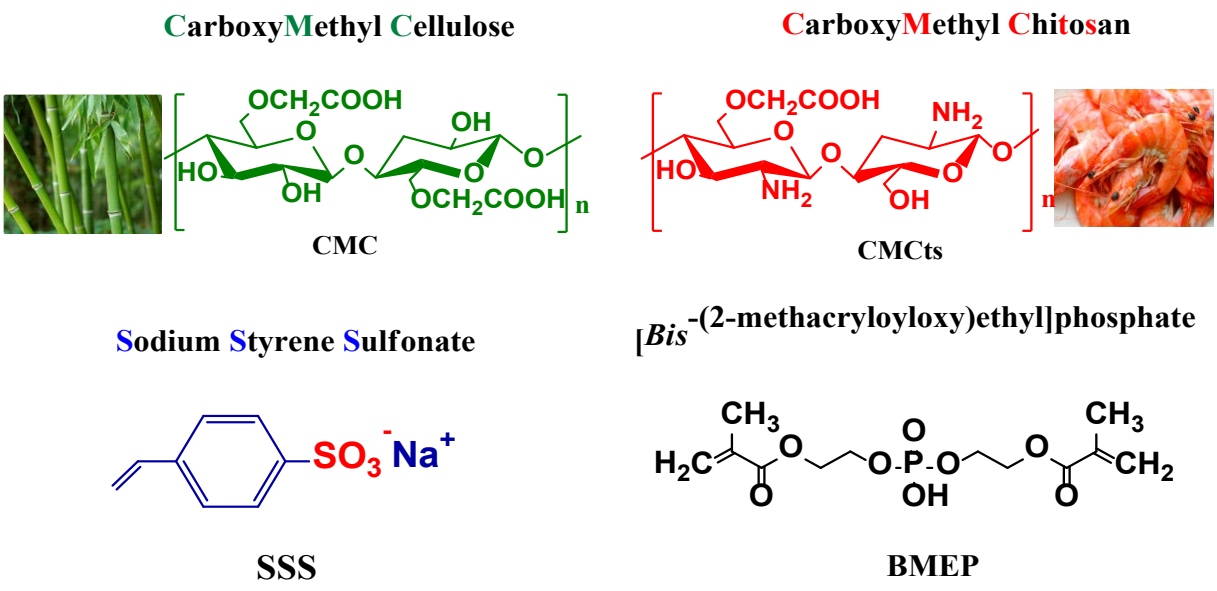

Figure 4. Chemical structures of main materials in current study.

II. Synthesis of samples

Although CMC hydrogel has outstanding basic properties for metal adsorption such as chelate-able with most of metal ions in solution and swell ability, it is necessary to modify CMC hydrogel by different ways. Gamma rays induced modification is a powerful and environment friendly method to propare new CMC-based hydrogels with desired property with is more advantageous than the chemical technique as mentioned in Chap.1-Sec.II.2. From the view point of hydrogels as polymeric adsorbents in Chap.1- Sec.II.1, modification of CMC hydrogel can be prepared by following preparation methods:

- Grafting one type of hydrophilic and active monomer onto CMC hydrogel to improve metal adsorption property of CMC hydrogel.

- Introducing a network reinforcer to the CMC hydrogel to improve the mechanical property of adsorbents.

- Varying functional groups in one adsorbent by interpenetrating of two independent cross-linked synthetic and/or natural polymers components contained in a network form to change its selective property.

In the current study, the three types of modified CMC-based hydrogel samples were synthesized from CMC, CMCts, SSS and BMEP in DW as follow:

1. *Gamma-ray-induced grafting of the active monomer SSS onto CMC structure (abbreviated as CS hydrogel)*

Basically, single hydrophilic CMC polymer units are cross-linked each other without any other chemical bonds between them to form CMC hydrogel. However, to raise the metal adsorption capacity of CMC hydrogel, a very active monomer SSS was grafted on CMC networks. It might be called as a grafted hydrogel type. Each aqueous solution of 20 wt% CMC and SSS in paste-like state with different CMC:SSS ratios of 1:0, 2:1, 1:1 and 1:2 was put into polypropylene (PP) tubes as in **Table 7**.

2. *Establishing cross-linked networks from CMC, SSS and BMEP (abbreviated as CSB hydrogel)*

It is cross-linked network of hydrophilic CMC polymer with BMEP monomer. The co-polymeric hydrogel networks might be non-covalently cross-linked structures formed from between –OH hydroxyl groups and $–CH=CH_2$ vinyl groups. A series of PP tubes containing the mixture of CMC, SSS and BMEP with concentration changing from 0.0 – 12.9 (m M) in DW as shown in **Table 8** to synthesize CSB hydrogels.

3. *Preparation of interpenetrating network adsorbent from CMC and CMCts polymers containing simultaneously SSS (abbreviated as CCS hydrogel)*

There were two independent cross-linked natural components: CMC and CMCts polymers. SSS was functionalized both of CMC and CMCts to enhance metal removal. Various ratios of CMC, CMCts and SSS content in DW as presented in **Table 9** were transferred into PP tubes.

Table 7. Different ratios of CMC and SSS for CS hydrogel synthesis

Recipe	CS 1:0	CS 2:1	CS 1:1	CS 1:2
CMC (g)	6.00 (0.36 mM)	4.00 (0. 24 mM)	3.00 (0.18 mM)	2.00 (0.12 mM)
SSS (g)	0.00 (0.00 M)	2.00 0.40 M	3.00 0.60 M	4.00 0.80 M
H_2O (ml)	24.0	24.0	24.0	24.0

Table 8. Initial composition for synthesized CSB hydrogel

Recipe	CSB 0.0	CSB 2.6	CSB 5.2	CSB 7.8	CSB 12.9
CMC (g)	2.00 (0.12 mM)	2.00 (0.12 mM)	2.00 (0.12 mM)	2.00 (0.12 mM)	2.00 (0.12 mM)
SSS (g)	4.00 (0.80 M)	4.00 (0.80 M)	4.00 (0.80 M)	4.00 (0.80 M)	4.00 (0.80 M)
BMEP (g)	0.00 (0.0 mM)	0.02 (2.6 mM)	0.04 (5.2 mM)	0.06 (7.8 mM)	0.1 (12.9 mM)
H_2O (ml)	24.0	24.0	24.0	24.0	24.0

Table 9. Material combinations for preparation of CCS hydrogel synthesis

Recipe	CCS -1	CCS-2	CCS-3	CCS-4	CCS-5
CMC (g)	3.00 (0.18 mM)	2.50 (0.15 mM)	2.00 (0.12 mM)	1.50 (0.09 mM)	1.00 (0.06 mM)
CMCts (g)	3.00 (0.28 mM)	2.50 (0.26 mM)	2.00 (0.18 mM)	1.50 (0.13 mM)	1.00 (0.09 mM)
SSS (g)	0.00 0.00 M	1.00 0.20 M	2.00 0.40 M	3.00 0.60 M	4.00 0.80 M
H_2O (ml)	24.0	24.0	24.0	24.0	24.0

III. Gamma irradiation

Earlier, hydrogels were usually synthesized by "classical" chemical methods. Although these ways allow to gain final products with desired properties, they still contain unwanted substances such as additives, initiators, crosslinking agents and monomers. These unwanted substances should be washed in complicated steps before using and may increase in production costs. One alternative technique for this situation is ionizing radiation. In the last few decades, it has been recognized as a very convenient method in the synthesis of hydrogels due to many advantages: no need to add any cross-linkers or initiators; easily controllable process, etc. Briefly, irradiation induced crosslinking and grafting process of polymer in paste-like state spend 3 main stages at least i.e. initiation, propagation and termination chains and may be described as in **Scheme 2**.

- Initiation step: At first, water molecules H_2O receive enough energy from γ-rays to create many energetic species like e_{aq}^-, $HO^\bullet$, $H^\bullet$, $H_2O^{\bullet+}$ radicals [52]. After that, those e_{aq}^-, $H_2O^{\bullet+}$, $HO^\bullet$ and $H^\bullet$ radicals attached to polymers and monomer chains resulting polymer and monomer radicals.

- Propagation step: Combination of those above radicals with other polymer and monomer molecules in the mixture forms new macro-radicals.

- Termination step: The reaction between macro-radicals in the mixture results in the formation of grafted or cross-linked hydrogel structure.

Each proposed mechanism for irradiation-induced synthesis of each type hydrogel has been described in following schemes.

Initiation

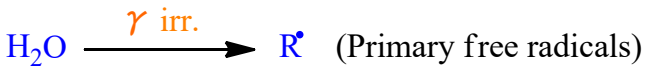

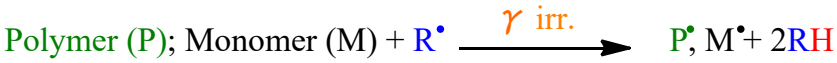

Propagation

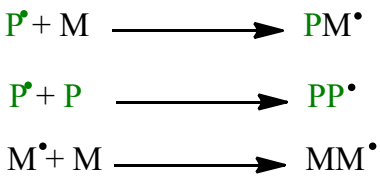

Termination

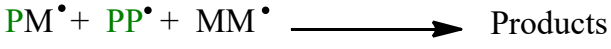

Scheme 2. Brief description of irradiation induced crosslinking and grafting process of polymer in paste-like state

To remove all air bubles, all prepared hydrogels were centrifuged at 10^4 rpm for at least 5 hrs. and then ^{60}Co γ-ray irradiated in the range doses of 10 – 100 kGy at the Center for Accelerator and Beam Applied Science (Kyushu University) (**Figure 5**). Herein, the irradiation dose means the specific dose which delivers to achieve a desire result in different materials. Upon completion of irradiation process, copolymerized hydrogels were showered with DW in order to extract any un-reacted chemicals. The final hydrogels were cut into 0.5×0.5×0.5 cm-cubes for further experiments.

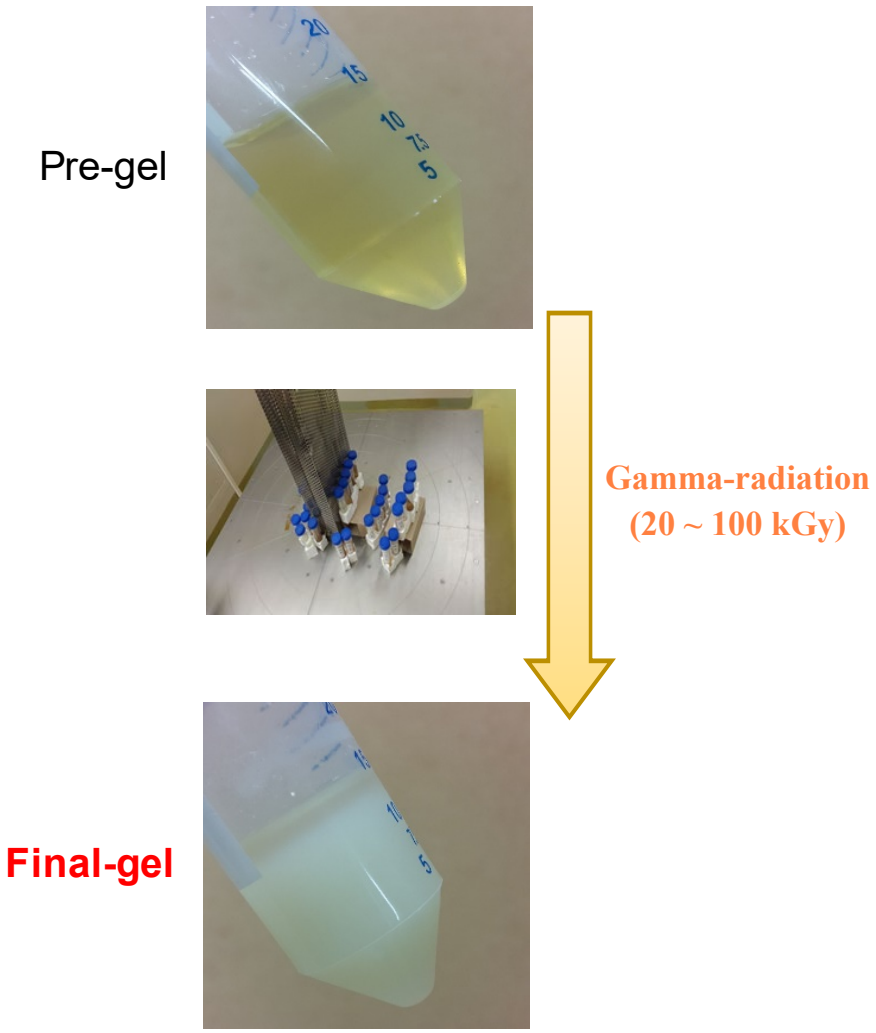

Figure 5. Samples irradiated at ^{60}Co gamma ray point source at Kyushu University center for accelerator and beam applied science.

IV. Characterization of samples

Hydrogel characterization is one of the most important sides of the polymer science and engineering applications. Since hydrogels are produced for this study it is important to determine the composition of the samples. Also gel content and swelling capacity determination is important because they affect the adsorption properties. Determination of thermos-physical and mechanical properties and surface characteristics are necessary for hydrogel processing.

1. *Gel fraction and swelling ability*

After the hydrogels were synthesized, the gel fraction (GF) and swelling capacity S_w were measured. Two these properties will influence directly on metal adsorption capacity of hydrogel. The GF in the sample was calculated by gravimetrically weighing its insoluble part after the extraction in DW for 48 hrs. at room temperature (**Figure 6**). The gelled parts were dried at 50 °C until getting constant weight. The GF was estimated accprding to the following equation **Eq. 11**:

$$\mathrm{GF}\ (\%) = \frac{W_\mathrm{d}}{W_0} \times 100\ , \qquad \textbf{Eq. 11}$$

where W_d is the weight of dry gelled part after extraction and W_0 the initial weight of dry gel.

The prepared hydrogels were dipped in DW for a certain time at room temperature. After wiping excess water at the surface of the gel, the weight of swollen gel was measured (**Figure 6**). Swelling ratio (S_w) of the blend hydrogels was calculated from the following **Eq. 12**:

$$S_\mathrm{w} = \frac{W_\mathrm{s} - W_\mathrm{d}}{W_\mathrm{d}}, \qquad \textbf{Eq. 12}$$

where W_s is the weight of the swollen gel and W_d the weight of dry gelled part.

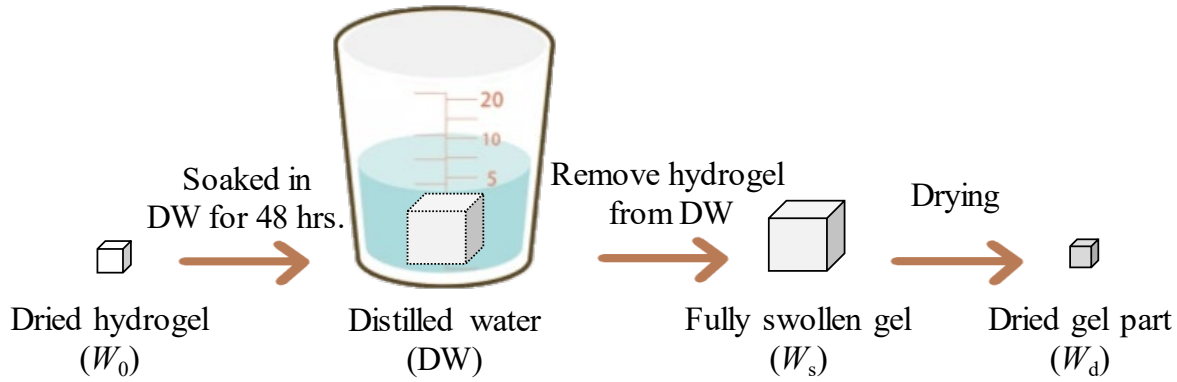

Figure 6. Calculation process of gel content of gelation and swelling ability.

2. *Fourier transforms infrared spectroscopy (FTIR) analysis*

To understand the nature of the hydrogels by themselves in FT-IR, we obtained their spectra first. Then each hydrogel's spectrum was compared with those of original componants'. FTIR spectra were obtained using the Jasco FT/IR 4100 instrument (Japan) by ATR method in the range of 400–4000 cm^{-1} after a background scan. Before FT-IR analysis, all samples in 0.5 mm-flat thin lamina were dried first at 50 °C until a constant weight.

The FTIR spectroscopy is a useful qualitative tool to determine composition of molecules which studies the interaction of the light with matter [53]. When we expose a sample to light, it will vibrate the chemical bonds in the sample that makes change in the spectrum since functional groups of a molecule absorbs the light at the same wavenumber regardless of the rest of the molecule. Like a fingerprint depending on the nature of the molecule. Vibration of chemical bonds has two main categories including stretching and bending. First, stretching vibration is the change in inter-atomic distance along bond axis. Second, the bending vibration is the change in angle between two bonds [53].

Polymers and monomers that we have used have different functional groups and expected to show a significant effect on the hydrogel spectra as they are synthesized. Various bands of reference adsorption peak are shown in **Table 10**.

Table 10. Some FTIR peaks of the hydrogel functional groups [54][55].

Absorption (cm^{-1})	Appearance	Group	Compound class
3550 – 3200	broad, strong	O–H stretching	Alcohol, carboxylic acid
1450 – 1300	medium	O–H bending	Alcohol, carboxylic acid
Around 3500	medium	N–H stretching	Primary amine
3400 – 2700	medium	C–H stretching	Alkane, alkene, alkyne
1650 – 1580	medium	N–H bending	Amine
1210 – 1163	strong	C–O stretching	Ester
1275 – 1075	strong	C–O stretching	Ether
1465 – 1375	strong	C–H bending	Alkane
1650 – 1566	medium	C=C stretching	Cyclic alkene
1372 – 1335 1195 – 1168	strong	S=O stretching	Sulfonate
1300 – 1200	strong	P=O stretching	Phosphate
1050 – 950	strong	P–O–C stretching	Phosphate

3. *The Carbon-13 Nuclear Magnetic Resonance (^{13}C-NMR) spectroscopy analysis*

^{13}C NMR measurement was more significant in determining the actual structure of the hydrogels since it is based on the chemical shift and peak intensities of simple spectra and thereby enabling the identification of carbon types, polymer composition and sequence distribution. This eventually facilitated the carbons reconstruction to obtain the actual structure.

Typical chemical shifts of organic compound in ^{13}C-NMR is displayed in **Figure 7**. ^{13}C-NMR spectrum was recorded on a NMR spectrometer (JEOL JNM-ECA-400, Japan) at Center of Advanced Instrumental Analysis (Kyushu University).

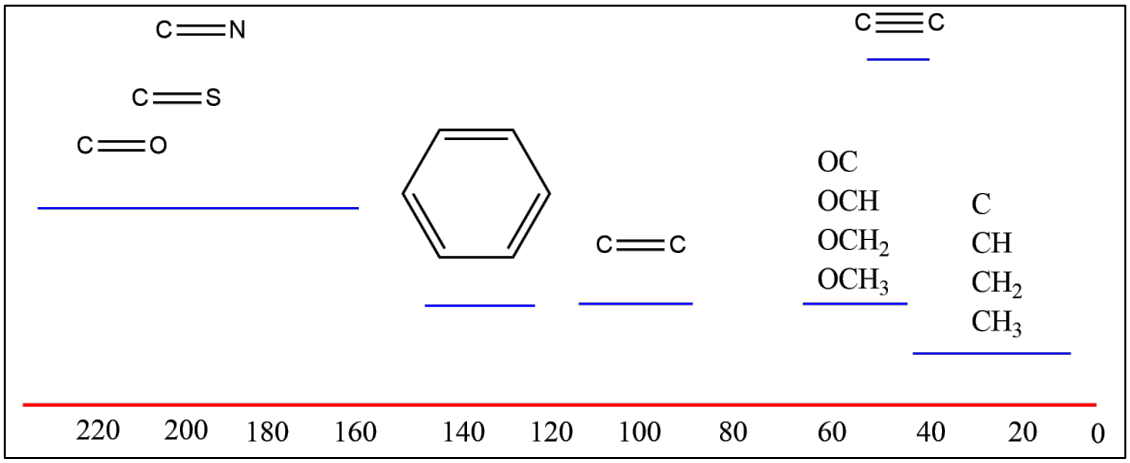

Figure 7. Typical chemical shifts of organic compound in ^{13}C NMR.

4. *Thermos-physical analysis*

The thermal gravimetric analyzis (TGA) was used to determine changes in weight in relation to changes in temperature. The weight loss measument gives information on changes in thermal stability, sample composition and kinetic parameters for chemical reactions in the sample. There are two tendencies of weight change in TGA mechanisms [56]:

- Weight loss explains following processes:
  - ✓ Decomposition: Chemical bonds are broken.
  - ✓ Evaporation: The volatiles are lost with elevated temperature.
  - ✓ Reduction: The sample interacts to a reducing atmosphere (hydrogen, ammonia, etc).
  - ✓ Desorption.
- Weight gain describes two progresses
  - ✓ Oxidation: The sample interacts with an oxidizing atmosphere.
  - ✓ Adsorption or absorption.

TGA was carried out on the STA 449 F3 Jupiter instrument (NETZSCH, Germany) over a temperature range of 20 – 800 °C with heating rate of 5 °C/min and N_2 flow rate of 40 mL/min.

5. *Surface characteristics by SEM and EDS measurements*

Scanning Electron Microscope (abbreviated as SEM) is a type of electron microscope that can produce high resolution images of the specimen surface using a narrow beam of electrons sweep across the sample surface [57]. Imaging is done by recording and analyzing the radiation emitted from the interaction of the electron beams with the specimen surface.

Energy dispersive X-ray spectroscopy (EDS) was a quantitative (the content of each element of the sample) and qualitative (the type of elements) analysis technique of observed surface samples [58]. This measurement was done simultaneously with analysis depth of a sample about 1 µm and able to identify all chemical elements on the periodic table, from boron to uranium. This ability for elemental isolation and identification was critical since it assists to prevent impurities by detecting any unwanted elements immediately after synthesis, and confirm that the obtained material contains only the desired constituents. Additionally, EDS detector can estimate the quantity of the constituent elements present in a sample, in form of weight percentage [58].

The surface morphology SEM (Scanning electron microscope) and surface elemental analysis EDS (Energy-dispersive X-ray spectroscopy) of hydrogel samples were estimated using Shimadzu Super scan SS-550 instrument (Japan) installed at Center of Advanced Instrumental Analysis, Kyushu University. The conductive carbon coater was used to pre-coat the sample surface before observing the microstructure at 15 kV in low vacuum conditions, with I_e= 99 A of the applied current. Sample irradiation was performed at a working distance of 10 mm, emitting backscatter electrons which were analyzed using a mounted detector, and utilized to reconstruct the topographical structure and compositional distribution of the sample surface. Analysis was carried out at different magnifications to exhaustively describe the hydrogel surface features.

6. *Compressive tests*

The tested hydrogels were splitted into 1.0×1.0×1.0 cm-cubes for the mechanical measurements as in **Scheme 3**. Each measurement was set up around 1 min. at room temperature (25 ºC). The compression force F of 0.000 – 0.137 N were applied to actual square area A of a hydrogel cube. The values of Poisson's ratio $\boldsymbol{\vartheta}$ and Young's modulus E were estimated from the slopes in linear region of the plots, [lateral strain $\boldsymbol{\varepsilon}_{\text{lat.}}$ vs. longitudinal strain $\boldsymbol{\varepsilon}_{\text{long.}}$] and [stress σ vs. longitudinal strain $\boldsymbol{\varepsilon}_{\text{long.}}$], respectively. Because the compressive force and longitudinal deformation vector have opposite movements along the z- axis direction, the σ and $\boldsymbol{\varepsilon}_{\text{long.}}$ values are negative. Three cubes of each the hydrogel sample were measured in order to ensure accuracy and the obtained data was averaged.

In this study, the Young's modulus is compressive modulus which calculated by the following **Eq. 13**:

$$\frac{F}{A} = E \times \frac{h - h_0}{h_0}, \qquad \textbf{Eq. 13}$$

where

F: Applied force (N),

h_0: Initial height (m),

h: Changed height (m),

A: Actual cross-sectional area (m^2),

E: compressive modulus (Pa).

From E data, it might be known whether a material shows elasticity.

The Poisson's ratio ϑ is the ratio of the lateral compression $\varepsilon_{\text{lat.}}$ and longitudinal extension $\varepsilon_{\text{long.}}$ as in **Eq. 14** in which minus sign means negative strain

$$\vartheta = -\frac{\varepsilon_{\text{lat.}}}{\varepsilon_{\text{long.}}} \qquad \textbf{Eq. 14}$$

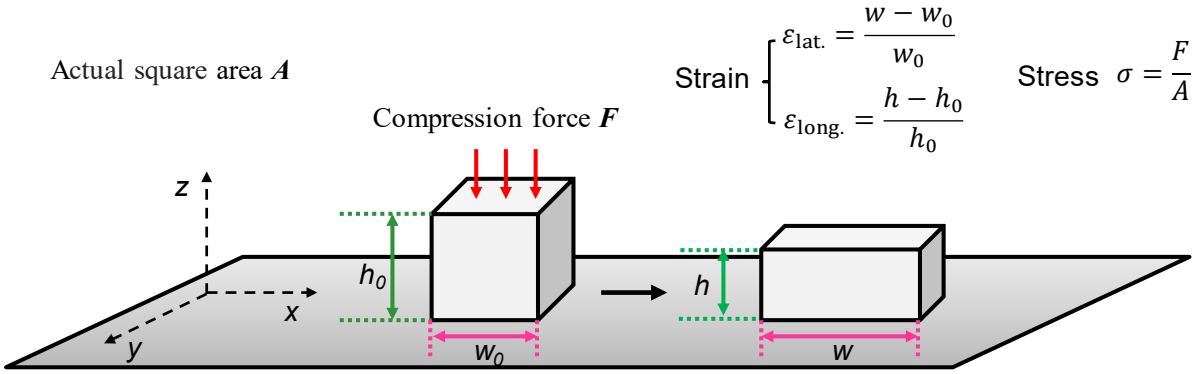

Scheme 3. The mechanical measument layout for prepared hydrogel samples.

V. Experiments for metal adsorption

The 0.5×0.5×0.5 cm-gel cubes (W, 0.200 g) were immersed in 0.04 L of adsorption solution (V) with 100 µg/L of initial concentration for each element, and left intact for 48 hours without stirring at 25 °C. The similar adsorption procedure on the single-ion solution experiment was carried out. The starting (C_0) and final-adsorption (C_f) metal concentrations in adsorption experiments (**Figure 8**) were measured by an inductively coupled plasma mass spectrometer (ICP-MS: Agilent 7700X, Japan) and the percentage of removed metal ions was determined as below:

$$\text{Removal (\%)} = \frac{C_0 - C_f}{C_0} \times 100\,, \qquad \textbf{Eq. 15}$$

In order to calculate metal adsorption capacity q (µg/g) of prepared hydrogel, the below equation **Eq. 16** is used:

$$q = \frac{(C_0 - C_f)V}{W}\,, \qquad \textbf{Eq. 16}$$

In addition, batch adsorption was carried out in 50 mL-polypropylene tubes containing stationary metal ion solution without stirring or shaking. The effect of various parameters such as different component, pH of metal solution, experimental temperature and weight of hydrogels on adsorption process were investigated. Influences of each factor were figured out while other variables were kept constant. Under the same controlled conditions, all the tests were repeated at least three times, and the measured values were averaged for the analyses.

VI. Desorption and reuse

Using the conventional method, the metal absorbed hydrogels were eluted in 0.5 M nitric acid for at least 48 hrs., and then, concentrations of the metal ions released from the adsorbent surface were detected by ICP-MS. After the desorption treatment, the respective adsorbents were taken out from the acid solution and washed in DW until their pH became equal to 7.00 at 25 °C, then the specimens were dried in oven at 50 ºC until constant dry weight. The dried adsorbents were re-used in the identical adsorption experiments in order to test their re-usability. This cycles of adsorption–desorption were repeated at least 4 times for all types of hydrogels in the present study, as presented in **Figure 8**.

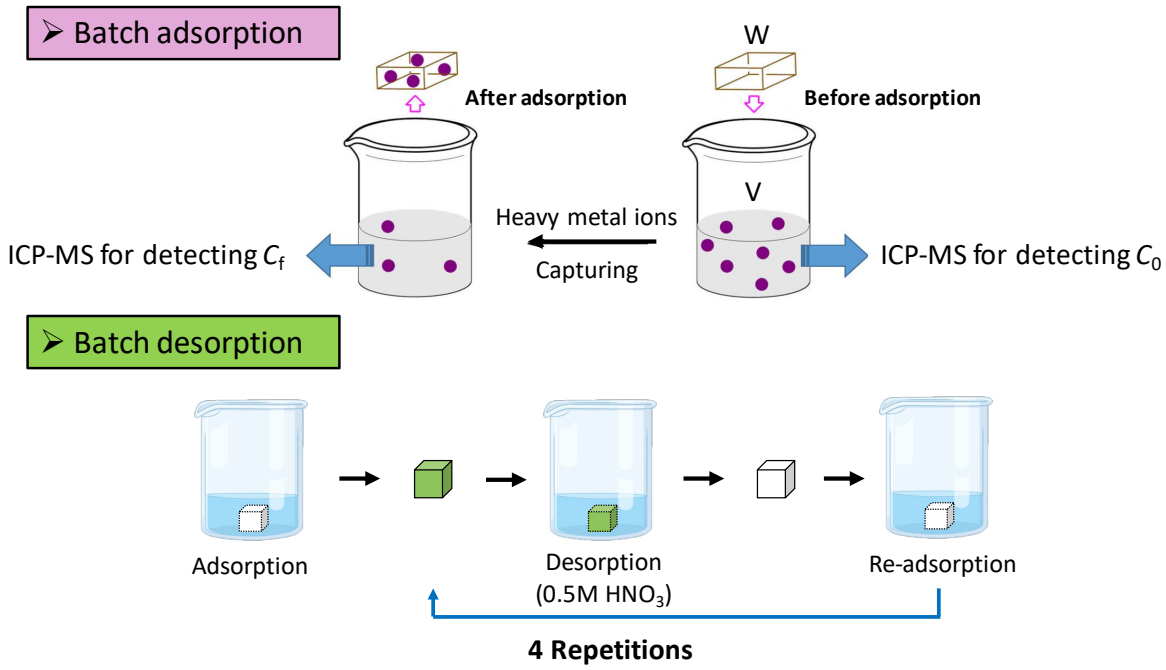

Figure 8. Experiment for determination of hydrogel adsorption capacity.

CHAPTER 3

IMPROVEMENT OF METAL ADSORPTION ABILITY OF CMC HYDROGEL

Considering the urgent need of changing CMC hydrogel to become a low cost and effective recovery agents to prevent heavy metal pollution as discussed in Chap.1-Sec.I and II, the first modifying of CMC hydrogel by graft-onto method under gamma ray irradiation was targeted. This graft-onto method offers the opportunity not only to adjust the length and density of grafting chains but also to improve the chemical and physical properties of hydrogels [59]. For example, some grafted hydrogels were carried out in many previous studies:: the alginate network grafted with polyacrylamide [60], the alginate network grafted with poly(N-isopropyl acrylamide) PNIPAM [61], poly(vinylidene fluoride) films grafted with sodium styrene sulfonate SSS [62] and the chitosan network grafted with PNIPAM [63].

SSS monomer containing sulfonate group was selected to graft onto CMC hydrogel network to enhance its metal adsorption performance. SSS, compared with other monomers has low toxicity, high thermal stability and especially, really high reactivity [64]. SSS is also known as a suitable vinyl monomer for preparing polyelectrolyte complex hydrogels by combination with polysaccharides [65]. The grafted CMC skeleton contained both active functional groups –COOH and $–SO_3^-$ synergistically within the same adsorbent which increase efficient extraction of heavy metal ions from aqueous solution.

I. Synthesis of grafted CMC hydrogel (abbreviated as CS hydrogel)

Scheme 4 shows briefly the proposed synthesis of the grafted hydrogel from CMC and SSS by using γ-irradiation. The $HO^{\bullet}$, $H^{\bullet}$ and $H_2O^{\bullet+}$ energetic species from H_2O molecules take H atoms from the –OH groups on CMC chains and CH_2=CH– group of SSS to form the new CMC and SSS macro-radicals. After that, random reactions of monomer and polymer radicals will react randomly together in order to form CS grafted hydrogel which have higher cross-linking and grafting density. Homo-polymerization of SSS by any radicals is possible but homo-polymers SSS do not cause appreciable unwanted effects on the final products.

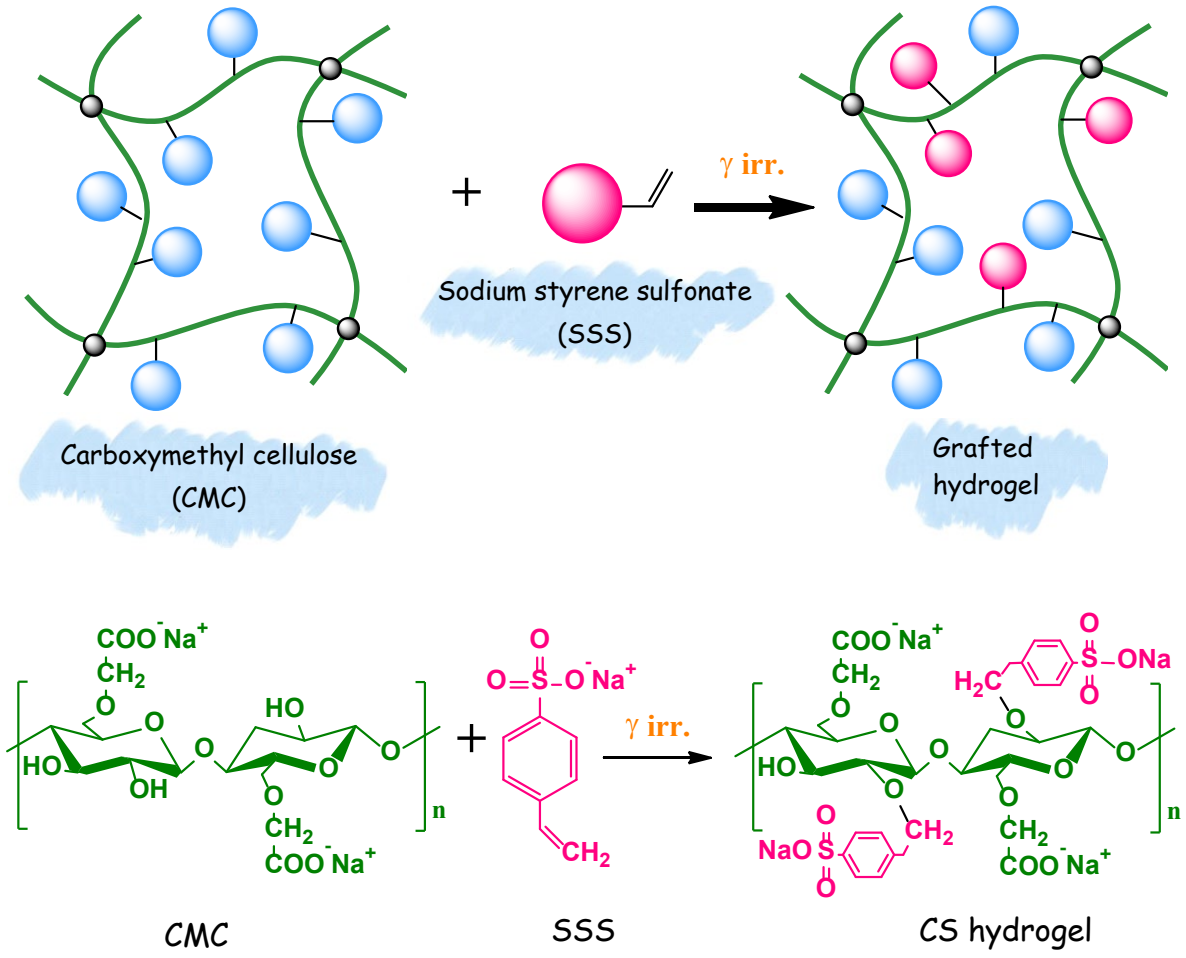

Scheme 4. A brief description of the proposed reaction for irradiation-induced grafting of SSS onto CMC.

II. Identification of prepared hydrogel structure

This step is very important for hydrogel production in order to make sure that the monomer SSS joined grafting process as expected. For basic and fast results the FT-IR and ^{13}C-NMR spectra was utilized.

1. *FT-IR analysis of prepared hydrogel*

Using FTIR we first produced the spectra of hydrogels. This is helpful to understand what to expect and what not to expect in the polymer spectrum. Since each of monomers/ polymers have different substituted group they are expected to give their characteristic peaks at different wavenumbers.

The FT-IR spectra of CMC, SSS and CS are displayed in **Figure 9.** The FTIR spectrum of CMC shows functional groups with absorption bands such as hydroxyl groups (–OH stretching) at around 3313 cm^{-1} as well as inter- and intra-molecular hydrogen bonds in cellulose molecules [24], carbonyl groups (C=O stretching) at 1600 cm^{-1}, hydrocarbon groups (–CH_2 scissoring) and O–H stretching in-plane at 1423 cm^{-1} and 1332 cm^{-1}, and ether groups (–O–) at 1000 – 1200 cm^{-1}.

In the case of SSS, the peaks in the 3100 cm^{-1} region represent vibration band of styrene. The adsoption signals at 1651, 1530 and 1400 cm^{-1} are assigned respectively to in-plane bending vibration of aromatic ring and the in-plane skeleton vibration of aromatic ring. The signals at 1042 and 988 cm^{-1} can be marked to the symmetric whereas the peaks 1187 and 1141 cm^{-1} antisymmetric vibration absorption peaks of –SO_3Na group.

In the CS grafted gel spectrum, in addition to the imprinted bands of CMC, some new absorption bands supporting the presence of SSS were observed. The 1034 and 1012 cm^{-1} bands correspond to –SO_3Na group whereas the bands found at 1195 and 1126 cm^{-1} come from S=O stretching vibration. The contemporary existence of these function groups on CS hydrogel is responsible for metal ion capturing process.

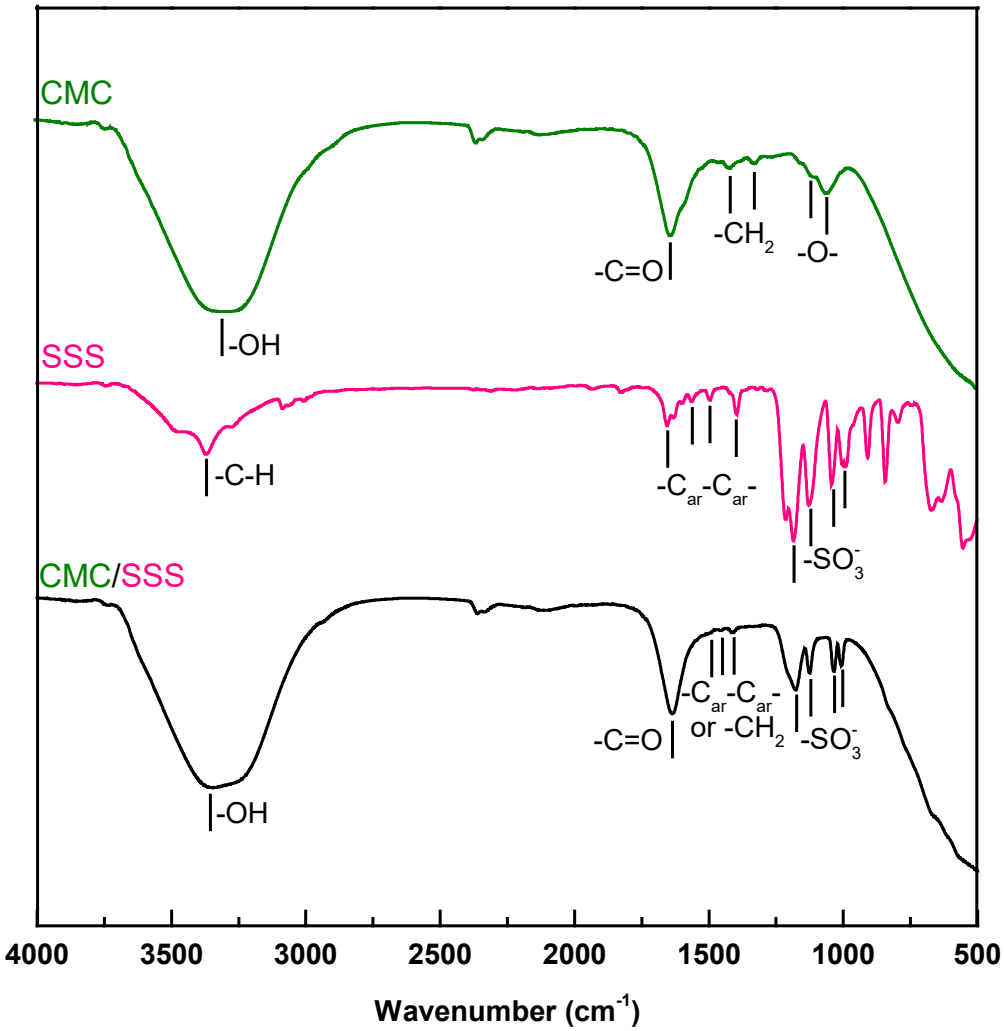

Figure 9. FT-IR of CMC, SSS and CS grafted hydrogel

2. ^{13}C-NMR recorded spectroscopy

The ^{13}C-NMR spectrum of CS is shown in **Figure 10** which includes characteristic peaks of six carbons on glucosamine ring of cellulose: 103.6 (C_1), 81.6 – 74.7 (C_2 – C_5) and 361.41 (C_6) ppm. In addition, the peak at 178.1 ppm is attributed to the carbonyl carbon (C_8) of the anionic group –COO−Na. The signals at 45.0 and 40.6 ppm (C_a and C_b, respectively) come from the SSS-monomer carbon-atoms near by the ether linkage to CMC. Peaks of aromatic carbons of the SSS appear at 148.2 ppm for C_c and, 126.8 ppm for C_d and C_e.

The signal at 141.9 ppm is assigned to the chemical shift for a C_f to a $–SO_3^-$ group. These spectral results demonstrated the appearance of both CMC polymer and SSS monomer in the CS hydrogel, i.e., SSS was sucessfully grafted onto the chain of CMC.

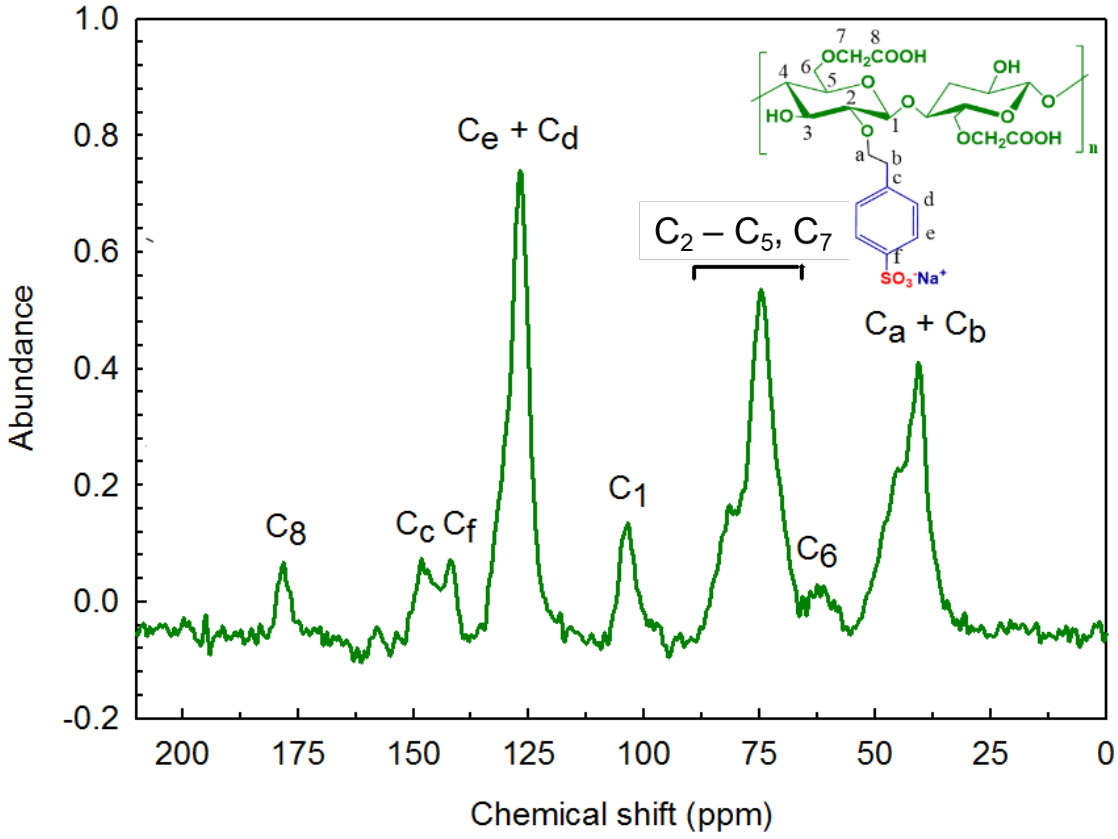

Figure 10. ^{13}C-NMR spectral characterization of CS hydrogel

3. *EDS and SEM*

a. EDS analysis

Results in **Figure 11** by EDS measurement confirmed that the CMC is comprised of only C, O and Na within its network. The total elemental composition by weight showed that C was the most abundant constituent and became less in the order of O and Na. The Pt-signal comes from the coating. The EDS of CS hydrogel in **Figure 11** was employed to further confirm the co-existence of CMC and SSS.

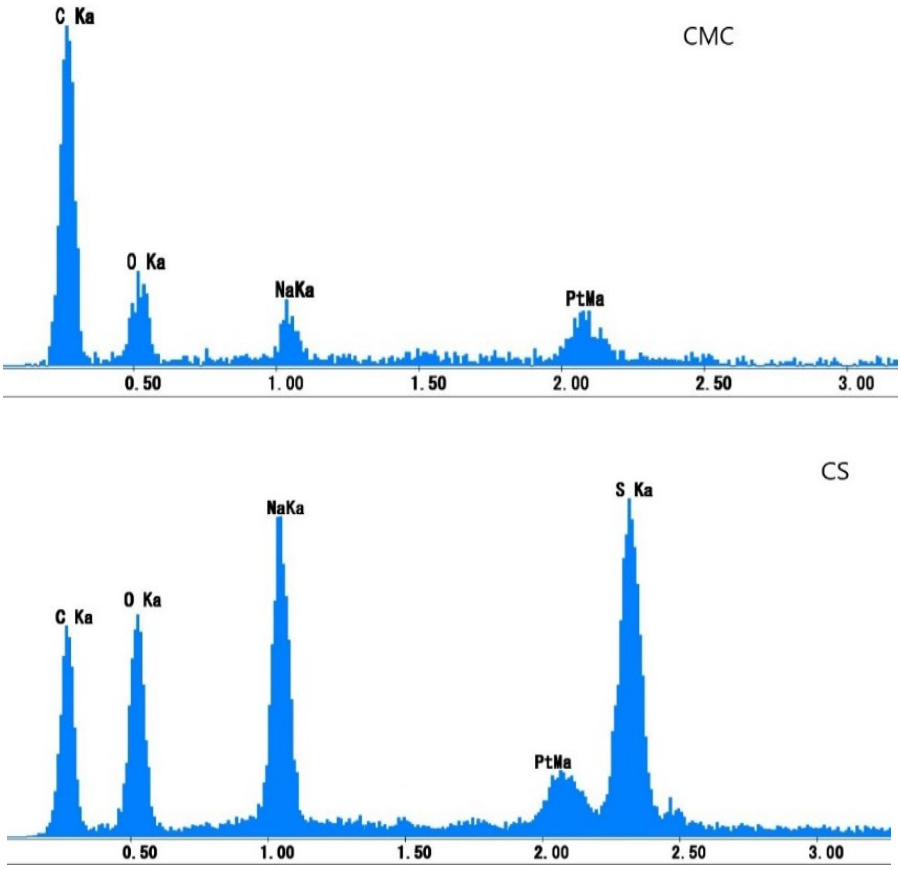

Figure 11. EDS spectroscopy of CMC and CMC/SSS (CS)

b. SEM

For the first type of studied hydrogel, we proceeded SEM examination to comprehend more the information of their surface morphology. As revealed in the SEM image (**Figure 12**), the CMC hydrogel showed a less rough external appearance. After grafting SSS onto CMC matrix, the surface of grafted hydrogel become rougher and has more pores with increasing of SSS amount and reducing of CMC contents. Thus, comparison of these figures demonstrates that grafting process had happened.

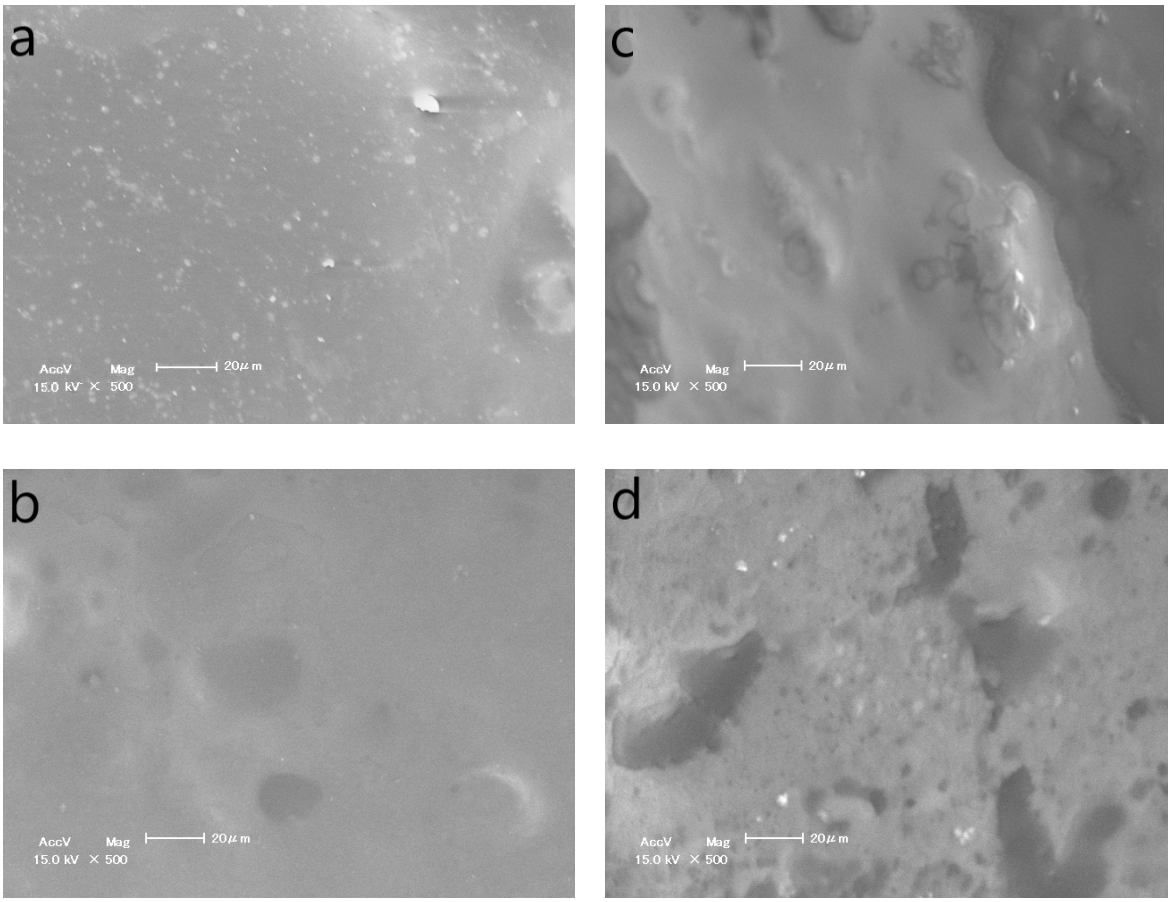

Figure 12. SEM observations of
(a) CMC, (b) CMC:SSS=2:1, (c) CMC:SSS=1:1 and (d) CMC:SSS=1:2 hydrogels.

4. *Other characteristics of prepared hydrogels*

a. *Water uptake measurement*

The swelling ability S_w (hypertonicity) or hydrophilicity of hydrogels is determined by polar functional groups such as hydroxyl (–OH), carboxylic (–COOH), amine ($–CONH_2$) and sulfonate ($–SO_3H$), etc., distributed in the hydrogel matrix [66]. In addition, hydrogel network has cross-linked polymer structures in a three-dimensional (3D) framework. In the swelling process of the hydrogel, there occur two stages including water penetration into the pores of the hydrogel and the expansion of the hydrogel circuit leads to plasticization and increases the volume of the polymer. Actually, it is due to the action of ionic force, Van der Waals force, hydrogen bonding or osmotic pressure, etc. The swelling ability of an absorbent hydrogel is related to its adsorption performance because it allows metal ions interpenertrate into the pores of hydrogels and then favors the binding between ions and active sites. The swell-able characteristic of hydrogel makes its application broader in various areas like wastewater decontamination, agriculture, the food industry, pharmaceuticals and even in hygienic products [67].

Figure 13 shows the dependence of swell ability of grafted hydrogel on SSS amount. The swelling capacity of grafted hydrogel increases with increasing in SSS concentration from 0.0 to 0.8 M and decreasing simutaneously in CMC amount from 0.36 to 0.12 mM . The highest Sw value was found for CS hydrogel with 0.8 M of SSS and 0.12 mM of CMC while the lowest Sw corresponds hydrogel synthesized from CMC only. Due to sulfonate group on SSS is strong hydrophylic group, it links easily with water molcules and expand the hydrogel volume. In contrast with increasing in swelling ability, the gel content was reduced when SSS was added more. It is caused by the gel part might come mainly from CMC polymers and SSS is as grafted part. A similar result has been reported by B. Rivas et al. who studied on co-ordinating of acryamide and SSS to synthesis Hg , Pb, Cd and Zn-adsorbent materials [68].

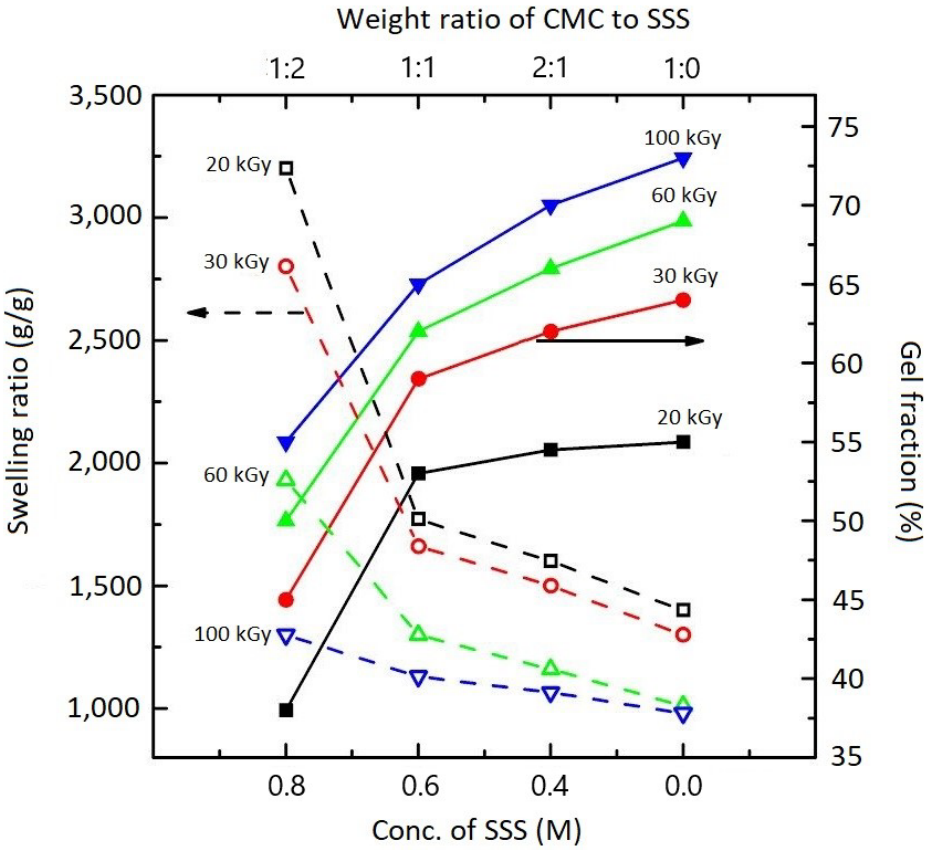

Figure 13. Gel fraction and swelling ratio versus SSS concentration.

b. *Thermo-gravimetric analysis TGA*

TGA of hydrogel enables a description of the massive loss process when it is fired at strictly controlled temperature from 25 up to 600 °C. The TGA analysis diagrams in **Figure 14** show comparison of two stages of mass loss of CMC and CS hydrogels. Firstly, 15 % and 30 % weight loss stage for CMC in the temperature range 17 – 220 °C and CMC in 17 – 415 °C temperature range, respectively corresponding to the evaporation and the de-crosslinking processes. Secondly, the decomposition stage of CMC starts at the range of 220 – 290 °C whereas CS decomposition is at 415 – 440 °C. The TGA graphs also show although both CMC and CS were dried at 50 °C during 24 hrs, in the vacuum oven, CS hydrogel still has much bounding water due to its stronger hydrophilicity. **Figure 14** also displays the temperature decomposition of CMC hydrogel is much lower than temperature decomposition of this grafted CS hydrogel.

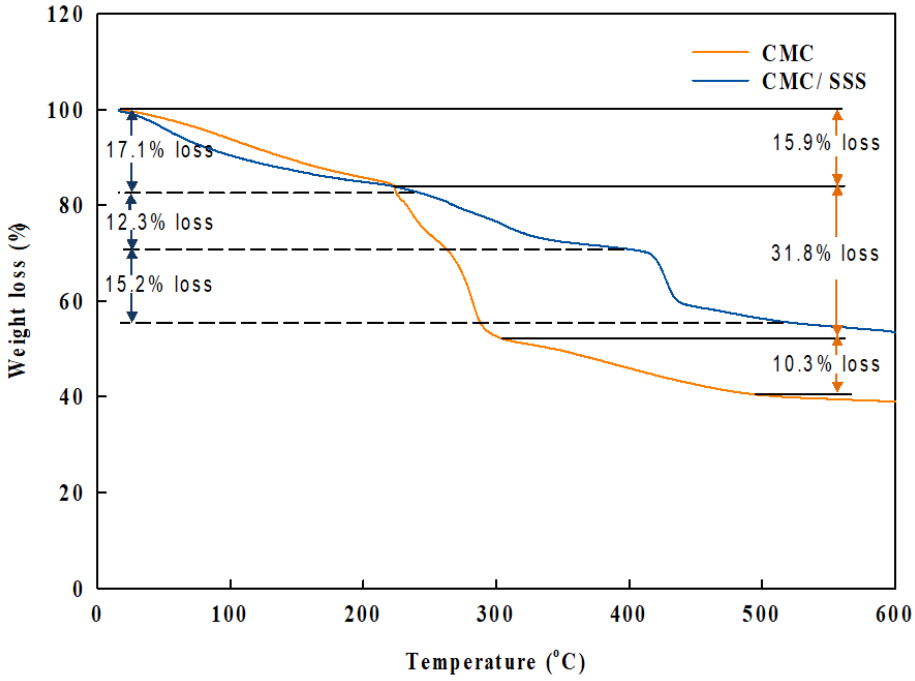

Figure 14. TGA profile of CMC and CS.

III. Metal ion adsorption performance of CS hydrogel

The modified CMC hydrogel performance was analyzed according to adsorption experimental designs described in Chap.2-Sec.V.

Batch adsorption experiments were done with a known weight of hydrogel adsorbent was immerced into concentrated analyte solutions in closed PP tubes at 25°C. The grafted CS gel with 0.5×0.5×0.5-cm-size (0.200 g) was dipped into 40 mL of solution containing different initial concentration of metal ions shown in **Table 11** for 24hrs. The pH was adjusted in the range 1–7 by 0.5 M-KOH and/or 0.5 M-HNO_3 solutions. The remaining metal ions in aqueous solution were determined by ICP-MS method, (Agilent 7700x Instrument, Japan).

1. *Effect of hydrogel composition*

During synthesis, the ratios of CMC and SSS were changed in order to examine whether the CS hydrogel can capture heavy metal ions through the ion exchange ability of the sulfonate group of SSS. Adsorption performance was tested against solution containing various ions of Pb, Cu, Zn, Cd, U, Cr, Mo, Mn, Fe and Ni in a batch adsorption experiment with the 100-time-diluted initial concentration as in **Table 11**. The measured pH value was 5.

As can be seen in **Figure 15**, a clear metal-ion-uptake dependence on CMC:SSS ratios was confirmed. The extraction percentage of metal ions increase with decreasing the weight ratio of CMC and increasing SSS amount. The CS gels with the ratio of 1:2 showed higher metal % removals at equilibrium, Mn (35.2 %), Pb (41.4 %), Cr (68.0 %) and Fe (33.5 %), compared with those of CMC hydrogels, 12.3, 27.0, 31.9 and 17.9 %, respectively. The CS hydrogel did not show particularly high selectivity to metal ions except for Cr (III), indicating the adsorption resulted from the electrostatic attraction; the most highly positive-charged Cr (III) ions can interact effectively with the negative –SO_3^- and –COO^- groups. In the similar way, the higher metal-adsorption capacity of the CS hydrogel than the CMC adsorbent can be explained because the former contains highly active –SO_3^- ($pK_a < 1$) groups in addition to –COO^- (pK_a ~4 – 5) groups whereas the latter, only –COO^- groups [69]. Another reason for the higher performance of the CS hydrogels than the CMC hydrogel is the CS hydrogel's higher swelling ability, which induces the easier diffuse of the metal ions in the CS hydrogel.

Table 11. Initial concentration of metal ions (µg/L).

Metal	Pb^{2+}	Cu^{2+}	Zn^{2+}	Cd^{2+}	U^{5+}	Cr^{3+}	Mo^{3+}	Mn^{2+}	Fe^{2+}	Ni^{2+}
Stock conc. (µg/L)	1,000	10,000	10,000	300	200	5000	7,000	5,000	30,000	1,000
200-time-diluted conc. (µg/L)	5	50	50	1.5	1	25	35	25	150	5
150-time-diluted conc. (µg/L)	6.7	67	67	2	1.3	33	47	33	200	6.7
100-time-diluted Conc. (µg/L)	10	100	100	3	2	50	70	50	300	10
50-time-diluted Conc. (µg/L)	20	200	200	6	4	100	140	100	600	20
25-time-diluted Conc. (µg/L)	40	400	400	12	8	200	280	200	1,200	40

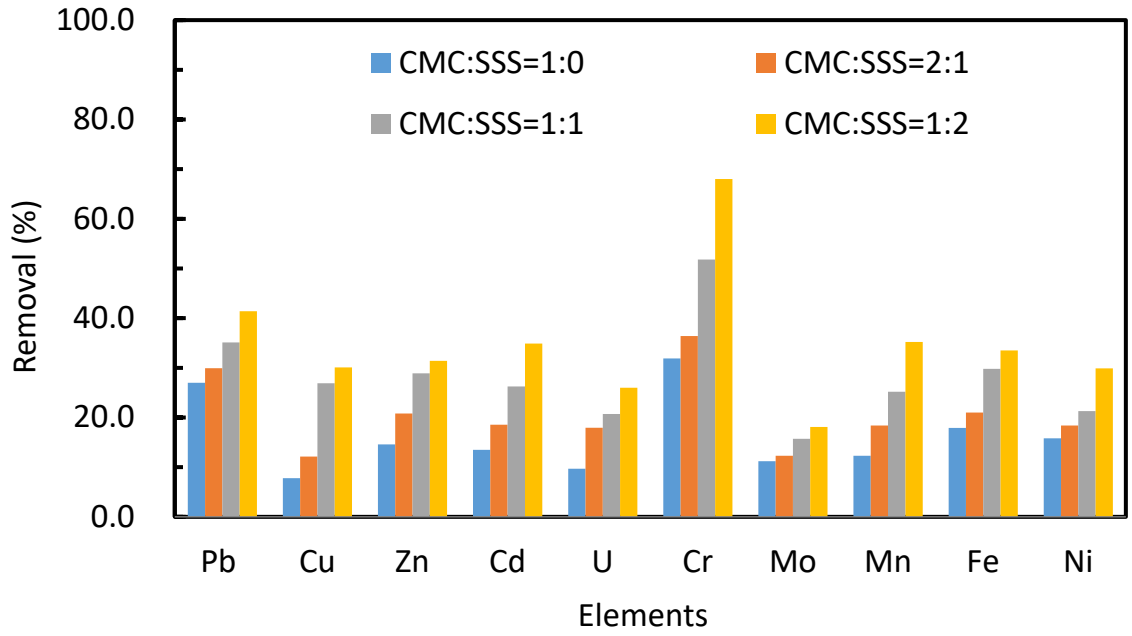

Figure 15. Dependance of the removal percentage for various metals on hydrogel composition at pH = 5.

2. *Effect of adsorbate solution pH*

Figure 16 illustrates the strong effect of pH of original metal ion solution on CS hydrogel's adsorption performance. All data show the best of the adsorption occurring over a pH range from 2 to 5. In this pH range (or adsorption edge), the functional groups are deprotonated and are free to bind with metal ions [70]. When moving pH to higher value > 5, the adsorption capacity is increased. This is caused from precipitation of metal ions and the mobility of the metal ions in solution was decreased in base media. These features have been mentioned as behaviors of metal ion adsorption in several previous adsorption studies and pH 5 was chosen to be the suitable pH for next studies.

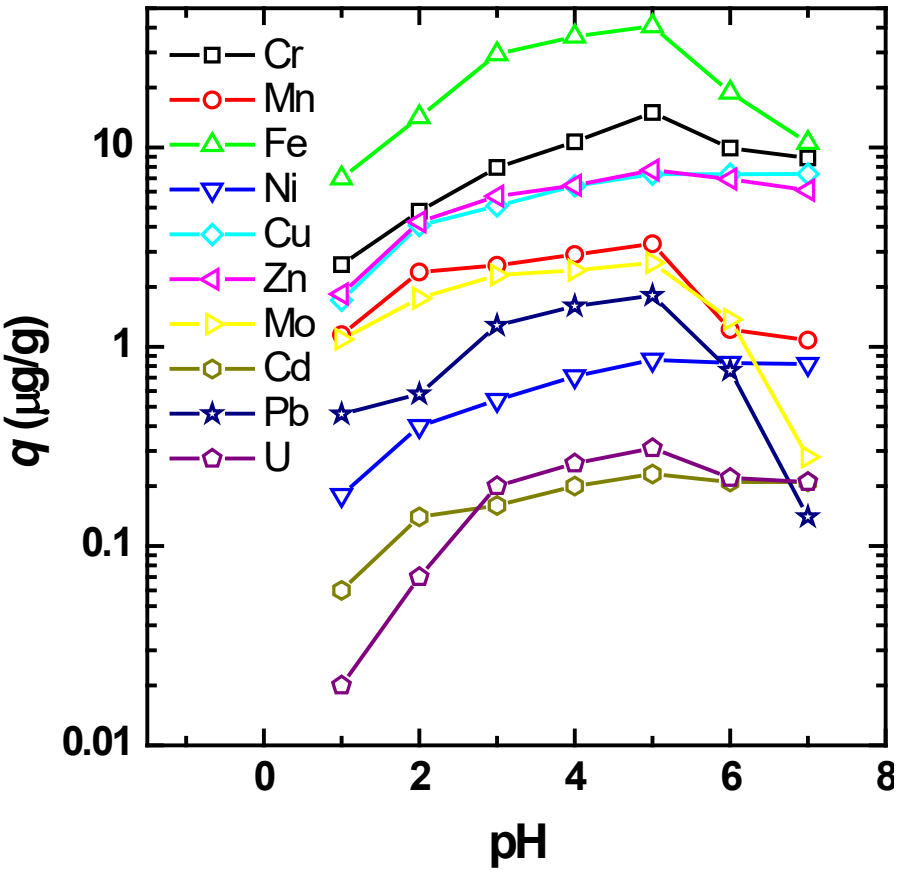

Figure 16. pH solution effect on the adsorption capacity of CS hydrogel for multi-elements.

3. *Kinetic study*

The kinetic of metal ion adsorption of CS hydrogels was studied at initial pH ~5 and initial concentration for each type of ions displayed in **Table 11**. The data in **Figure 17** indicated adsorption occurred quickly during 600 mins., and reached a maximum around 1560 mins., after then became almost constant up to 2880 mins. Commonly, adsorption involves three processes. The initial process is a rapid reaction happened on the surface. The next process is slow adsorption when available surface-adsorption-sites are decreases gradually. The last process is the slow pore-diffusion of metal ions into the polymer matrix [Chap.1-Sec.II-4.d, [Chap.1-Sec.II-4.d, [47]].

To elucidate the adsorption kinetics of an adsorbents at fixed concentration, two commonly kinetic models in which the pseudo-first order (**Eq. 6**) and pseudo-second order (**Eq. 7**) kinetic models were used [Chap.1-Sec.II-4.d,[45]].

$$\frac{\mathrm{d}q_t}{\mathrm{d}t} = k_1(q_e - q_t)\,, \qquad \textbf{Eq. 6}$$

$$\frac{\mathrm{d}q_t}{\mathrm{d}t} = k_2(q_e - q_t)^2\,, \qquad \textbf{Eq. 7}$$

where q_t and q_e (µg/g) are the weights (µg) of adsorbed-metal ions per gram of adsorbent at a time t and at equilibrium time (min.), respectively and k_1, k_2 are the rate constants of adsorption.

The kinetic results of adsorption were examined by both of the pseudo-first-order and the pseudo-second-order models as shown in **Figure 17** and **Table 12**. From the better fitting-correlation-coefficient (R^2), the pseudo-second-order kinetic model can be adopted to interpret the metal adsorption on the CS hydrogel. In addition, the q_{cal} values derived from the fitting utilizing the pseudo-second-order kinetic model show good agreement with the experimental q_{ex}'s. These results suggested that the pseudo-second-order model describe well the adsorption process. The adsorption rates of CS hydrogels for metal ions were probably controlled by the chemical process, i.e., the chemisorption involving valence forces through sharing or exchange of electrons between adsorbent and adsorbate, not the physisorption [71]. In fact, SSS and CMC have strongly active $–SO_3^-$ and $–COO^-$ groups, respectively. So the metal ion could be absorbed by interaction with $–SO_3^-$ and $–COO^-$ groups of CS hydrogel.

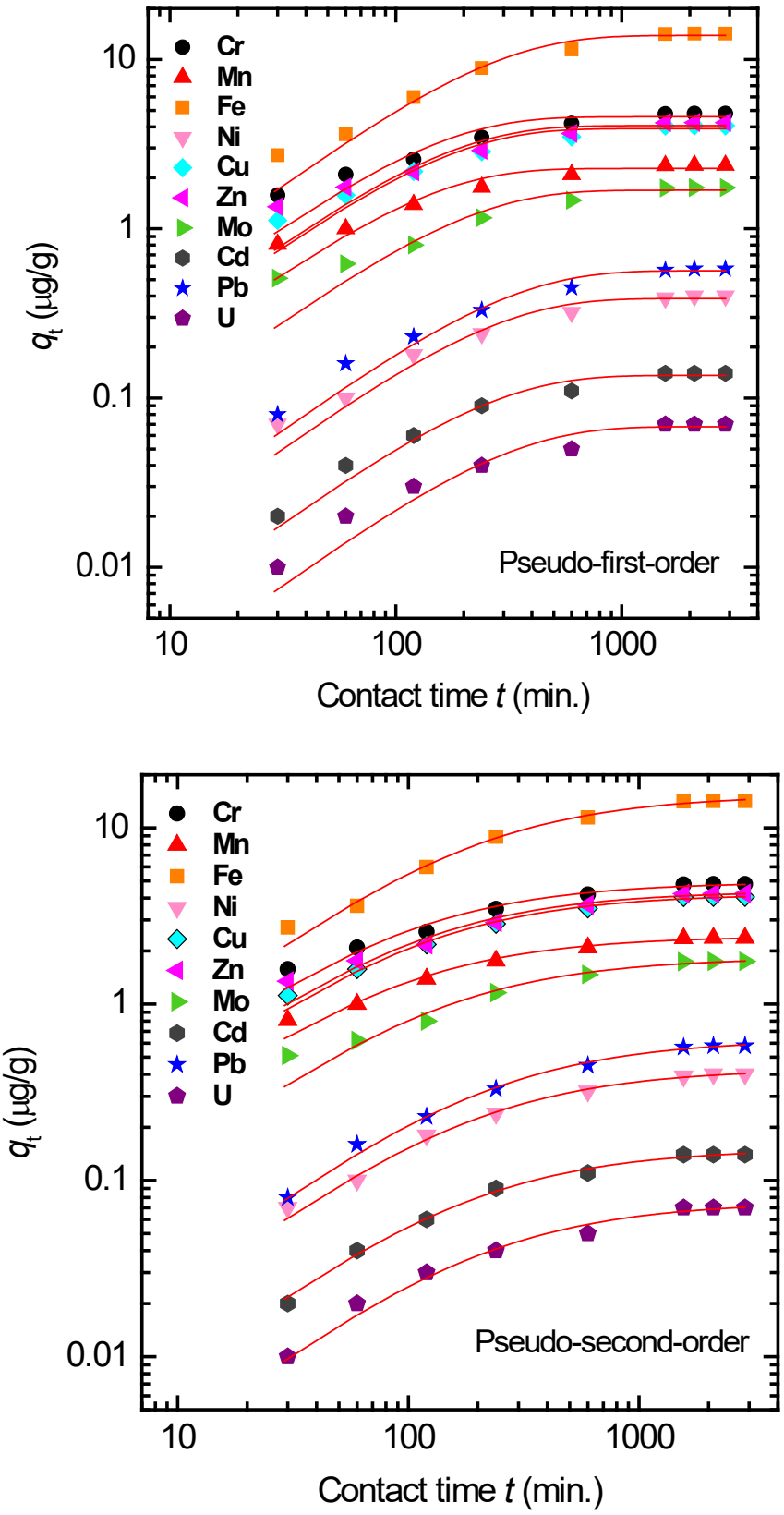

Figure 17. Kinetic studies for adsorption capacity of CS hydrogels.

Table 12. Calculated kinetic results of metal adsorption by CS hydrogel adsorbent.

Metal	Pseudo-1st-order model				Pseudo-2nd-order model		
	q_{cal} (µg/g)	k_1(1/min)	R^2	q_{ex}(µg/g)	q_{cal}(µg/g)	k_2 (g/[µg min])	R^2
Cr	14.3	0.0080	0.968	14.97	15.4	0.0007	0.996
Mn	3.17	0.0044	0.976	3.29	3.51	0.0016	0.996
Fe	38.8	0.0086	0.964	40.65	41.7	0.0003	0.995
Ni	0.81	0.0058	0.981	0.86	0.90	0.0084	0.998
Cu	7.18	0.0035	0.983	7.34	8.01	0.0005	0.996
Zn	7.55	0.0035	0.981	7.71	8.48	0.0005	0.986
Mo	2.54	0.0054	0.976	2.64	2.78	0.0026	0.988
Cd	0.22	0.0053	0.983	0.23	0.24	0.0278	0.999
Pb	1.70	0.0110	0.951	1.81	1.82	0.0087	0.993
U	0.29	0.0067	0.980	0.31	0.32	0.0285	0.997

4. *Equilibrium isotherms*

In order to evaluate the adsorption capacity of CS hydrogel for metal ions in solution, equlibrium isotherm experiments were carried out. Among many isotherm models, the two-parameter Langmuir and Freundlich models in non-linear form were employed due to their simplicity and easy interpretability [45][72]. Initial concentration of metal ions for this experiment is in **Table 11**.

The Langmuir isotherm is used to approximately calculate the maximum adsorption capacity of CS hydrogel according to **Eq. 3** [Chap.1-Sec.II-4.c, [46]]:

$$q_e = \frac{q_{\max} K_L C_e}{1 + K_L C_e}, \qquad \textbf{Eq. 3}$$

where

C_e: the equilibrium concentration of adsorbate (µg/L),

q_e: the adsorbed-metal weight (µg) per gram of adsorbent at equilibrium (µg/g),

K_L: Langmuir isotherm constant (L/µg),

q_{max}: the maximum monolayer coverage of metal ion capacity (µg/g).

The Freundlich model is used to describe the adsorption process and the inhomogeneous surface of adsorbent materials by **Eq. 4** [Chap.1-Sec.II-4.c, [46]]:

$$q_e = K_F C_e^{\frac{1}{n}}, \qquad \textbf{Eq. 4}$$

where

K_F : Freundlich constants (µg/g),

C_e : the equilibrium concentration (µg/L),

n: empirical parameter.

The metal ion uptake increased with elevating initial metal-ion concentrations (**Figure 18**). The fitting of experimental data by both of the Langmuir and Freundlich models in **Figure 18** suggests that a mono-layer adsorption of multi-elements on the CS hydrogel surface is appropriate to describe this phenomenon.

The Langmuir constant K_L or the adsorption equilibrium constant, which is found to be a maximum for U (0.723 L/µg [**Table 13**]) in the case of CS hydrogels, is related to the adsorption energy and the affinity of the binding sites. Therefore, the higher binding energy for U than those for others in the experiments was ascribed to the strongest electrostatic interaction between U and adsorbent. As given in **Table 13**, the highest monolayer capacity (q_{max}) of the CS adsorbent for high capturing of Fe^{2+}, Zn^{2+} and Cr^{3+} were found to be 79.8, 30.3 and 36.7 µg/g, respectively. This priority could be resulted from higher initial concentration. Similar trends are reported by Jin Joo et al. which studied removal of multi-elements from wastewater by spherical chitosan/gelatin hydrogel particles [73].

Table 13. Caculated Langmuir and Freundlich parameters for metal adsorption by CS hydrogels.

Metal	Langmuir isotherm			Freundlich isotherm		
	q_{max} (µg/g)	K_L (L/µg)	R^2	K_F (µg/g)	n	R^2
Cr	36.7	0.0140	0.970	2.28	2.12	0.899
Mn	8.78	0.0198	0.966	0.702	2.25	0.888
Fe	79.8	0.0054	0.990	6.162	2.86	0.913
Ni	2.67	0.0694	0.975	0.305	1.91	0.916
Cu	25.2	0.0061	0.986	0.707	1.82	0.940
Zn	30.3	0.0052	0.981	0.659	1.71	0.937
Mo	7.19	0.0107	0.976	0.382	2.09	0.918
Cd	0.42	0.577	0.989	0.168	2.98	0. 896
Pb	3.60	0.151	0.984	0.842	2.69	0.890
U	0.58	0.723	0.995	0.2515	2.79	0.930

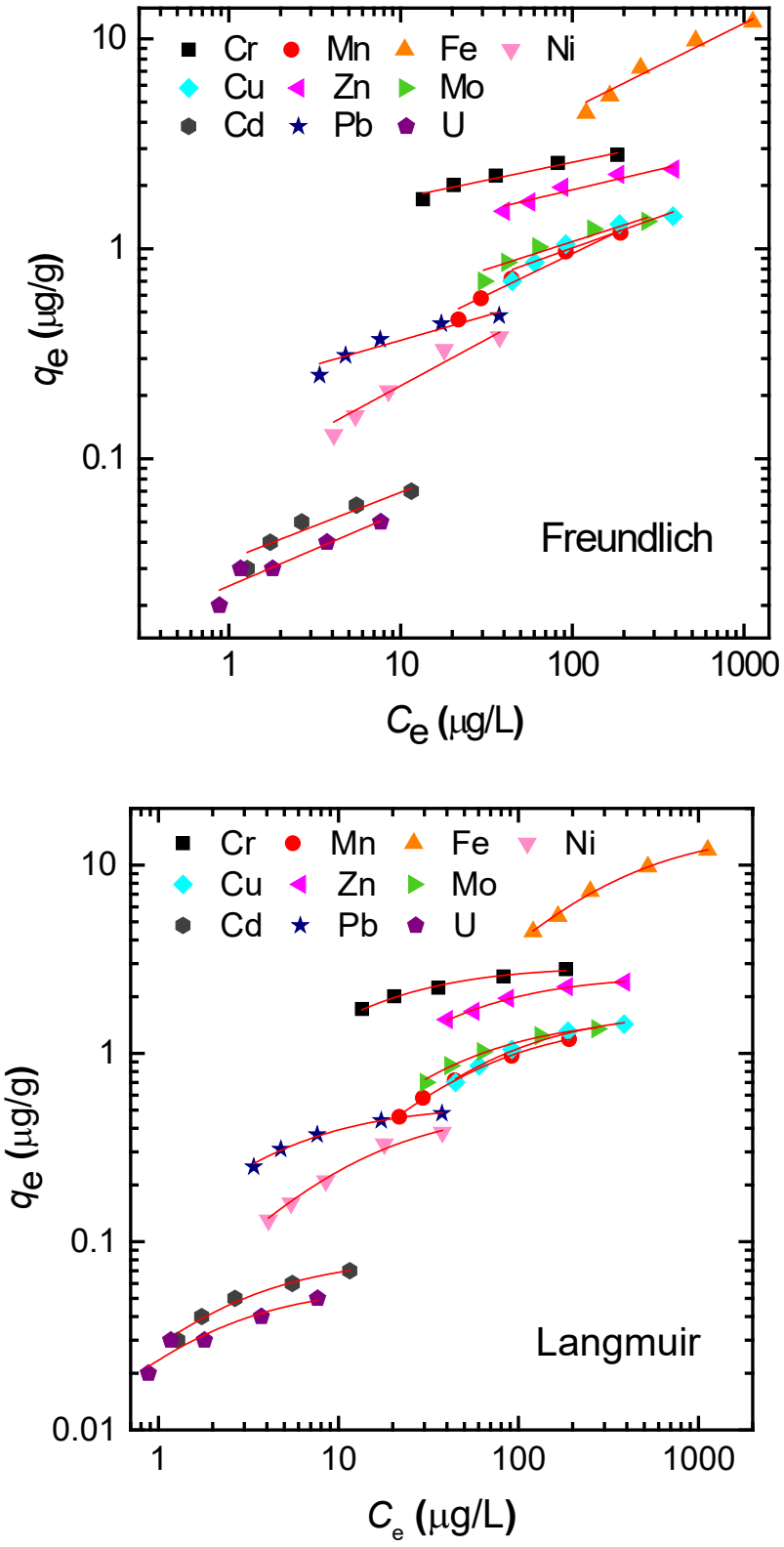

Figure 18. Freundlich and Langmuir isotherm fitting curves for metal ions adsorption by CS hydrogel.

5. *Desorption metal ions from CS adsorbent and reusability*

What happens to adsorbent after its use in water treatment process? This is an important question when developing new adsorbent materials, for example biomaterials, etc. If the metal-loaded hydrogel is released to environment, it may have some negative influences on humans and ecology. For the first type of hydrogel in this study, we also discussed about its reusability. Hara et al. [74] found that the majority of the adsorption processes are physical processes. So that spent hydrogel can be regenerated after most desorption in acidic media. This is a simple and quite cheap process. In studying metal desorption from the hydrogel matrix, the adsorbent was immersed into a small volume nitric acid 0.5 M to recover of the main adsorbed metal and regenerate the adsorbent for re-use. Since CS hydrogel was a fragile material with weak connections between the network-polymer chains, some of the surface parts will be easily disintegrated into small pieces and dispersed in the water on swelling during washing in deionized water, which caused decrease in the recoverable metal-amount through decrease in the remaining-portion volume as shown in **Figure 19**; considerable decease was observed after only 2 cycles of adsorption-desorption process.

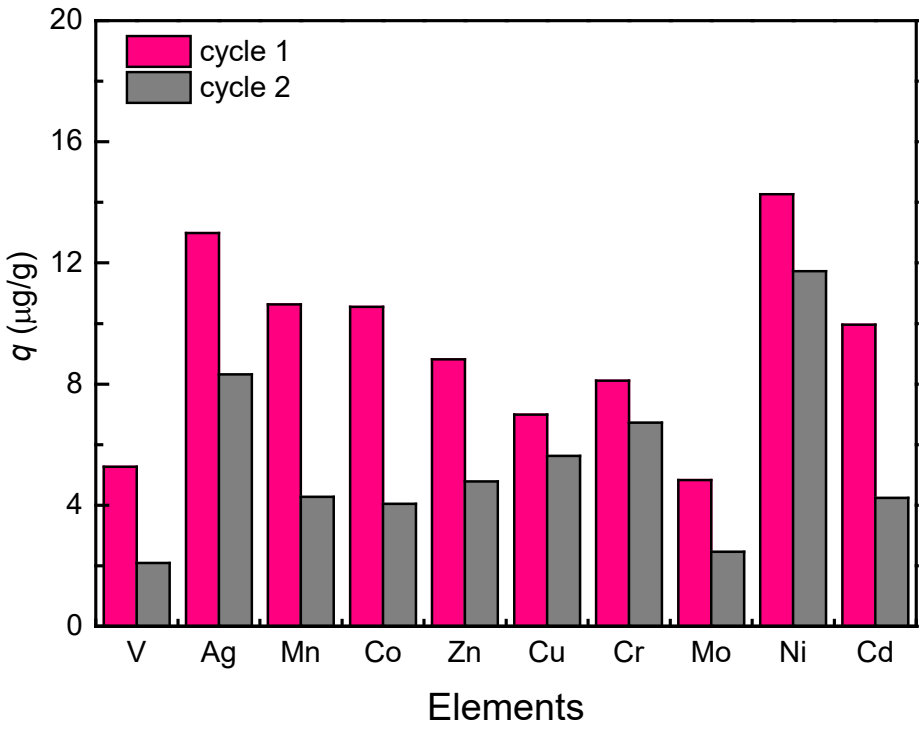

Figure 19. Regeneration of CS hydrogel.

IV. Conclusion

One of the shortest ways to make the human body susceptible to heavy metal poisoning is eating and drinking metal residues in contaminated food and water. This becomes a noticeable and serious problem for the health of humans, especially for people living in the areas where dirty sewage without the proper treatment leaks from factories and industrial zones. Even though there are well established solutions for capturing heavy metal ions in aquatic environment, their usage is usually limited by cost. Hence, there exists a need to develop an efficient, cost-effective and eco-friendly method for the heavy metal removal from industrial waste fluids. In the present chapter, we recommend a novel method of using radiation induced grafted hydrogel type from CMC and SSS to remove heavy metals in water. The main highlight of this primary experiment is the utilization of only the monomers/polymers and water to attain gelation with gamma irradiation. We successfully demonstrated a possibility to achieve the multi-element adsorption by a kind of adsorbent. The results also revealed the effectiveness of grafting active sites like $–SO_3^-$sulfonate groups onto adsorbent structure for promoting pollutant adsorbing functionality. In the experiment described in the present section, the CS hydrogel with 1:2 of CMC:SSS ratio showed highest functionality for the metal removal (**Figure 15**). However, a difficulty for practical use was also revealed, inability in the repetitive use, for example, the metal adsorption capacity of the CS-1:2-hydrogel decreased considerably after 2 cycles of the adsorption-desorption iteration (**Figure 19**).

The limitation of the repetitive use came from the CS hydrogel's insufficiency in the mechanical strength enduring the large volume change during the regeneration treatment. In this situation, the hydrogel adsorbent with high strength was noticed as an important material, because the reuse of the adsorbent is indispensable from the view point of the practical use in environment-friendly and economic conditions. Along the lines, the development of the CMC-based hydrogel with higher strength became a guide to the new research for more practical CMC-based hydrogel-adsorbent, which will be described in the following chapters.

CHAPTER 4

ENHANCING REUSABILITY OF SSS-GRAFTED CMC-HYDROGEL

Following the previous chapter, we designed and fabricated a CS hydrogel which had higher mechanical strength by increasing crosslinking points inside CMC hydrogel matrix as in such scientific papers [22][75], which is described in this chapter. Method for increasing hydrogel strength was characterized by the blend of CMC polymer and SSS monomer with another monomer (Bis[2-(Methacryloyloxy)Ethyl] Phosphate, abbreviated as BMEP) adopted as a cross-linker.

In the experiment described in the present chapter, we used BMEP, a phosphate ester well known as a reinforcer, in order to strengthen the CMC-based hydrogel matrix for the purpose improving reusability as well as the high metal-adsorption capacity. BMEP has been known to have hydrogen-bond forming functionality and high affinities for various metal ions [76], which meet the several conditions necessary for the application for improving environmental problems. In additions, BMEP's hydrolyability and bio-degradability can promote the water uptake ability of hydrogel in basic media [77]. Moreover, the BMEP-cross-linked hydrogels are also reported to capture bacteria as well as absorbing metal ions [78]. With these promising properties, the author determined to adopt BMEP as an additional cross-linker expecting both of reinforcement of the CS hydrogel's network and promotion of the metal-ion adsorption-capacities for resolving the problem revealed in the previous chapter: inability of the repetitive use of the CS hydrogel adsorbent.

As was done in the experiments described in the previous chapter, gamma irradiation was also utilized to form the network and to graft SSS and BMEP to CMC glucose. As described in the preceding chapters, the gamma irradiation method has advantage over ordinal chemical methods to produce the modified CMC hydrogel from the viewpoint of unnecessity of toxic chemical initiator-agent and of production at room temperature, by which the final products are very pure and sterile [51].

I. Reinforcing of SSS-grafted-CMC hydrogel network (abbreviated as CSB hydrogel)

In the process of grafting of BMEP to CMC network, two vinyl groups of BMEP react with CMC polymer chains during the chain propagation, which forms another type of cross-linked structure in addition to those formed by plural CMC-polymers. As was depicted in the preceding chapter, the unsaturated $–CH=CH_2$ group of SSS can be also grafted on CMC network. All of above-mentioned reactions were initiated at the same time by species of e_{aq}^-, $HO^\bullet$, $H^\bullet$, $H_2O^{\bullet+}$ radicals from H_2O under gamma irradiation process [52]. As a result, hydrogels (abbreviated as CSB hydrogel) with rigid and complicated structure was estimated to be constructed, as shown in **Scheme 5**.

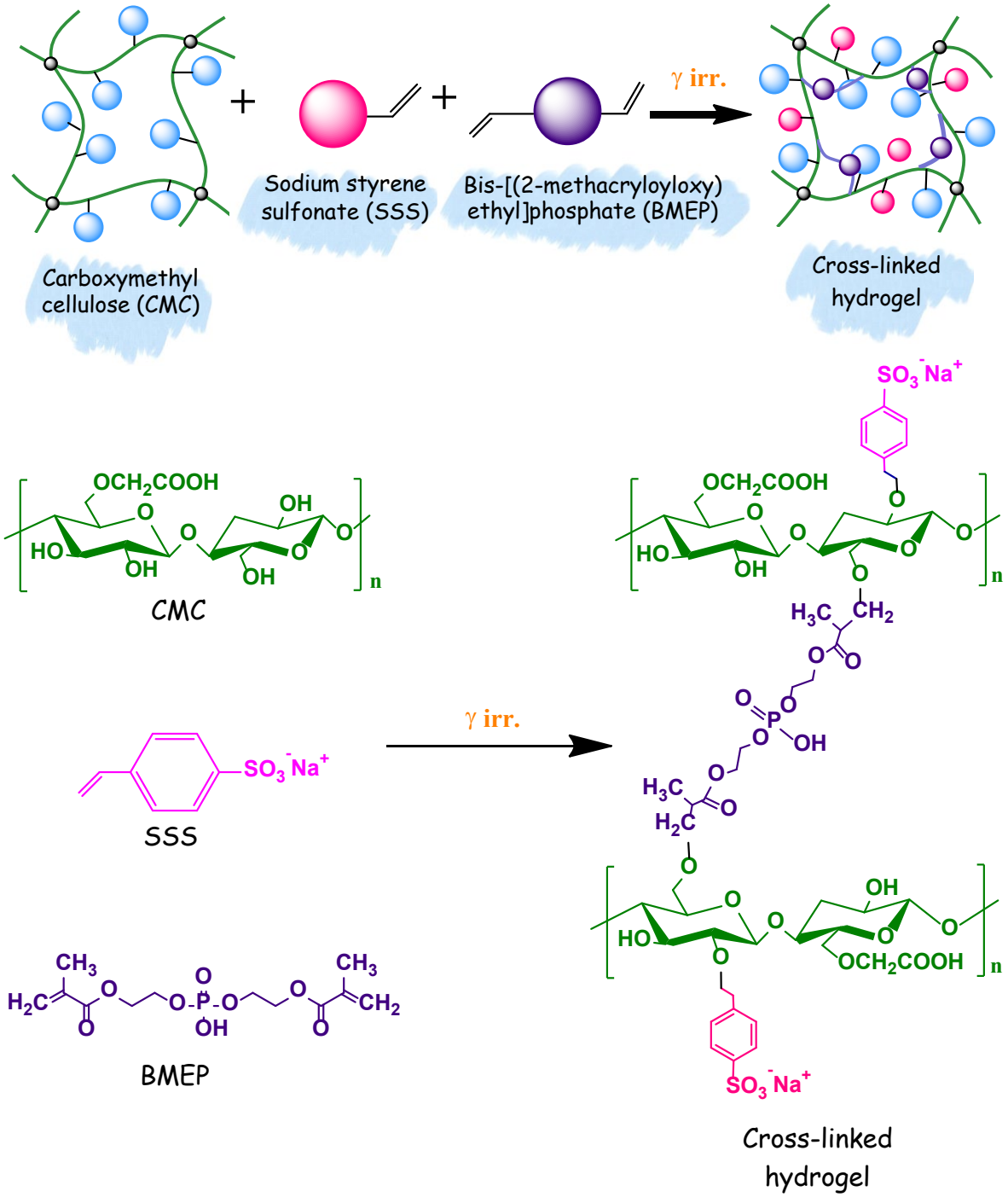

Scheme 5. Proposed associate structure of CMC, SSS and BMEP in prepared hydrogel.

II. Characterization of CSB hydrogel

1. *FT-IR spectra analysis*

Figure 20 presents the FT-IR spectra of all components in the CSB hydrogel. Firstly, the CMC spectrum shows a strong peak at 1657 cm^{-1} ascribed to –C=O of acid or ester (stretching vibrations). The typical signal at 1068 cm^{-1} due to secondary alcohol C–OH (the stretching vibration) [79].

The SSS network has been demonstrated by the characteristic peaks at 1403, 1537 and 1655 cm^{-1} for the aromatic ring ($–C_{ar}–C_{ar}$ bonds). Intense peaks of stretching vibrations at 992 and 1042 cm^{-1} are typical of symmetric S=O, but this region is also dominated by –P=O and P–O–C of phosphonate group which resonate with these wavenumbers [77]. Additional peaks at 1240 and 1410 cm^{-1} are for asymmetric –S–O in $-SO_3Na$ group [79].

Nevertheless, from the spectral findings of CSB hydrogel, new vibrational bands emerged at wavenumbers at 1002, 1052, 1145 and 1189 cm^{-1}. Appearance of these new bands seemed attributed to replacement of the secondary alcohol C–OH group with sulfonate group of SSS and the characteristic stretching vibrational bands at 987 and 1161 cm^{-1} of phosphonate group could not be identified. On the result, the author considered that the phosphonate-group peaks might not be distinguished by the intense stretching vibrational bands of $–SO_3^-$ groups in the same spectral region, which would be attributed to much higher SSS concentration (800 mM) than that of BMEP (2.6 – 12.9 mM) in the present CSB hydrogel. Therefore, they carried out an additional measurement intended to make clear the existence of the BMEP-crosslink between CMC macro-molecules by producing the hydrogel only composed of CMC and BMEP by gamma irradiation method (abbreviated as CB hydrogel). As observed in the spectrum of the derived CB hydrogel (**Figure 20**), confirmed were the existence of characteristic stretching vibrations corresponding to P–O–C and P=O at 1030 and 1126 cm^{-1}, respectively.

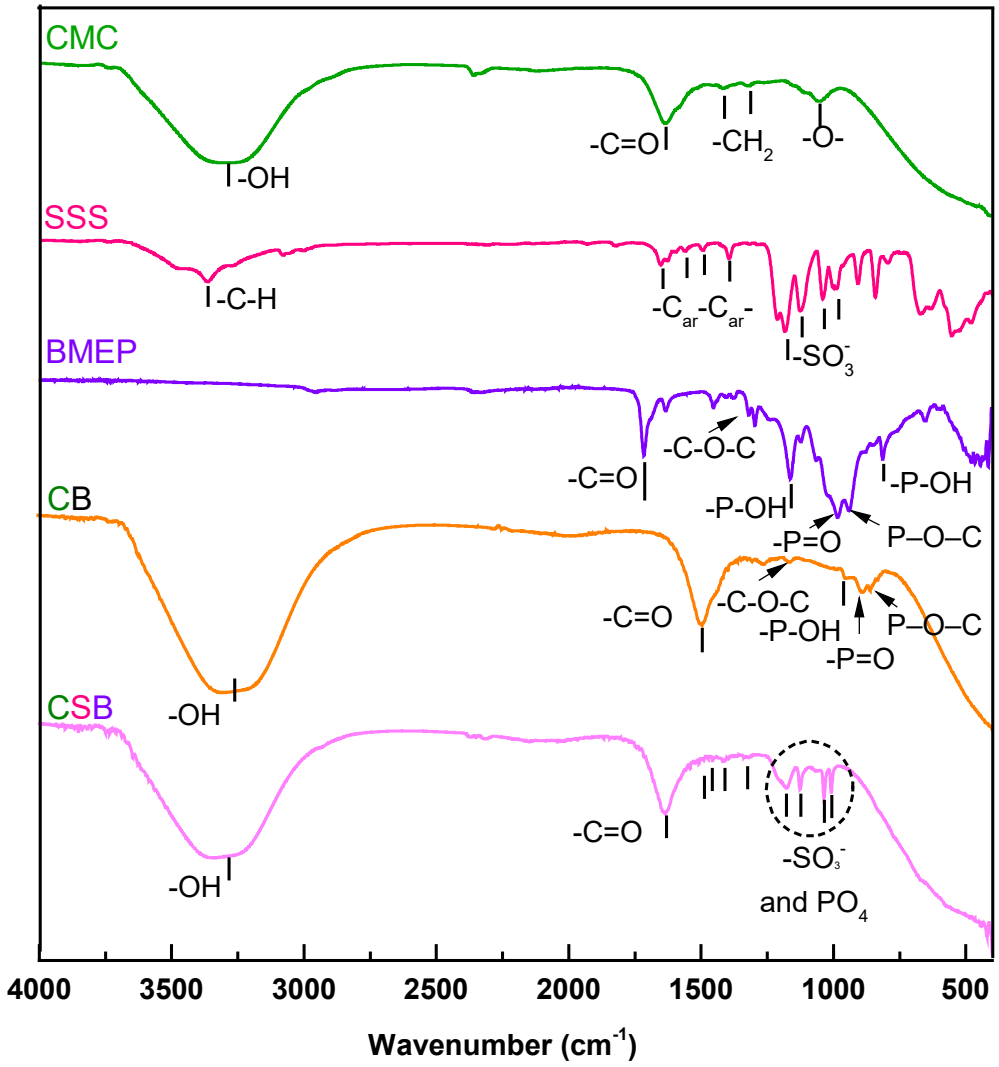

Figure 20. FT-IR spectra records of pure materials (CMC, SSS, BMEP) and CMC/SSS/BMEP (CSB) hydrogel.

2. *^{13}C-NMR Nuclear magnetic resonance spectroscopy*

^{13}C analysis was also performed for CSB hydrogel, of which the observed spectrum is in **Figure 21**. The sets ascribed to carbon–carbon linkage ([C_b, $C_{2'}$, $C_{3'}$]) and those to carbons with oxygen single bond (C_a, [$C_{1'}$, $C_{5'}$, $C_{6'}$], [C_6, C_7]) were identified (0 – 80 ppm) in the measurement. The signal at 110 ppm is attributed to carbon–double oxygen (C_1) and the intense peak at around 74 ppm comes from the carbon–carbon connection in glucose rings (C_2 – C_5). The resonated carbons in the aromatic ring of SSS, [C_d, C_e], C_f, and C_c are at 127, 142 and 149 ppm of chemical shifts, respectively. The chemical shifts at 160 – 185 ppm usually agree with the sp^2 hybridization and the de-shielding influence of the C=O in either carboxylic acid ([C_8, $C_{4'}$]) or an ester group.

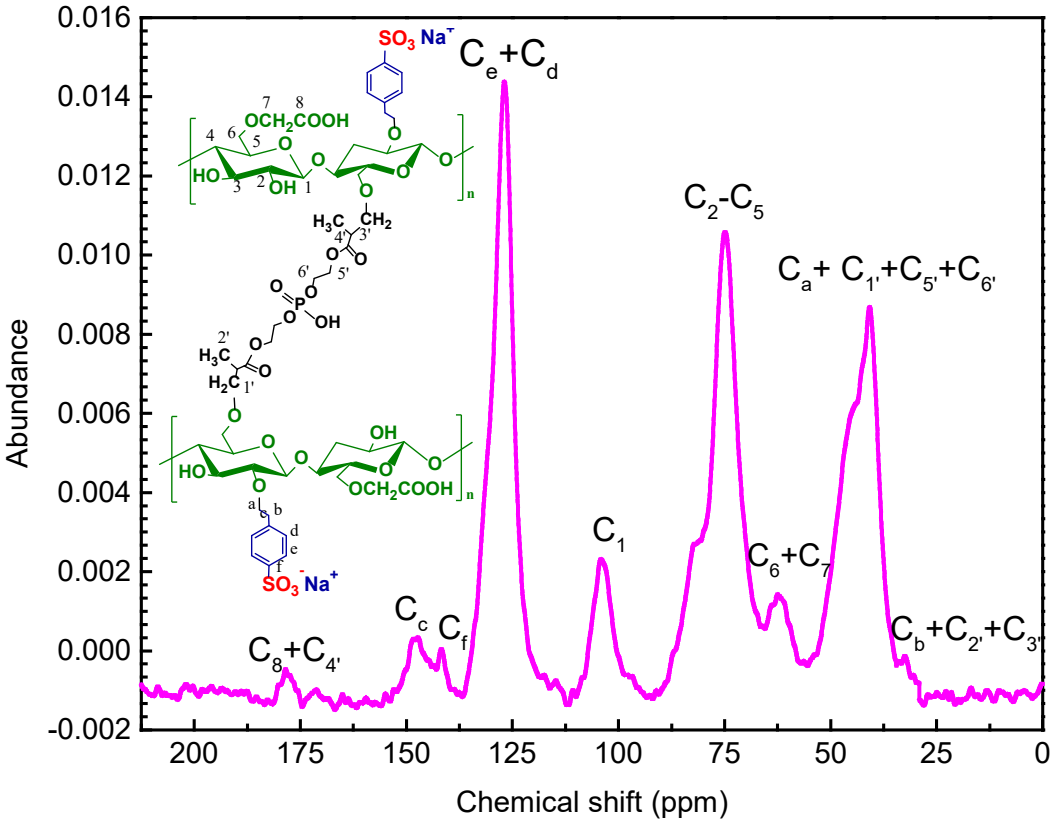

Figure 21. ^{13}C-NMR analysis of CSB hydrogel.

3. *EDS and SEM*

a. EDS analysis

In order to examine the net amount of BMEP incorporated into CSB hydrogel, EDS measurement was carried out by adopting CSB 2.6 hydrogel as a specimen (containing the lowest concentration, 2.6 mM of BMEP, **Table 8**) taking into account of EDS detector's high sensitivity to recognize many chemical elements, in addition, a control experiment was also performed for CSB 0.0 (without BMEP, **Table 8**). The detected elemental data inside the CSB hydrogel after the analyses are illustrated in **Figure 22**.

The element analysis spectrum certifies the existence of BMEP-origin phosphorus element in CSB hydrogel, in addition to C, O, Na and S. This result demonstrates that BMEP successfully cross-linked CMC polymers. As presented in **Figure 22**, one of the notable results was revealing quantitative amounts of C, O, Na, S and P in both CSB 0.0 and CSB 2.6 samples, of which the results confirmed that the CSB 2.6 hydrogel comprised P in contrast to CSB 0.0. The total elemental composition by weight showed that the content of C increased from 43.59 % to 49.88 % after BMEP introduction whereas the O and Na content decreased a little indicating the replacement of $–CH_2COO$-Na groups with BMEP-reinforcer. The contents of S were almost equal between CSB 0.0 and CSB 2.6 hydrogels, which confirms that introducing BMEP did not affect on the grafting SSS process onto CMC. Due to adding too small BMEP weight of 0.02 g, compared with other weight of CMC (2.00 g) and SSS (4.00 g) during CSB hydrogel synthesis, the P weight percentage on the CSB 2.6 was only 3.38 %. The EDS analysis results clearly demonstrated the simultaneous presence of CMC, SSS and BMEP inside of the final CSB hydrogel.

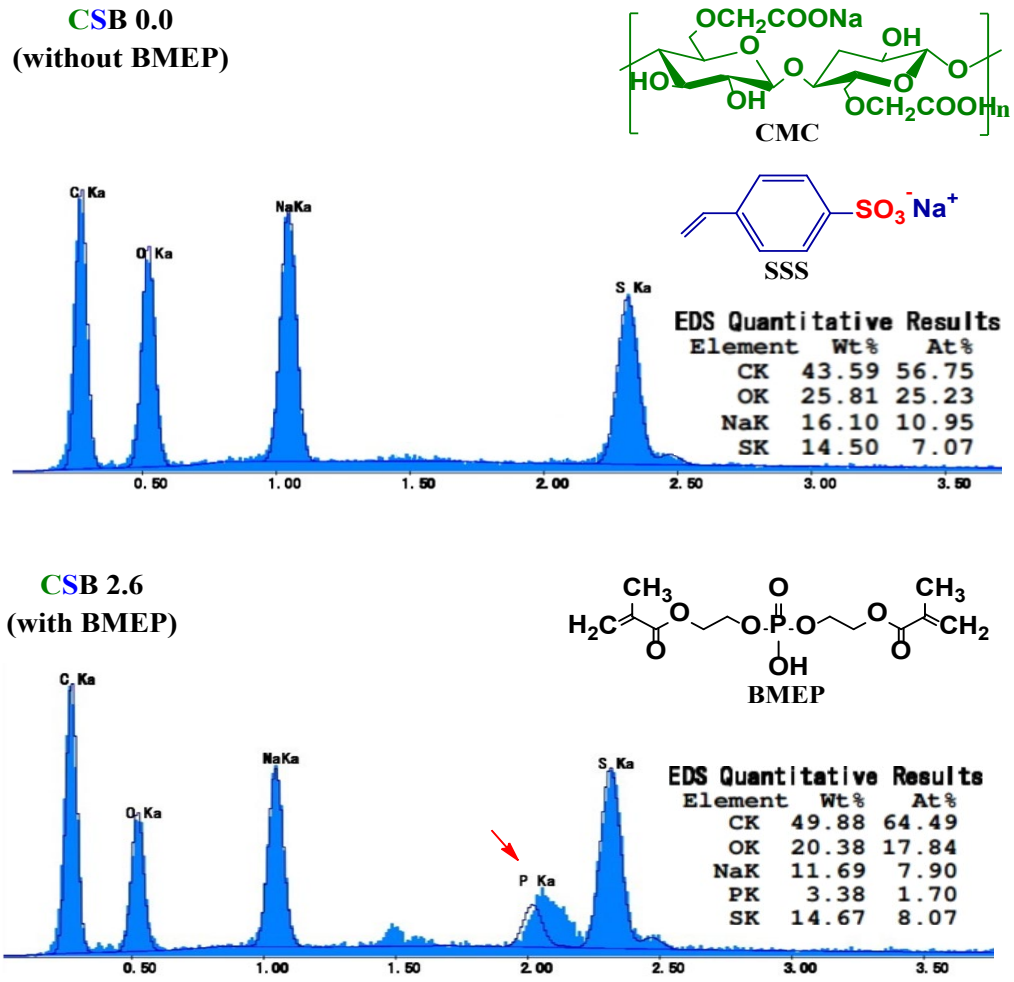

Figure 22. EDS map of CSB before and after phosphonation.

b. SEM images

In order to investigate the distribution and compatibility of BMEP with CS network, observed were SEM images of CSB 0.0, CSB 2.6, CSB 5.2, CSB 7.8 and CSB 12.9 hydrogels' surface.

Figure 23a is a SEM image of CSB 0.0's (without BMEP) surface. The profile shows a porous and wavy surface, which seem to function as a transport channel promoting diffusion the multi-element ions into the interior hydrogel matrix. The spongy surface is caused by lower crosslinking centers and active sites. Conversely, after further adding of BMEP as observing SEM images in (**Figure 23b – e**) with increasing BMEP content, the surface of CSB hydrogels changes significantly. They become high homogenous and much smoother. It might be because BMEP disperses more evenly and interacts with CS hydrogel to form crosslinking network between polymers and monomers, leading to decreasing in distance among macromolecular chains. This implied that BMEP joined and uniformed the architecture of hydrogel chains.

With the aim of developing the practical adsorbent, both of mechanical strength and permeability to the metal-ion solution are important, in spite that they are mutually exclusive. To the author's judgement, CSB 2.6 hydrogel seems the best choice from the viewpoint of reconciliation between the strength and adsorption capacity.

CSB 0.0

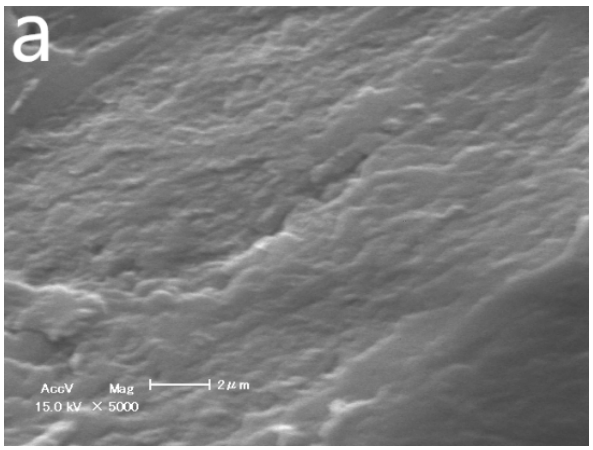

CSB 7.8

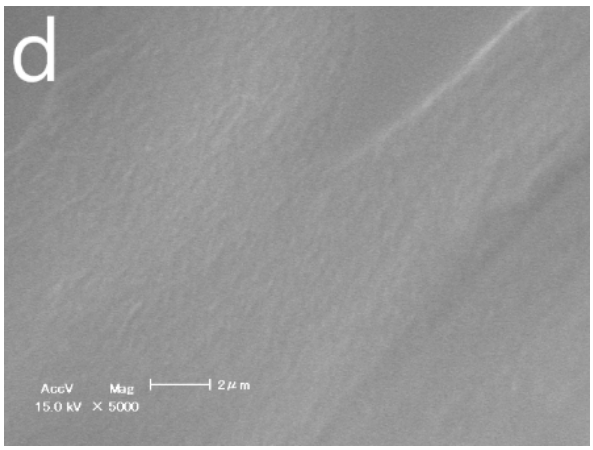

CSB 2.6

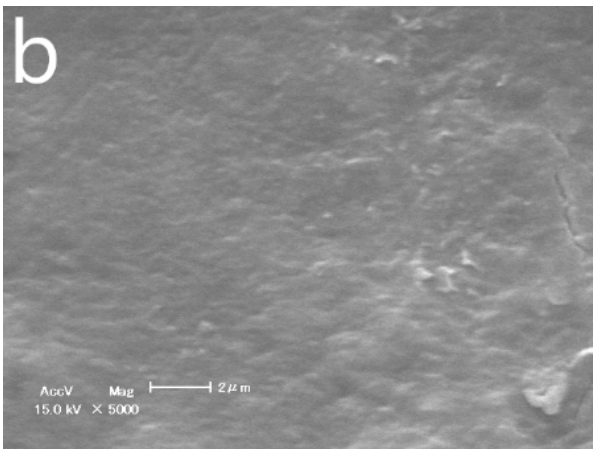

CSB 12.9

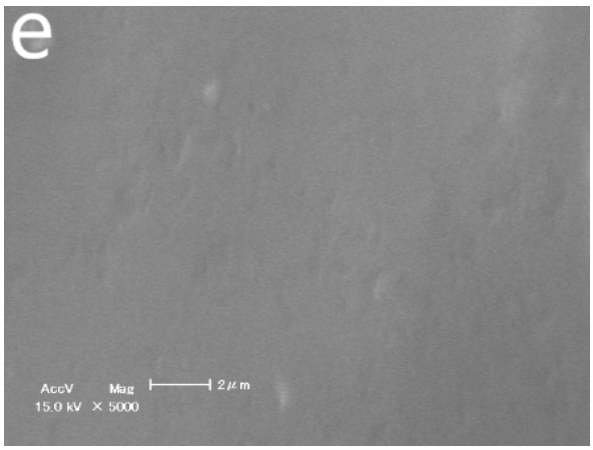

CSB 5.2

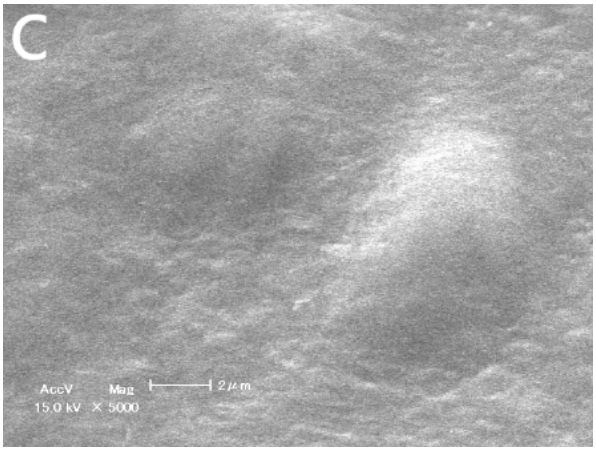

Figure 23. SEM surface morphology photos of CSB hydrogels:
(a) without BMEP and (b) – (e) with different BMEP contents (Mag. ×5000).

4. *Other characteristics of prepared hydrogels*

a. Swelling capacity test

Using BMEP to increase the strength of CSB hydrogel may cause deceasing of its swelling ability and then metal adsorption capacity. The high degree of swelling helps metal ions interpenetrate into the inside of the network and it is known the swelling property of hydrogels depends on external condition such as light, pH, temperature and salinity as well as inherent factors, density of hydrophilic group and density of crosslinking points in hydrogel, etc. [80]

Primary investigations on the swelling degrees of CSB hydrogels with different amounts of BMEP were conducted by immersing CSB hydrogels in DW for a prolonged period (24 hrs). As described in **Figure 24**, it was observed that the gel fractions increases and the water-imbibition amount decreases with increasing BMEP content. The gel content showed a maximum (~80 % at 60 kGy-irradiated dose) at 12.6 mM of BMEP concentration, at the same time, the swelling ratio showed the lowest value. Such a feature can be explained as follows: the CSB hydrogels with higher BMEP concentration will be tougher via larger number of crosslink points in the network and will more effectively suppress the expanding force caused by ionized $–SO_3^-$ and $–COO^-$ groups.

As is described in previous chapter, the hydrogel without BMEP swelled significantly in water and indicated a promising potential as metal capturing material however, the hydrogel absorbing large amount of water became tight, easily cracked and broken into small pieces which make difficult the repetitive use of the CS hydrogel. The experimental result in the present section indicates that by incorporating suitable amount of BMEP into the hydrogel (namely, CSB hydrogel), the modified hydrogel can have both of the high metal-ion adsorbing capacity and durability against iterative adsorption-desorption-regeneration cycles, necessary for the practical adsorbent. From the present experiment, the most promising CSB hydrogel for the repetitive use was produced in the conditions: 2.6 mM of BMEP and 40 kGy of gamma irradiation which has 40 % of the gel fraction and 500 g/g of swelling ratio [weight ratio of swollen to as-synthesized hydrogel].

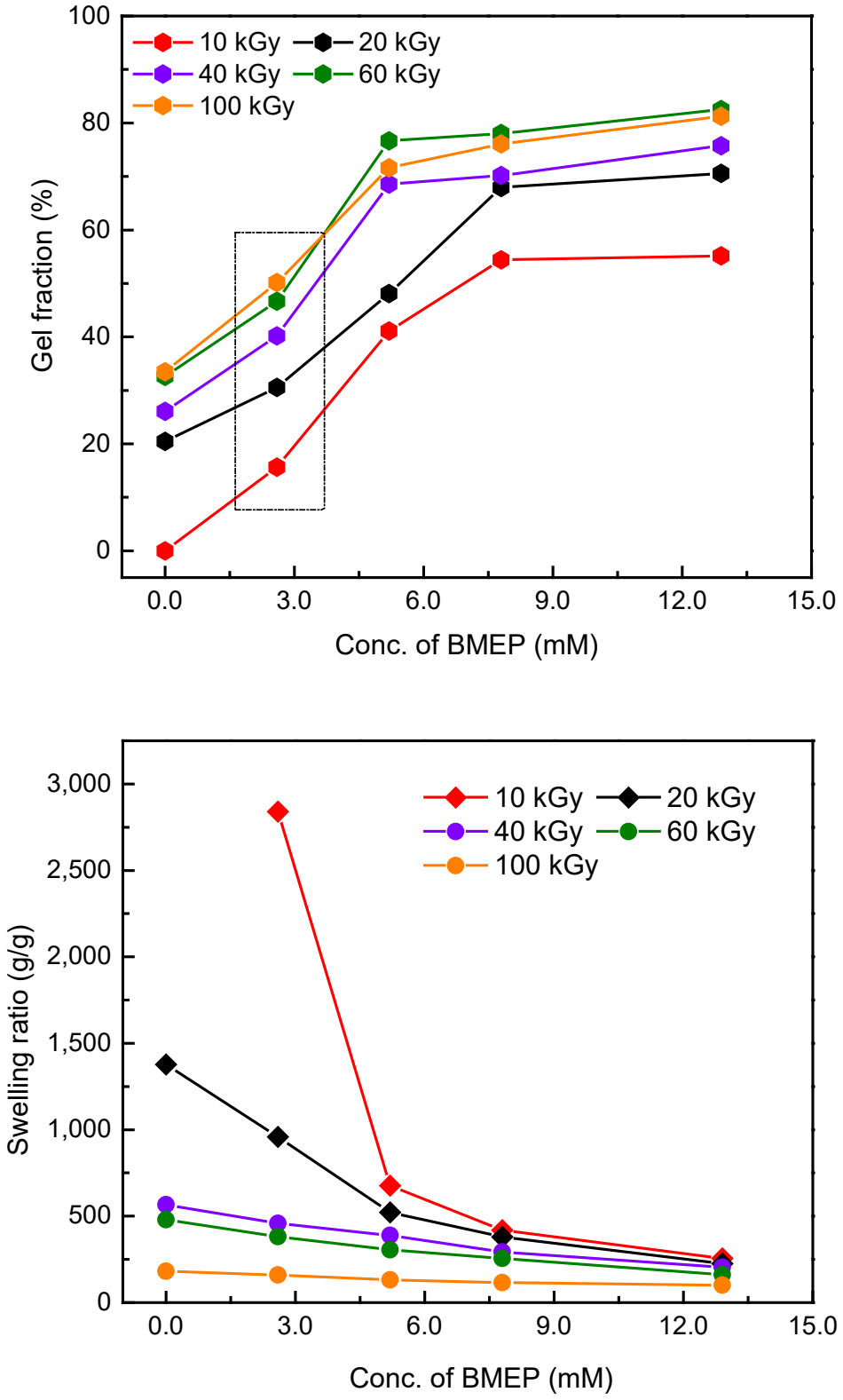

Figure 24. The (a) gelled part percentage and (b) equilibrium swelling abitlity of CSB hydrogels.

b. Visible mechanical testing and calculated compressive modulus related to elasticity property of hydrogels

Adsorbent's mechanical strength is important from the viewpoint of its reusability, which is indispensable in the practical application. For example, as is described in the preceding chapter and section [64], though CS hydrogel showed high metal-adsorption ability, the hydrogel was thought not to be used in the practical application: during the adsorption-desorption-regeneration cycle, the cracking and peeling occurred at the hydrogel's surface, which lessened adsorbing capacity via the volume decrease. In order to prevent such a feature, increase in the elastic stiffness is very important. Along this line, the author grafted BMEP to CS network as second cross-linker in order to strengthen the hydrogel's network. For examining the effectiveness of introduction of BMEP, simple elasticity measurements were performed for CSB hydrogels with different BMEP content, as described in this section.

The mechanical features of CSB hydrogels with different BMEP content are summarized in **Figure 25**, **Figure 26** (a), (b) and **Table 14**. The BMEP-added CSB 2.6 – 12.9 hydrogels featured higher elastic stiffness than CSB 0.0 hydrogel (without BMEP), namely, CS hydrogel. The and Poisson's ratio of the CSB 0.0 hydrogel were 2.76 kPa and 0.47, respectively, compressive modulus, for example, CSB 12.9 hydrogel had 5.75 kPa of compressive modulus and 0.35 of Poisson's ratio. Because increase in the compressive modulus and decrease in Poisson's ratio indicate toughening of the hydrogel network, it is demonstrated that introduction of BMEP significantly enhance the mechanical strength of CSB hydrogels.

The hydrogel with strong bonds in the network is difficult to be deformed and is easy to recover to original form. In the measurements described in the present section, it was demonstrated that the introduction of more amount of BMEP increased the strength of the hydrogel via the creation of higher number of cross-links in the hydrogel's network. However, increase in the crosslink points will induce the smaller mesh-sized network, in which the diffusion of the fluid become slower; this feature is not favorable from the viewpoint of capturing capacity. Therefore, a optimal concentration of BMEP should be determined to make the CSB hydrogel with both of high mechanical strength and high metal adsorption capacity.

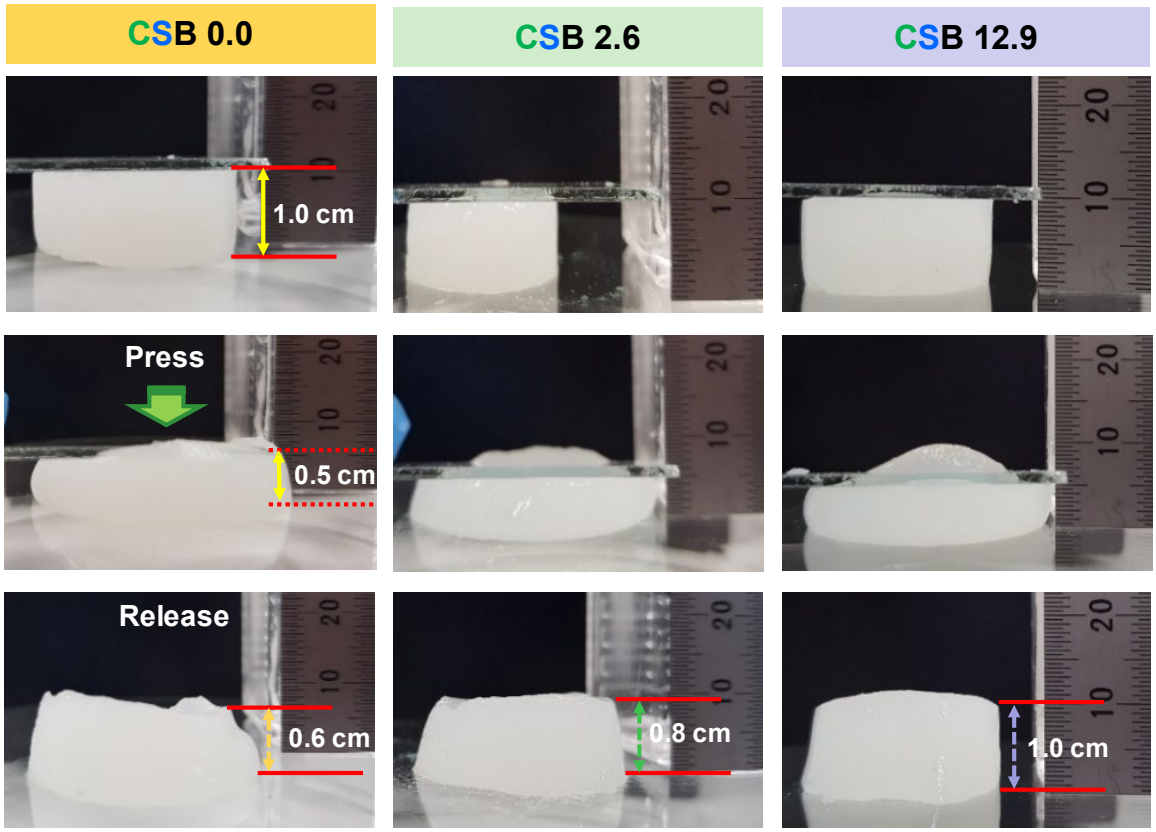

Figure 25. Visible compression tests demonstrate the CSB hydrogel recovers their original shape.

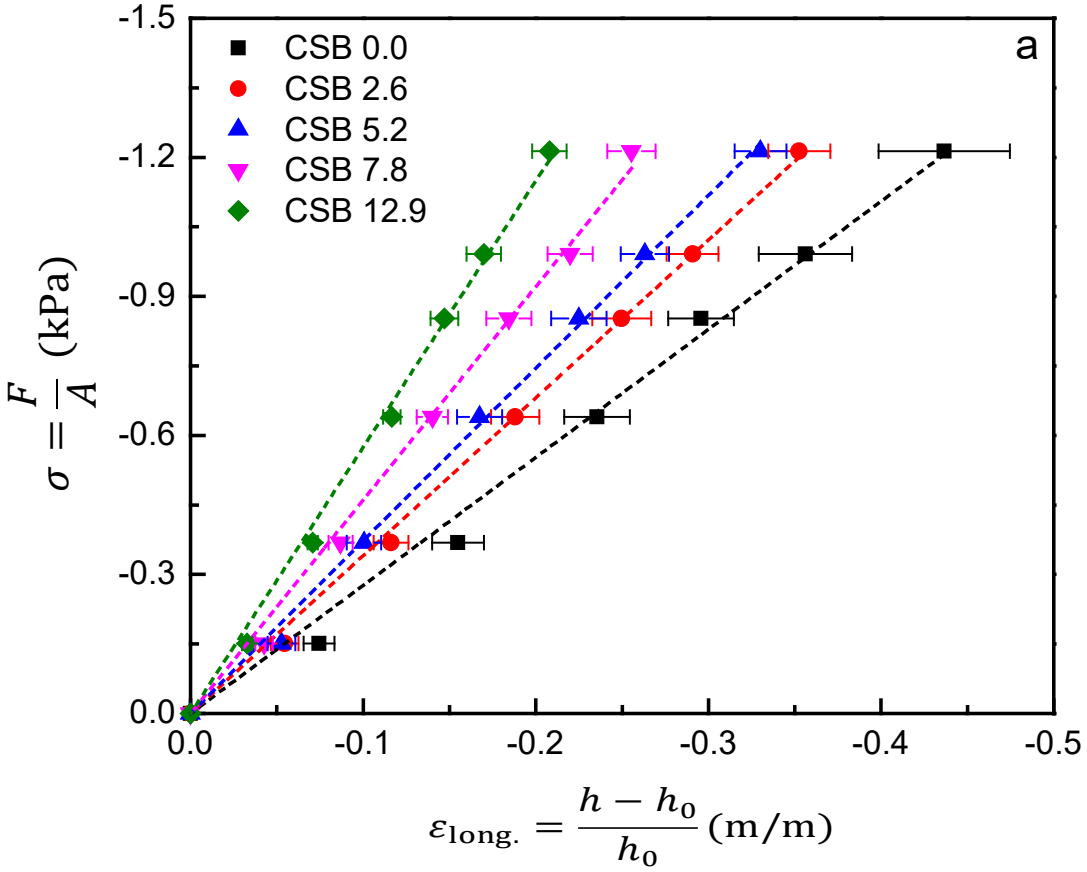

Equation	$\frac{F}{A} = E \times \frac{h - h_0}{h_0}$				
Residual Sum of Squares	0.00794	0.00207	0.00291	0.0049	0.00437
Pearson's r	0.998	0.999	0.999	0.999	0.999
Adj. R^2	0.997	0.999	0.999	0.998	0.998
		Value	Standard Error		
■ CSB 0.0	Intercept		--		
	Slope		0.05		
●	Intercept		--		
	Slope		0.03		
▲	Intercept		--		
	Slope		0.04		
▼	Intercept		--		
	Slope		0.06		
◆	Intercept		--		
	Slope		0.08		

Figure 26 a. σ vs. $\varepsilon_{\text{long.}}$ fitting plots at σ = 0.00 – 1.21 (kPa) for the CSB hydrogels.

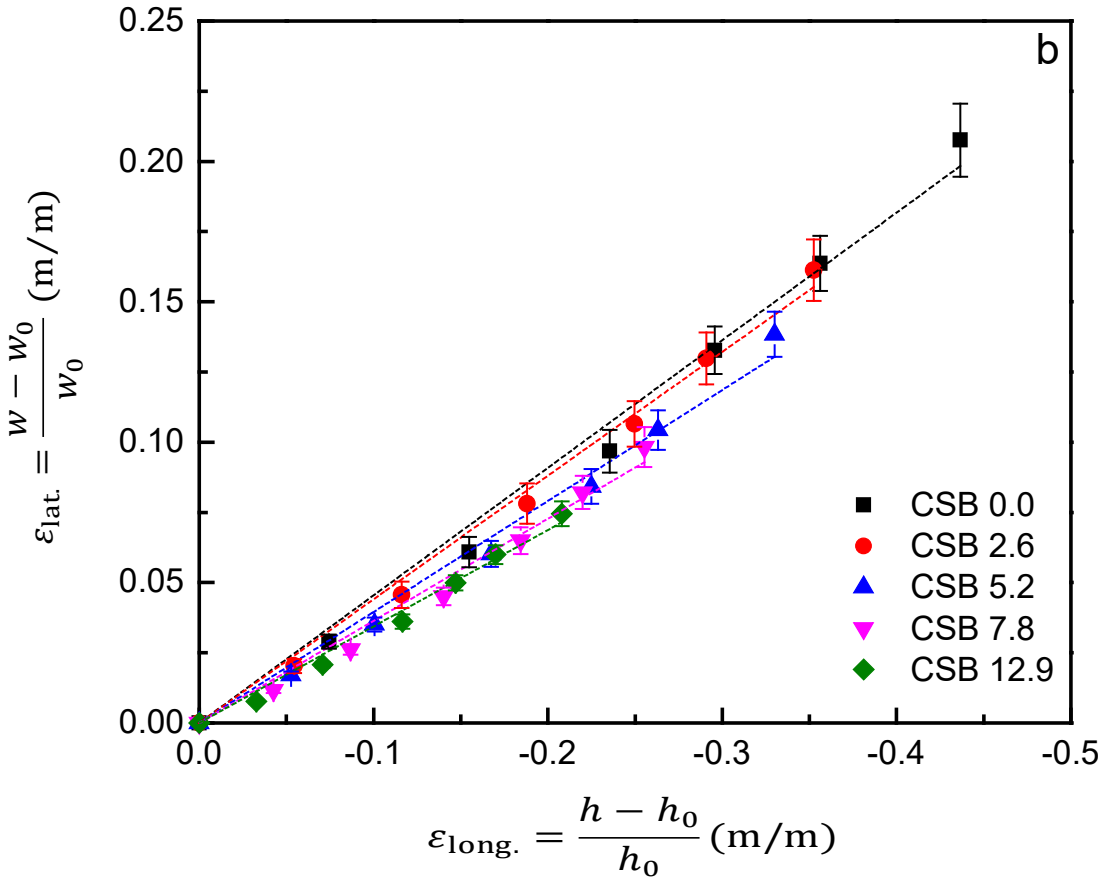

Equation					
Residual Sum of Squares	3.08 E-4	1.17 E-4	1.55 E-4	1.16 E-4	5.34 E-5
Pearson's r	-0.998	-0.999	-0.998	-0.997	-0.998
Adj.	0.996	0.997	0.995	0.994	0.995
		Value	Standard Error		
■	Intercept		--		
	Slope	-0.45	0.010		
●	Intercept		--		
	Slope	-0.44	0.007		
▲	Intercept		--		
	Slope	-0.39	0.009		
▼	Intercept		--		
	Slope	-0.36	0.010		
◆	Intercept		--		
	Slope	-0.34	0.008		

Figure 26 b. $\varepsilon_{lat.}$ vs. $\varepsilon_{long.}$ fitting plots at σ = 0.00 – 1.21 (kPa) for the synthesized hydrogels.

Table 14. The calculated values of Poisson's ratio and Young's moduli for the CSB hydrogels.

Samples	Young's moduli, *E* (kPa)	Poisson's ratios, ϑ
CSB 0.0	2.76	0.45
CSB 2.6	3.40	0.44
CSB 5.2	3.73	0.39
CSB 7.8	4.61	0.36
CSB 12.9	5.75	0.34

III. Metal adsorption performance

1. Metal adsorption in competitive condition

In this section, described are CSB hydrogels' metal-ion capturing capacities from aqueous mixtures, which are the most important properties as an adsorbent. In the investigation, 40 mL aqueous solutions containing simultaneously equal amount of Mo, Cr, Mn, Zn, V, Ag , Cu, Cd, Co and Ni ions with 100 μg/L of initial concentration for each element were prepared as described in Chap.2-Sec.V, then their pH's are adjusted to ~5 by using HNO_3 0.5 M solution. On the other hand, the CSB hydrogel-cubes (0.5×0.5×0.5 cm3 {0.200 g}) with different compositions (CSB 0.0, CSB 2.6, CSB 5.2, CSB 7.8, and CSB 12.9 as in **Table 8**) were prepared and washed with DW for 5 hrs. After these preparations, the CSB hydrogels had been immersed in the pH-adjusted metal-ion aqueous mixture for 48 hrs without stirring at room temperature (25 °C).

Figure 27 shows the removal ratios of Mo, Cr, Mn, Zn, V, Ag , Cu, Cd, Co and Ni from the multi-metal-ion aqueous solutions by the CSB 0.0, CSB 2.6, CSB 5.2, CSB 7.8, and CSB 12.9 hydrogels. As can be seen from the figure, removal efficiency of every metal ion was observed to be lower in the CSB hydrogels with higher BMEP ratio, in spite that all of the CSB hydrogels contain the same amounts of metal-ion adsorbing group, namely SSS and CMC.

Among the CSB hydrogels except for CSB 0.0 hydrogel (CS hydrogel) examined in the present investigation, CSB 2.6 hydrogel showed the highest metal-ion capturing capacity. As described in Chap.2 Sec.II.2 [**Table 8**], CSB 2.6 hydrogel was composed of 2.00 g of CMC, 4.00 g of SSS and 0.02 g (2.6 mM) of BMEP and showed a high metal removal performance comparable to CS hydrogel (CSB 0.0 hydrogel) [**Figure 27**] even though its swelling degree was considerably smaller than CS hydrogel [**Figure 24**].

For these results, the author considers as follows taking into account of ionization property of BMEP: Because BMEP contains an ionizable phosphate group and 2 bind-able vinyl groups in a molecule, it works as a metal-ion capturing group as well as a cross-linker connecting CMC chains. Therefore, compared with CS hydrogel, when BMEP amount is small as in the case of CSB 2.6, the lowering of metal-ion capturing capacity with finer mesh (described above) can be compensated by the larger amount of the metal-ion capturing groups (phosphate groups).

The **Figure 27** and **Table 15** also demonstrate other interesting characters on the metal-ion capturing capacity of CSB 2.6 hydrogel: in the competitive condition in the coexistence of Mo, Cr, Mn, Zn, V, Ag , Cu, Cd, Co and Ni, CSB 2.6 hydrogel showed high ion-adsorption capacities for a wide range of the metal ions with a weak selectivity for them: the order of the adsorbed metal-ion amount was

$$Mo < V < Zn < Cr < Cu < Mn < Cd < Co < Ag < Ni.$$

As depicted in **Figure 27** and **Table 15**, CSB 2.6 hydrogel showed relatively higher capturing functionality to Ni^{2+} and Ag^{+} than other coexisting metal ions. The probable explanation for the higher Ni^{2+} and Ag^{+} selective capturing capacity might be as follows:

- Ni^{2+} has the smallest covalent radius (124±4 pm), compared with other ions: Co^{2+} (126±3 pm), Cu^{2+} (132±4 pm), Mn^{2+} (139±5 pm) or Ag^{+} (145±5 pm), etc., indicating easy mobility of Ni^{2+} ions in solution and high possibility to come across the active site of the adsorbents.
- Ag^{+} has higher electronegativity (Pauling scale) 1.93 which can attract electrons from binding sites on hydrogel structure towards itself, whereas the electro-negativities of Ni, Cu, Co and Cd are 1.91, 1.90, 1.88 and 1.69, respectively.
- The HSAB concept as mentioned in Chap. 1-Sec.II.4. a., Ni^{2+} in solution can be a relatively hard acid while Ag^{+} is considered as a soft acid. The O ligands on the carboxyl, phosphate or hydroxyl groups are able to hard bases. As a result, Ni^{2+} has stronger bindings with those functional groups, leading to a little higher adsorption capacity for Ni^{2+} ions, compared for Ag^{+} ions.

Although Mo^{3+} has the highest electronegativity (2.16 [81]) among the examined metal-ions in the present experiments and a high-mobility single lone-electron in the outermost 5s-shell, one Mo^{3+} ion is thought to be necessary to link with at least 6 active sites on an adsorbent, whereas Ni^{2+}, only two binding sites or Ag^{+} needs one.

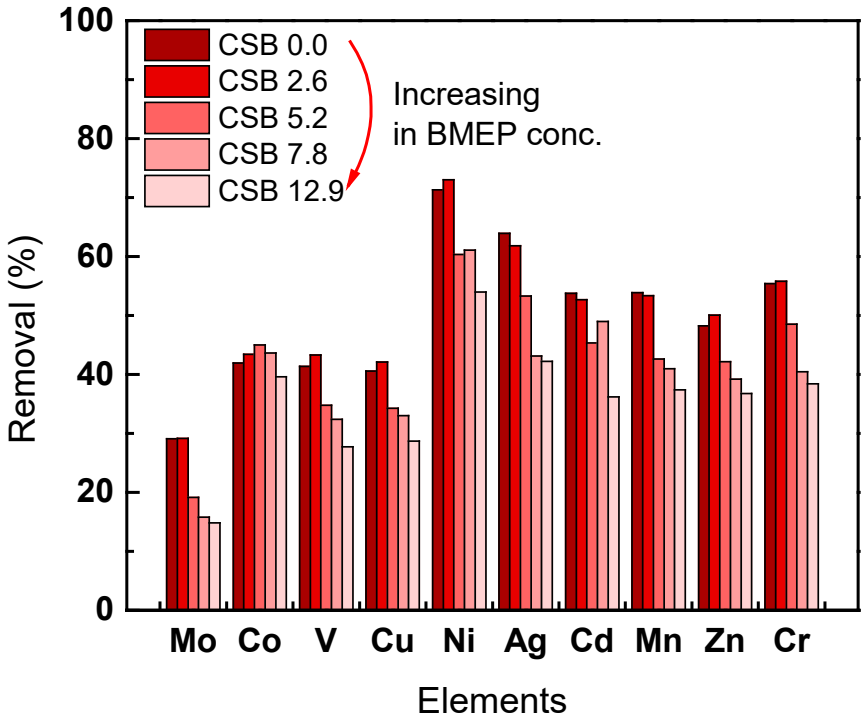

Figure 27. Multi-element capturing in solution by CSB hydrogels.

Table 15. Adsorption capacities of CSB hydrogels for multi-elements.

Hydrogel code	Metal ion adsorption capacity (µg/g)									
	V (V)	Ag (I)	Mn (II)	Co (II)	Zn (II)	Cu (II)	Cr (III)	Mo (III)	Ni (II)	Cd (II)
CSB 0.0	6.19	12.7	8.78	8.29	7.33	8.17	10.9	5.82	14.1	10.7
CSB 2.6	6.52	12.2	8.50	8.54	7.86	8.29	11.0	5.74	14.4	10.4
CSB 5.2	5.48	10.2	7.32	6.89	6.10	6.58	9.63	3.71	12.3	9.96
CSB 7.8	4.29	9.45	7.01	6.93	5.84	6.26	8.37	4.32	12.8	10.1
CSB 12.9	3.28	9.17	6.56	6.94	5.22	5.61	7.90	2.94	10.1	8.04

2. *Metal adsorption in non-competitive condition*

Nickel (Ni) is a silver-white metal with a glossy surface and is one of the five ferromagnetic elements. The mechanical properties of Ni are hard and malleable. So Ni is used quite a lot in mechanical industries. Under normal environment, Ni is very stable in the air because of its low reactivity toward oxygen. Nickel is commonly contained in foods and drinking water due to environmental pollution caused by human activities. Short-time exposure to Ni in foods or water can induce an allergic reaction to some men [82]. In addition, animal experiments also show that long-term exposure to Ni can result in loss of fertility and/or developmental disorders [83]. Though there is currently no maximum Ni level for food in Europe [84][80], it is reported that Ni in drinking water for human and in natural mineral water exceeding 20 µg/L causes serious health impairments [85]. Accordingly, the Ni-removal treatment for Ni-rich water before being accessible to the public is mandatory.

Silver (Ag) is a precious metal which has been exployed widely in industry for long times ago because of its wonderful characteristics such as ductility, luster, thermal and highest electrical conductivity, corrosion and oxidation resistance, reflectivity of any metal, , antimicrobial[80]. As a result, silver from industrial activities discharged into water system. In addition, mining effluents also contain appreciable amounts of Ag since Ag is usually distributed with relatively low content in massive base metal ores. From the toxicity point of view, Ag ions in wastewater are not as harmless as people usually thought. Actually, Ag ions have more posing risks to aquatic organisms than copper or mercury [86][87][88] and the accumulation of Ag ions in organisms (including humans) can cause numerous diseases and disorders [89][90]. Besides, as a matter of fact, world silver demand which steadily increases by around 2-2.5% annually, has exceeded production since 2005. About 18-20% of the world's silver demand is supplied by recycling photographic wastes [82][91]. In summary, it is essential to efficiently and economically recover silver from industrial wastewater and effluents.

In the previous experiments measuring individual-metal-ion adsorption from their aqueous mixture, CSB 2.6 hydrogel showed the highest capacity among the CSB hydrogels containing different BMEP amount from 2.6 to 12.9 mM, indicating possibility for a promising adsorbent. In addition, CSB 2.6 hydrogel was also revealed to exhibit especially high capturing capacity for Ni^{2+} and Ag^{+}. Because Ag is a precious metal and Ni, simultaneously useful and toxic, there will be high importance of its recovery as a resource and/or removal as a harmful substance. Therefore, the author considered that more detailed studies on Ni and Ag adsorption by CSB 2.6 hydrogel were necessary as a basis for developing adsorbents with higher capturing capacities for Ni and/or Ag. Therefore, in the present study, Ni and Ag adsorption from respective single-ion aqueous solutions were investigated as an experiments for obtaining more quantitative result in a simplified condition.

For Ni and Ag batch adsorption experiment, CSB 2.6 hydrogels of 0.100 – 0.600 g were immersed into original aqueous concentrated solutions of Ag and Ni single metal ion solutions and the change in concentration of the residual solution was measured using ICP/MS instrument (Agilent, Japan). The initial concentrations (C_0's) and pH's of Ni^{2+} and Ag^{+} aqueous solutions were set at 100 µg/L and 5, respectively, which were the same conditions with the previous adsorption experiments from multi-element aqueous solution. The adsorption parameters are summarized herein in **Table 16**.

Table 16. Parameters of single metal adsorption experiments.

Hydrogel	CSB 2.6							
Initial adsorbent weight m_0 (g)	0.100	0.100	0.200	0.200	0.400	0.400	0.600	0.600
Tested Element	Ni	Ag	Ni	Ag	Ni	Ag	Ni	Ag
Solution volume V (mL)	40	40	40	40	40	40	40	40
Initial concentration C_0 (µg/L)	100	100	100	100	100	100	100	100

In **Figure 28** and **Table 17**, illustrated is an overview of the adsorption feature and performance parameters obtained in the present experiments. In the case of CSB hydrogel, the usage was thought to be more effective for Ni adsorption than for Ag ions, owing to much higher K_d values and % removal (over 90 %) for Ni.

In addition to the high extraction efficiencies over 80 % in the present experimental conditions, the author also noticed that the apparent adsorption performance (q) had a negative correlation with the initial adsorbent weight (m_0) in both of the adsorption experiments performed with single Ni^{2+}- and Ag^{+}-ion solutions: the apparent adsorption capacities were lower for the adsorbents with larger initial weights.

This experimental results were thought to come from the availability of adsorbent's vacant adsorptive-sites for the adsorbate-ions migrating into adsorbent against friction force caused by the interactions with the surrounding network. The feature that higher apparent capturing-efficiencies for the adsorbents with lower mass can be explained as follows: Because adsorbate permeation into adsorbent is only controlled by the conditions related to interaction between adsorbent's network and adsorbates, adsorbate's penetrating depth will not be unaffected by adsorbent's volume, therefore, the volume ratio of the adsorbed portion to that of the whole adsorbent can be lower in the adsorbents with larger volumes (weights) during some limited adsorption period, namely, the lower apparent adsorption efficiencies in the adsorbents with larger weights.

An overview of adsorption experiments and obtained results is illustrated in **Figure 28** with supporting data in **Table 17**. Initial findings for single ion Ni (II) and Ag (I) adsorption were noticed that the adsorbent dosage relative to adsorption performance. In all cases, the applied adsorbent weight was increased, causing the adsorption capacities were declined, even the extraction efficiencies were maintained of over 80 %. It is due to the availability of vacant adsorptive sites of the adsorbent for ions under osmotic pressure. At a lower dosage of adsorbent, the binding sites might be employed sufficiently, leading to a higher adsorption capacity. However, at a higher mass of adsorbent, due to the existence of osmotic pressure, the adsorption would readily reach equilibrium even though more active sites are available for adsorption.

The selective adsorptiony of the CSB hydrogel for Ni ions might be analyzed by the distribution coefficient K_d (mL/g) which is defined in **Eq. 1** (Chap.1 Sec.II.4.a). Higher K_d implied that more metal ions are extracted from the solution into the hydrogel network, signifying higher adsorption efficiency by the hydrogel in capturing the metal ions. In this case, the CSB hydrogel was more suitable for Ni adsorption owing to the much higher K_d values and % removal in excess of 90 % compared with Ag ions.

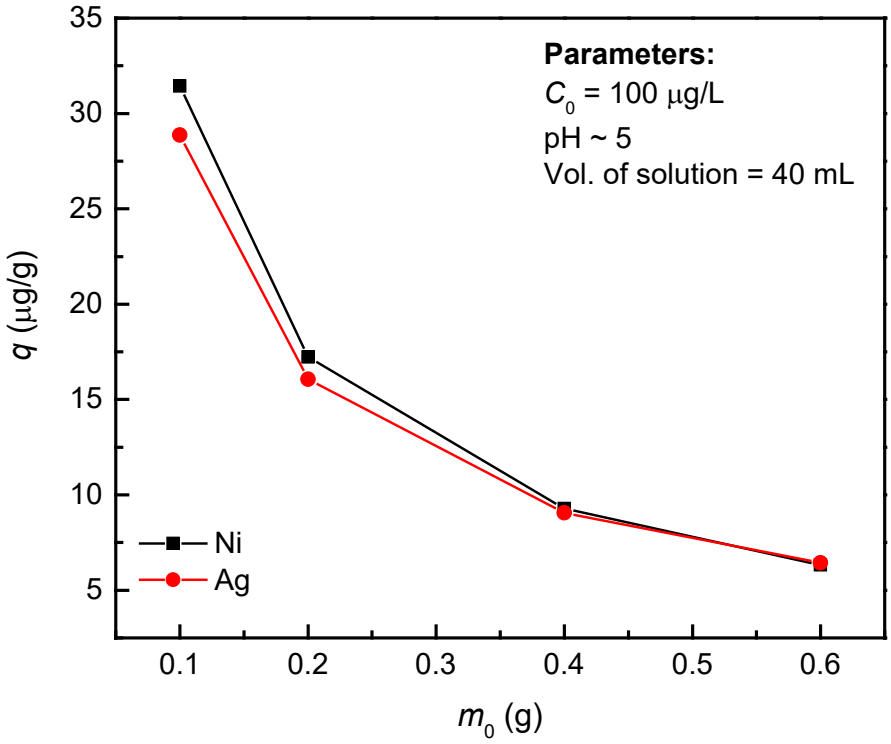

Figure 28. Ni and Ag adsorption in non-competitive conditions.

Table 17. Results on the adsorption performance of CSB hydrogel for Ni and Ag single ion metal solutions.

	Ni (II)			Ag (I)		
m_0 (g)	q (µg/g)	Removal (%)	K_d (mL/g)	q (µg/g)	Removal (%)	K_d (mL/g)
0.100	31.44	81.91	1.744	30.86	79.84	1.524
0.200	17.22	90.33	1.787	17.06	88.92	1.534
0.400	9.28	94.84	1.804	9.06	94.11	1.569
0.600	6.32	96.52	1.820	6.43	96.01	1.606

3. *Effect of pH*

Because the CSB hydrogel's adsorptions for metal ions were thought to be considerably influenced by the activity of the functional group sensitive to pH, it seemed important to investigate pH dependence of the equilibrium adsorption capacity. Therefore, in the present experiments, the simultaneously adsorbed amounts of Mo, Cr, Mn, Zn, V, Ag , Cu, Cd, Co and Ni by CSB 2.6 hydrogels (0.5×0.5×0.5 cm) from 40 mL aqueous mixture with the same initial concentrations of 100 µg/L of each metal ion were measured in a range from pH=1 to 8, adjusted by adding appropriate amounts of aqueous 0.5 M-KOH and/or 0.5 M-HNO_3 solutions into the adsorbate solutions, as shown in **Figure 29**.

As shown in **Figure 29**, the adsorption capacities of CSB 2.6 hydrogels for all of the metal ions were very low at pH=1 and 2, this may be because almost of the functional sites, i.e. $–SO_3^-$, $–COO^-$ and $–PO_4^-$, could be protonated (namely deactivated), which could result in the reduction of number of available adsorption sites. In a region around pH=4 – 5, the uptake capacities for Mo, Cr, Mn, Zn, V, Ag , Cu, Cd, Co and Ni were remarkably higher than other parts and had maxima for all the metal ions, indicating that the functional groups worked better in this pH range than other parts. This phenomenon could be explained by the fact that the ionized form of functional groups $–SO_3^-$, COO^- and $–PO_4^-$ exist in a range pH from 4.20 to 6.40, namely, the more functional groups for metal ion adsorption could be available in this pH range. Above pH=6, the adsorbed amount of the metal ions by CSB hydrogels were lower than the range pH=4 – 5. This could be because many of the metal ions precipitated by forming metal hydroxide precipitates in spite that $–SO_3^-$, $–COO^-$ and $–PO_4^-$ groups might be highly ionized in this pH region.

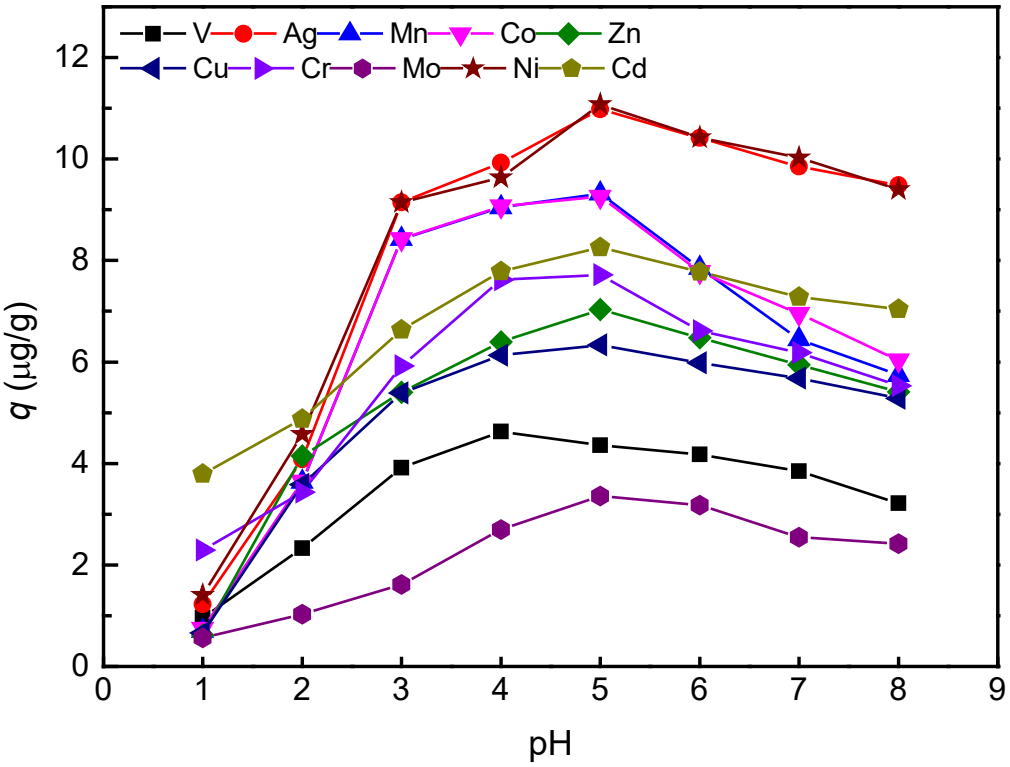

Figure 29. pH dependent adsorption capacity of CSB hydrogel for multi-elements in solution.

4. Adsorption kinetics

The evolutions of metal-ion adsorptions for Mo, Cr, Mn, Zn, V, Ag , Cu, Cd, Co and Ni by CSB 2.6 hydrogel at room temperature were measured in a time range up to 72 hrs. to confirm the maximum duration for the most effective hydrogel performance as shown in **Figure 30**. Batch adsorption experiments by CSB 2.6 hydrogel onto original aqueous concentrated solution (40 mL) of multi metal ion solutions (initial concentration 100 µg/L for each metal ion).

Looking at the time dependence of the metal-ion adsorptions by CSB hydrogels in **Figure 30**, CSB hydrogel seemed capture all the types of metal ions with almost the same time-dependence and the adsorptions continued for a long period. The adsorption equilibrium was not achieved up to ~24 hrs, which might come from the competition among metal ions to be bound with functional groups in the CSB hydrogel.

With referring to the experimental results described in the previous chapter related to metal ion's interaction with functional groups on hydrogel [Chap.3-Sec.III-3], the obtained kinetic data were also analyzed by adopting pseudo-2nd-order kinetic model represented by **Eq. 7** [Chap.1-Sec.II-4.d [45]]; if a non-linear dependence might be revealed in the plot of q vs. t, the adsorption mechanism could be indicated to be dominantly sharing or exchange of electrons between functional groups and metal ions.

The numerical analyses were conducted by utilizing using Origin 9.0 software (OriginLab, USA.). The adsorption kinetic analyses revealed high non-linear curve fits with high correlation coefficients R^2's and low χ^2's values [Chap.1-Sec.II-4.d]. In addition, it could be easily recognized in **Table 18** that the respective calculated values of q_e are highly close the experimental ones for all the metal ions.

As shown in **Table 18**, the calculated adsorption rates depended on the size of captured metal ions in aquatic environment. Comparing the data of ionic radius of the hydrated metal ions and adsorption parameters in **Table 18**, it could be said that Cu with the highest radius could rapidly interact with CSB hydrogel surface, namely the highest value of k_2, on the other hand, the CSB hydrogel showed the highest adsorption capacity (q_e) for smaller ions such as Ni.

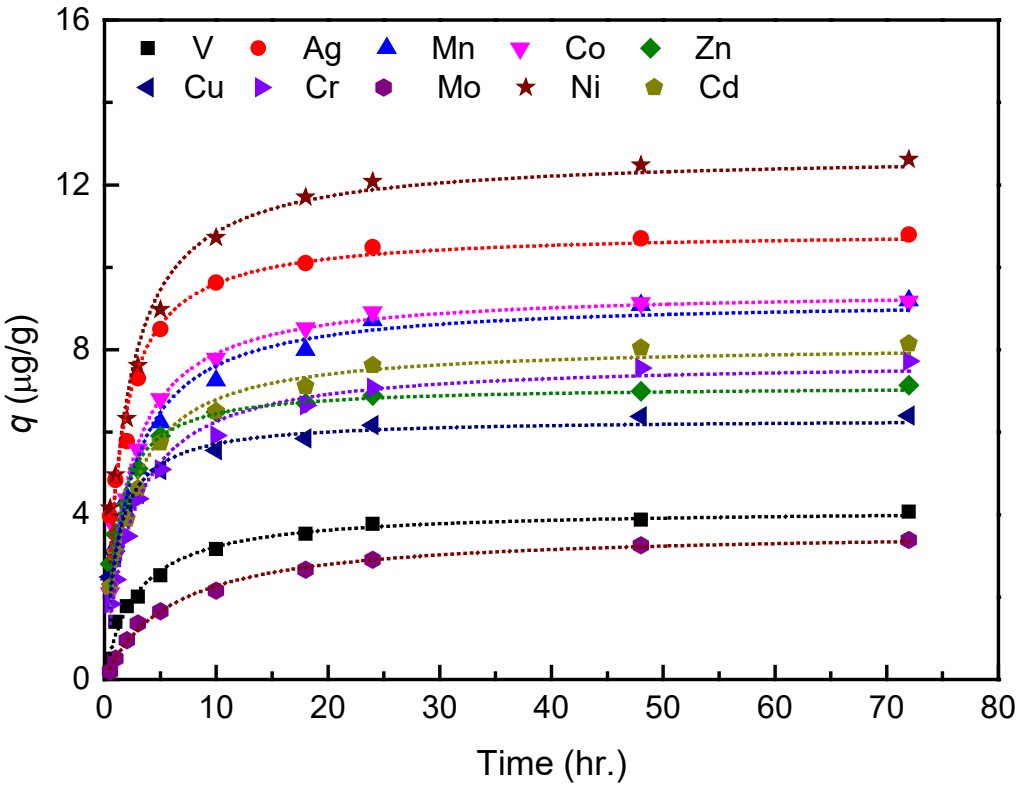

Figure 30. Time dependent adsorption of CSB hydrogel for multi elements in aquatic environment

Table 18. Overview of ionic radius of hydrated metal ions in aqueous solution [92] and the pseudo-2nd-order kinetic model analysis of CSB hydrogel adsorption behavior for multi-element.

		Experimental	Calculated pseudo-2nd-order kinetic analysis			
Metal ions	Ionic radius (Å)	q_e	q_e	k_2	R^2	χ^2
V (V)	0.80	4.07	4.13	0.085	0.986	0.020
Ag (I)	0.98	10.79	10.88	0.069	0.968	0.211
Mn (II)	0.86	9.19	9.23	0.050	0.975	0.150
Co (II)	0.74	9.17	9.45	0.053	0.991	0.058
Zn (II)	0.74	7.13	7.12	0.134	0.976	0.059
Cu (II)	0.92	6.39	6.32	0.149	0.974	0.050
Cr (III)	0.62	7.71	7.73	0.055	0.986	0.064
Mo (III)	0.76	3.38	3.62	0.046	0.995	0.006
Ni (II)	0.71	12.61	12.74	0.044	0.969	0.326
Cd (II)	0.96	8.15	8.13	0.062	0.977	0.106

5. *Adsorbent re-use*

The re-usability of CS hydrogel was low because of the low mechanical strength as described in Chapter 3. One of the most important subjects in the present investigation (Chap.4) was improving the re-usability by introducing BMEP into CS hydrogel, namely producing CSB hydrogel.

In **Figure 31**, the experimental features during the examination of the re-usability of CSB 0.0 hydrogel (namely CS hydrogel) and CSB 2.6 hydrogel are displayed. In the experiments, iteration of adsorption-desorption (in 0.5 M of HNO_3 acid solution) process were conducted at least 4 times. As for the adsorbate, 100 μg/L of Ni aqueous solution was chosen for this experiment since CSB hydrogel showed a high adsorption capacity for Ni ion in the aqueous solution under a competitive condition. In every desorption process, it was confirmed by ICP-MS apparatus that almost of Ni captured to CSB hydrogel desorbed.

Figure 32 shows Ni-removal-degree change of CSB 0.0 (namely CS hydrogel) and CSB 2.6 hydrogels during the cycle of adsorption-desorption iteration. As can be seen from the figure, CSB hydrogel continued to absorb Ni with no noticeable decrease whereas CSB 0.0 showed the adsorption decrease as described in Chapter 3: the capturing performance of CSB 2.6 hydrogel was around 81% after the 4th adsorption-desorption cycle, on the other hand, CS hydrogel, 56%. The experimental results in the present investigation demonstrated that CSB hydrogel is a promising adsorbent from the viewpoint of its re-usability as well as the high metal-ion capturing capacity.

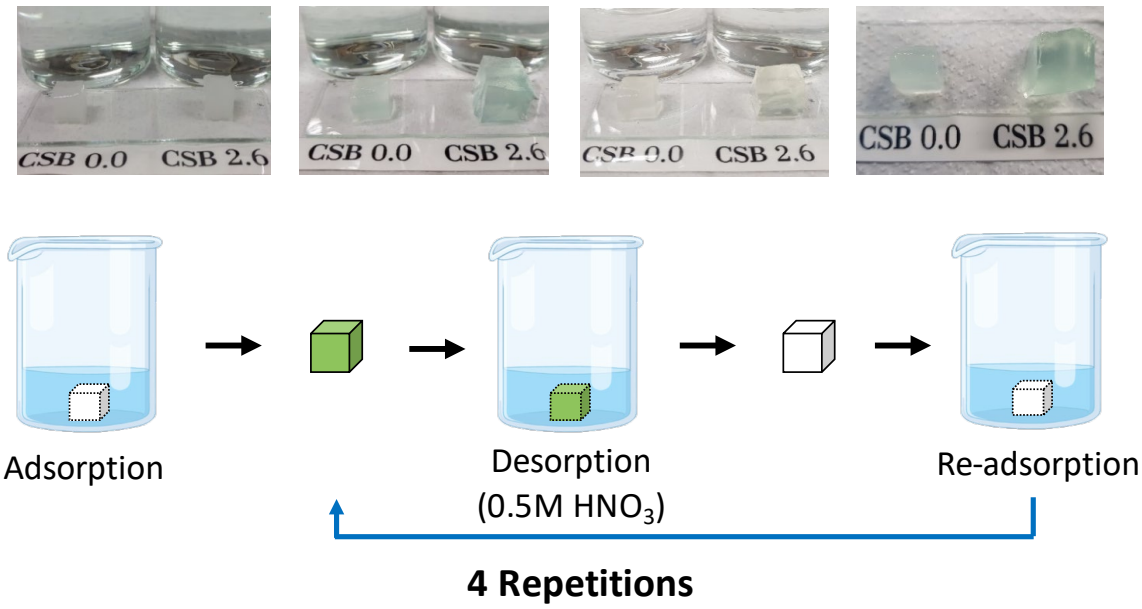

Figure 31. Simple recycle process of Ni-absorbed hydrogel.

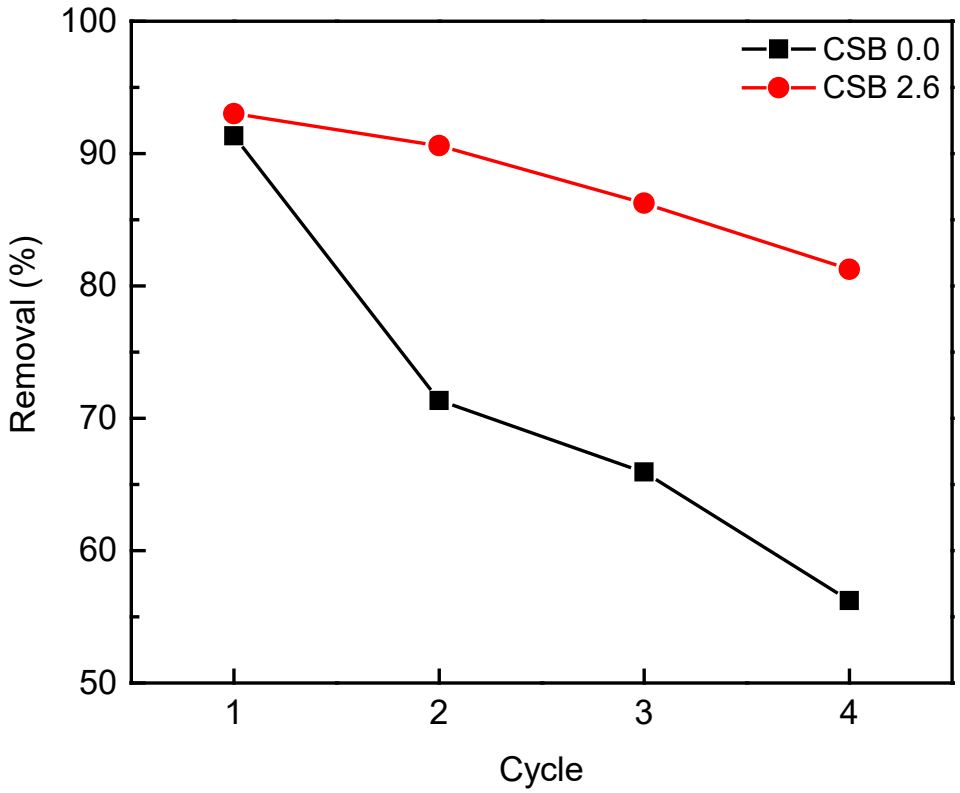

Figure 32. Ni-removal recycles by CSB hydrogels

IV. Conclusion

The CS hydrogel used for metal adsorption in the previous study possesses weak mechanical property, causing low re-usability. In this chapter, we successfully overcame this disadvantage by designing and composing a new kind of hydrogel with introducing BMEP as a reinforcement agent into CS hydrogel. The ɤ-irradiation during gelation process still proves that it is a "clean" method. No any additional reagents, such as polymerization initiator, cross-linking agent nor reaction accelerator was used. The processed product is very pure without any chemical initiator or related impurities remaining on the modified surface.

The newly formed absorbent, CSB hydrogel does not show noticeable swelling capacity but exhibits higher mechanical property (0.45 of Poisson's ratio and 3.4 kPa of compressive modulus) than CS hydrogel. CSB hydrogel maintains multi-metal capturing effectiveness comparable to CS hydrogel. Particularly, FTIR, SEM, and EDS analyses confirm the existence of varying active sites including $–SO_3^-$, $–PO_4^-$, $–COO^-$, and –OH groups which allow the efficient capturing of Ni^{2+} ion. Furthermore, the modified hydrogel can maintain a high metal removal of ~81 % after 4 adsorption-desorption routines. These exciting results make the CSB a promising heavy metal absorber that can be used in wastewater treatment systems.

CHAPTER 5

STRATEGY FOR SELECTIVE SSS-GRAFTED CMC ADSORBENT

For treatment of wastewaters, high sorption capacity of all (or most of) metal ions is required. However, it is more realistic to develop selective recovery method for a specific metal ion from mixture of metal ions to allow re-use of recovered metal ion in some cases. Previous chapters showed that modified CMC-hydrogels i.e. CS and CSB hydrogels are advanced materials for multi elements adsorption from solution. Especially, CSB hydrogel can remove efficiently for both nickel Ni^{2+} and silver Ag^{+} under the competitive condition. In this chapter, we would like to consider the required scpecifications of CMC-based hydrogel in Ag^{+} selective adsorption from the mixture of multi-elements because Ag has precious, useful but toxic property. Preparation of low-toxic and biodegradable adsorbent is still of the main purpose in terms of environmental safety in our study.

According to the HSAB concept [36] (Chap.1-Sec.II.4.b), Ag ion is characterized as a soft Lewis acid. Therefore, Ag has strong affinity toward nitrogen (N) atoms which is a relatively soft base via lone pair electrons. A hydrogel adsorbent with functional groups containing N atoms indeed has exhibited good performance in the adsorption of silver metal ions [93][94][95].

In recent years, Carboxymethyl chitosan (CMCts), a biopolymer, is industrially attractive in adsorption because it is widely available and environmentally safe. Unlike CMC with only active carboxyl group, this natural-origin polymer includes both amino and carboxyl groups which define its stronger complexation properties towards metal ions. CMCts is also characterized by its high percentage of N, present in the form of amine groups that can be responsible for Ag metal ion binding.

In order to enhance selective Ag (I) adsorption ability and re-usability of CMC hydrogel, we attempted to compose a new eco-hydrogel from 2 polysaccharides carboxymethyl cellulose (CMC) and carboxymethyl chitosan (CMCts). More importantly, grafting sodium styrene sulfonate (SSS) on polysaccharide backbones for rising active sites. Gamma-induced irradiation was still applied. This new synthezied adsorbent can be called an interpenetrating network (IPN) hydrogel which is defined and classified as follow: "*Polymer comprising two or more networks that are at least partially interlaced on a molecular scale but not covalently bonded to each other and cannot be separated unless chemical bonds are broken*" as per IUPAC [96] and **Figure 33**. With these CMC and CMCts polymer networks are interpenetrated, the resulting hydrogel exhibited much improved mechanical properties and re-usability.

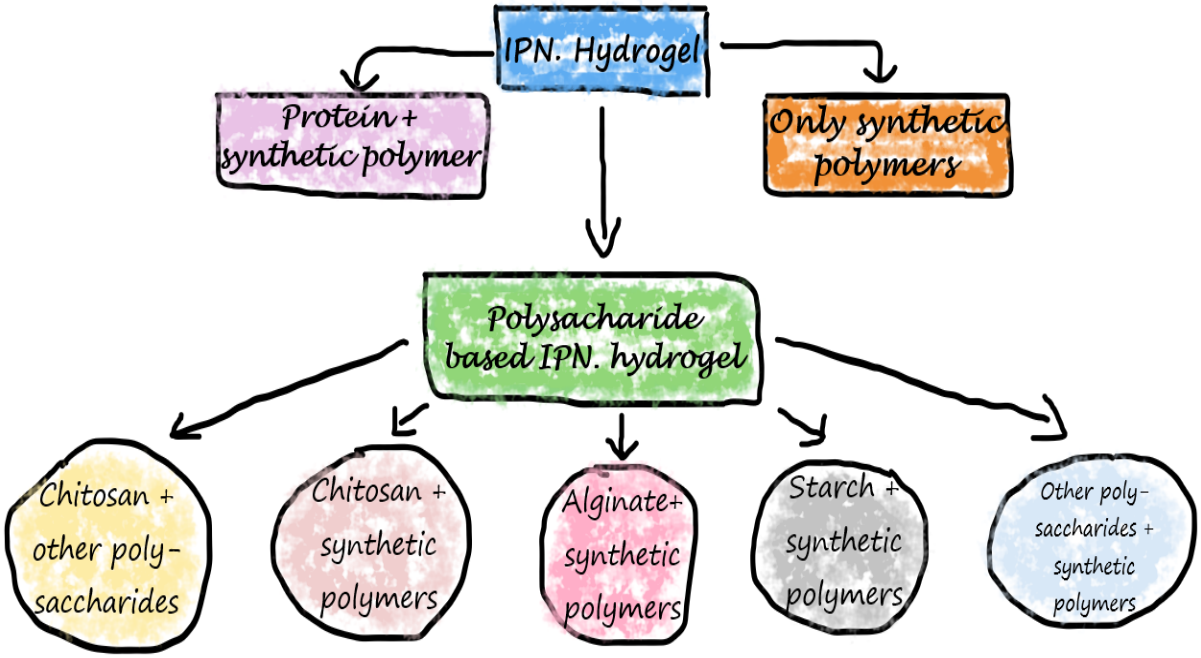

Figure 33. Some possible associations of hydrophilic polysaccharides used to synthesis IPN hydrogels [97][98][99].

I. Composing of selective IPN CMC-based hydrogel (abbreviated CCS hydrogel)

In the study for synthesis of binary gelling system, it was possible that hydroxyl group of CMC, amine group of CMCts and vinyl group of SSS monomer were attacked by many $HO^{\bullet}$, $H^{\bullet}$ and $H_2O^{\bullet+}$ energetic species from water to create new macro radicals [100][101]. After that, these polysaccharide polymer and vinyl monomer radicals react randomly and as a result, the hydrogel products with two kinds of interpenetrated cross-linked networks as well as higher grafting density are obtained. It is possible radical reactions between CMC and CMCts polymeric carbohydrates might be compatibilized by co-regeneration and electrostatic interaction to obtain CCS hydrogel. A supposed mechanism for binary hydrogel or CCS hydrogel synthesis is nearly same as the brief proposed synthesis of the grafted hydrogel from CMC and SSS and is displayed in **Scheme 6**.

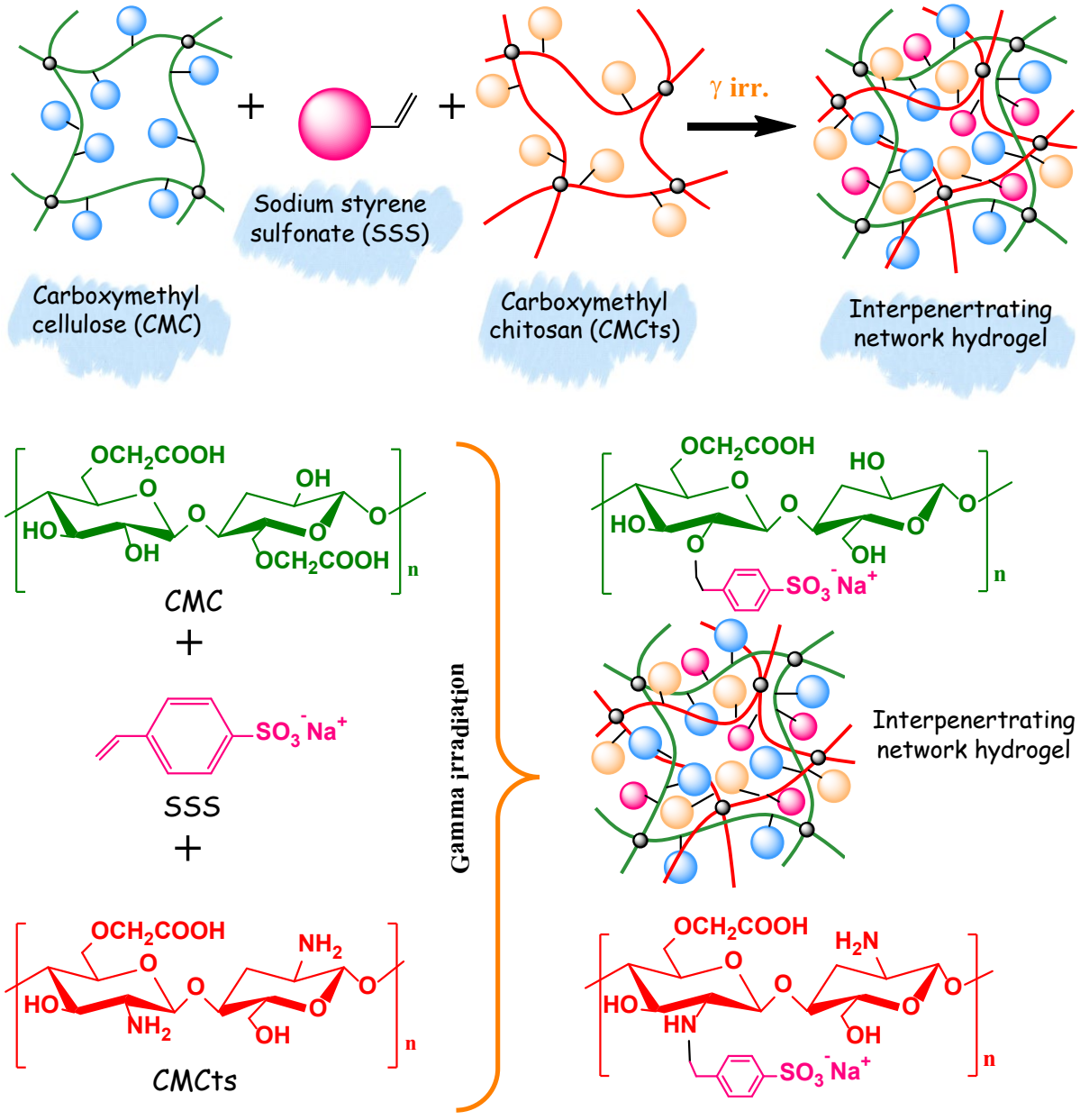

Scheme 6. Proposed composing of CCS hydrogel from CMC and CMCts.

II. Recognization of CCS hydrogel

1. FT-IR spectrum

The synthesis of studied IPN hydrogel CCS is based on blending process between CMC and CMCts in parallel in grafting reactions of SSS onto these polysaccharides. FTIR spectrum of CCS hydrogel (**Figure 34**) has all relevant peaks of CMC: 3346 cm^{-1} (free O–H stretching vibration in cellulose chains), 1651 cm^{-1} (the carboxylate group), 1332 cm^{-1} and 1423 cm^{-1} (C–H and O–H stretching vibrations in CMC plane), 1076 cm^{-1} (the C–O–C stretching of glycosidic ether) [102]. The FT-IR spectrum of CCS also displays the characteristic absorption bands of CMCts at: 1598 cm^{-1} (N–H stretching vibration), 1430 cm^{-1} ($–COO^-$ stretching vibration) and 1056 cm^{-1} (C–O stretching of secondary –OH group). Supportably, the new peaks on the CCS hydrogel spectrum at region of 1653, 1516 & 1400 cm^{-1} are signed for $–C_{ar}–C_{ar}$ bonds; two types of peaks at 1187 & 1141 cm^{-1} and 1042 & 988 cm^{-1} presented respectively for stretching of S=O and $–SO_3Na$ group [62], indicating the presence of SSS in the CCS sample. This newly detected functional groups in IPN hydrogel CCS were likely responsible for the high swelling and metal adsorption capacity [101][103].

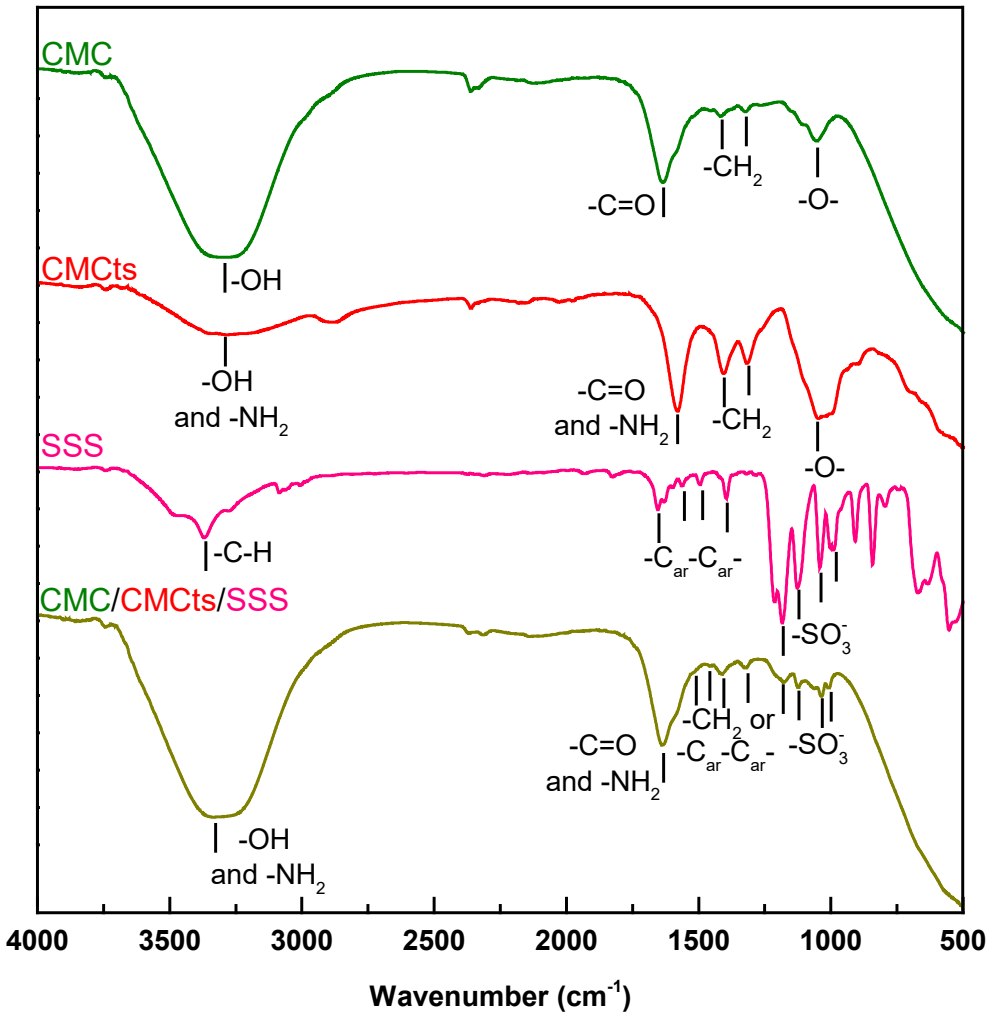

Figure 34. FT-IR records of CMC, CMCts, SSS and CCS interpenetrating polymeric hydrogel.

2. ^{13}C-NMR Nuclear magnetic resonance spectroscopy

From **Figure 35**, the ^{13}C-NMR spectroscopy of CCS hydrogel validated the earliest resonances in 35 – 40 region of C–C (C_b) or C–N single bond (C_2, C_a). The next signals in an area of 58 – 62 might be C-OR bonds like Carbons at positions a', 2', 6 and 7 in the molecular of hydrogel. The highest signal at around 74 ppm is for C–C of glucose rings (C_3, $C_{3'}$, C_4, C_5). The peak at 110 ppm is corresponded to O–C–O at 1' and 1 ($C_{1'}$, C_1). The CCS hydrogel exhibited the resonances of the SSS in the aromatic region of 126, 142 and 149 ppm ([C_d, C_e], C_f and C_c). The last peak at 178 ppm is from C=O bonding, (C_8 in an acid or ester). All above-mentioned ^{13}C-NMR results can be the evidence of the occurrence of SSS, CMC and CMCts in the CCS polymerization.

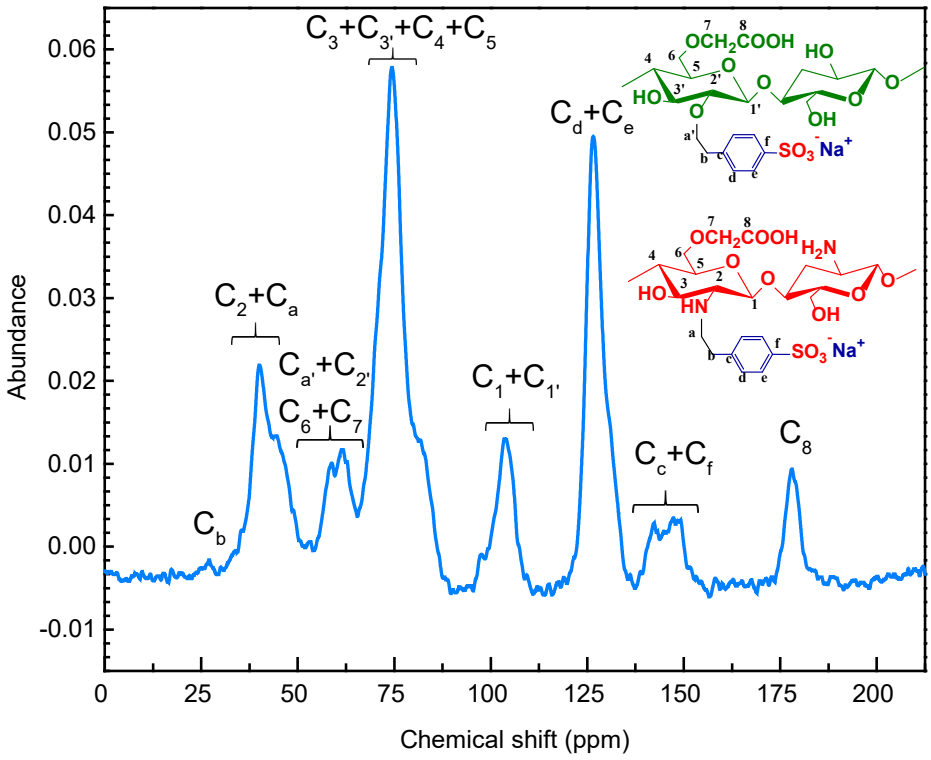

Figure 35. ^{13}C-NMR record of CCS hydrogel.

3. *EDS and SEM analysis*

a. *EDS*

EDS technique was used to analyze element or to describe chemical composition of CCS hydrogel. As described in Chap.2 Sec.IV.5, EDS spectrum is formed from the interaction of electromagnetic radiation and matter, and then analyzes the X-rays emitted from matter during interaction with electromagnetic radiation. Because each element has a geometric atomic structure, it has different scattered X-rays energy. Based on the gotten EDS spectrum, all elements can be identified.

The EDS spectra of interpenetrating polymeric hydrogel (CCS) and CMC/CMCts are showed in **Figure 36**. As shown in the figure, all peaks corresponding to presence of C, N, O and Na elements from CMC/CMCts copolymers were observed (except for a pre-coat conductive signal Pt [platinum atom]). In addition, it was also confirmed that SSS was clearly joined on the CCS synthesis because the CCS hydrogel spectrum has an additional peak of S element compared with that of CMC/CMCts copolymers.

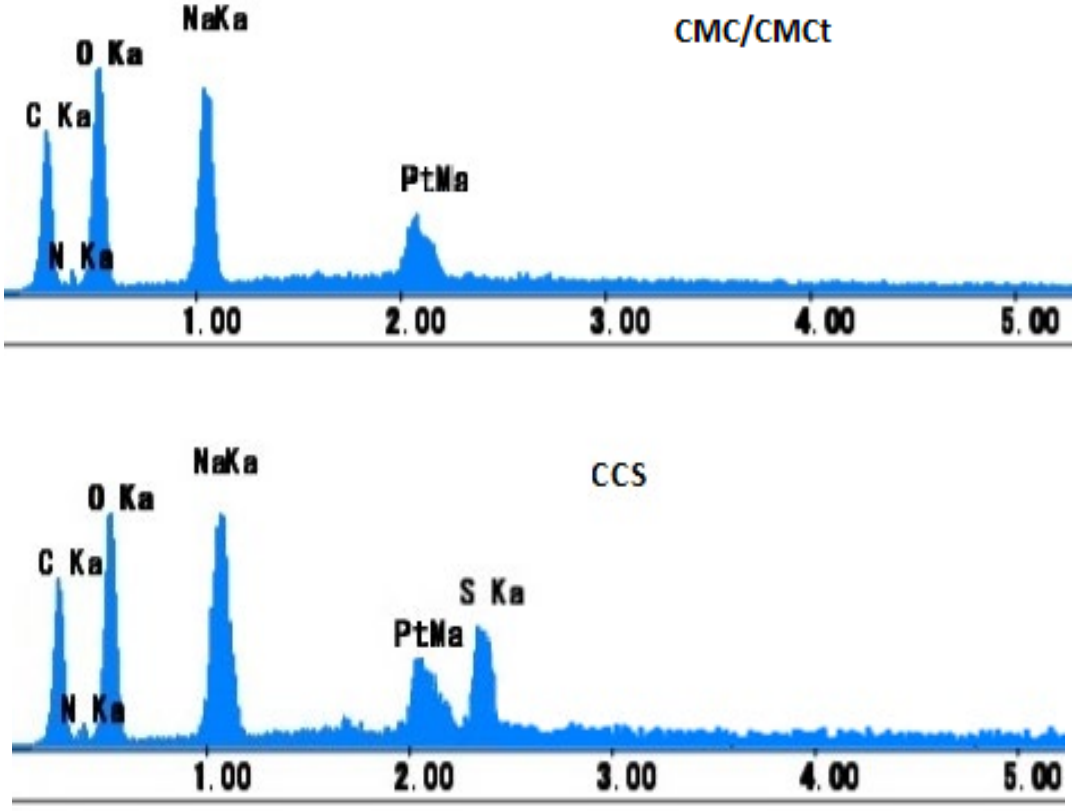

Figure 36. EDS spectra of CMC/CMCts and CMC/CMCts/SSS (CCS).

b. SEM

The SEM images to comprehend the surface of hydrogel samples including CMC, CMCts, CMC/CMCts and CCS are summed in the **Figure 37**.

It can be easily seen from the figure, the observed surface of CMC, CMCts hydrogel and CMC/CMCts hydrogel were wavy and granule, smoother but weakly rugged and almost smooth with parallel lines, respectively. Seemingly three SEM photograph images of CMC, CMCts and CMC/CMCts surfaces were quite similar. The resemblance of these surface images can be explained by compatibility of CMC and CMCts polymers resulting from their almost identical molecule-structures: they can tend to clump together, which might lead to the formation of tight structures with high-density network-crosslinking points during crosslinking process under the gamma irradiation [34].

On the other hand, after adding SSS into the mixture of CMCts and CMC during CCS synthesis, the surface morphology became considerably different. Various holes and gaps might be created by existence of SSS during the grafting and crosslinking process. These holes and gaps looked like to interconnect to each other and to form capillary channels, which might indicate the priority of the grafting process of SSS onto CMC and/or CMCts skeletons to the connection processes of CMC and CMCts polymers during gamma irradiation; in such a situation, bulky and porous structures could occur and their surface would be rough. In addition, the presence of sulfonate group ($–SO_3^-$), amine ($–NH_2$) and carboxylate ($–COO^-$) groups in the CCS hydrogel would greatly increase the affinity for H_2O molecules because these functional groups are reported to act as a H-bond donor or an acceptor [104], therefore, H-bonds among CMC, CMCts and SSS could also make CCS hydrogel's surface more irregular [105]. CCS hydrogel with rougher hydrophilic surface areas with more cavities would have smoother contact area to the migrating aqueous solvent which can cause higher permeation property with H_2O, which would indicate that CCS hydrogel would potentially enhance the internal diffusion of metal ions.

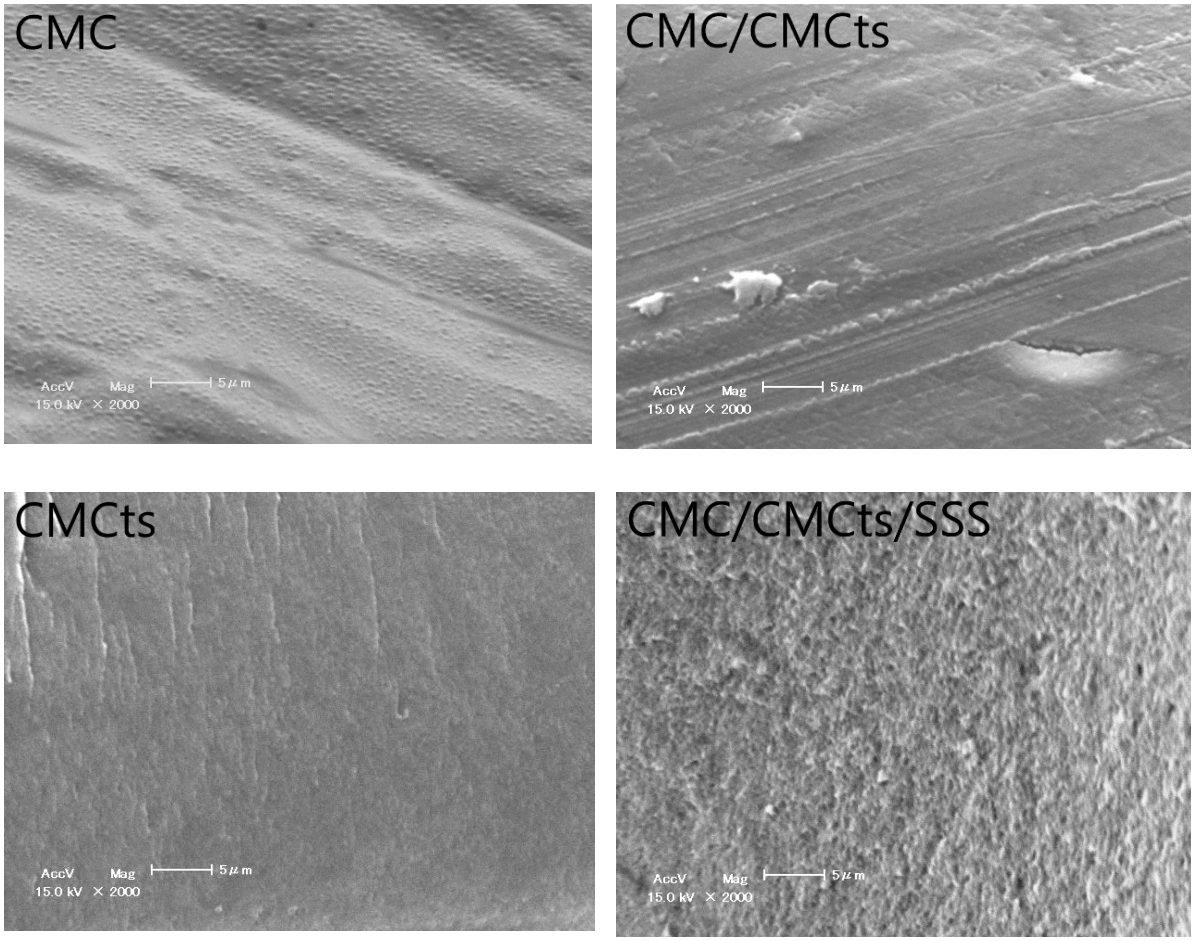

Figure 37. The surface morphology SEM of CMC, CMCts, CMC/CMCts and CCS (Mag. ×2000).

The usual usage of SEM photograph is to distinguish the surface patterns qualitatively, such as “rough” or “smooth” as described above. However, the photograph itself has more information than the qualitative ones. In order to extract more quantitative information from SEM photograph, the author conducted 2-dimensional (2D) Fourier Transform analyses of the SEM photographs of CMC, CMCts, CMC/CMCts and CCS hydrogels. By utilizing the analyses, the author could successfully extract the more quantitative information on the surface patterns of the hydrogels and make clear the difference and similarity of them more in detail.

In the present study, in order to derive the 2D Fourier Transformed image, commonly used two-dimensional fast Fourier transform (2D-FFT) method was adopted by utilizing an image processing software (NIH ImageJ, http://rsb.info.nih.gov/ij).

The procedures were as follows: Before converting to the 2D-FFT Power Spectra, the original SEM photographs were converted to 8-bit grayscale TIFF files and cropped to 256×256 pixels corresponding to 19.4×19.4 μm area in real space with a resolution of 0.0758 μm/pixel (**Figure 38a)**. By operating the software, the 2D-FFT images of the SEM surface pattern were derived as shown in **Figure 38b**. Bright horizontal and perpendicular lines crossed at the center in the 2D-FFT images appeared from the step-like brightness difference on the edge of the image, which were not originated from the hydrogels. 3 dimensional distribution of the 2D-FFT power spectrum were plotted in **Figure 38c,** in which z-axis corresponds to the power-spectrum intensity.

	CMC	CMCts	CMC/CMCts	CCS
a	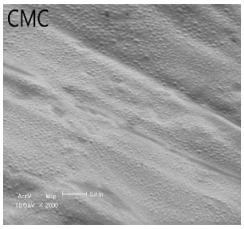	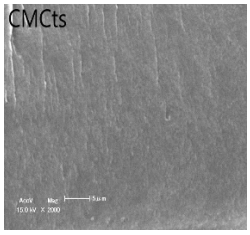	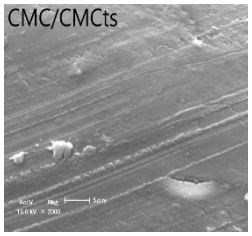	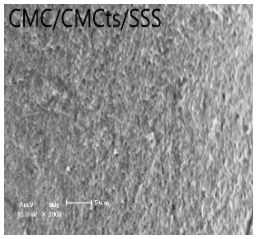
b	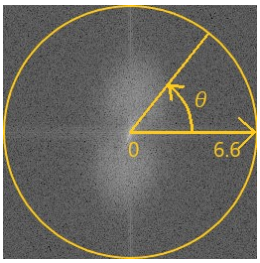	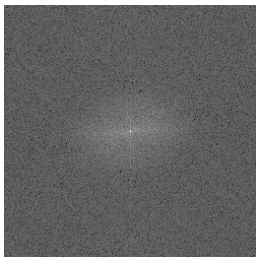	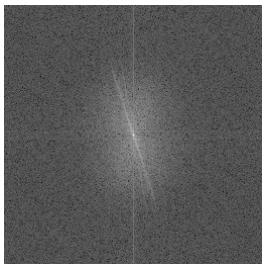	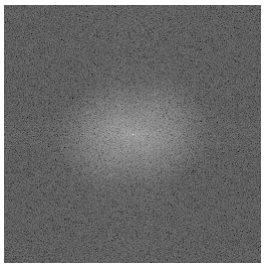
c	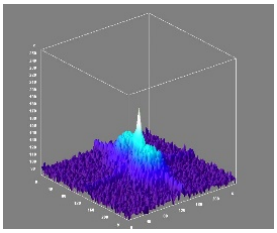	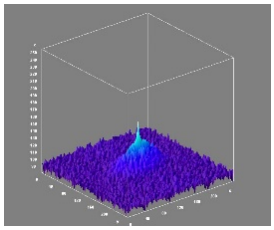	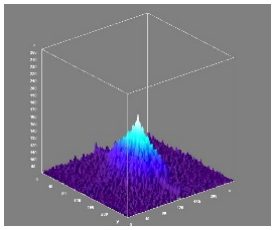	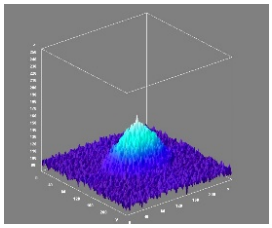

Figure 38. 2D-FFT analysis of hydrogels: (a) Original SEM photos; (b) 2D-FFT power spectrum results; (c) 3D-images of power spectra.

To characterize hydrogel microstructure, the power spectrum is computed and analyzed in two different methods. First, we look for the orientation distribution by calculating the average intensity depends on the angle. For each angle between 0 and 180° (1° increment), all pixels within the radius of 128 pixels, i.e. 128/19.4 = 6.6 μm^{-1} were examined. The CMC and CMC/CMCts computed data in the **Figure 39** show the characteristic of isotropic material. However, the broad distribution around 73° for CMC and the peak at 107° for CMC/CMCts are corresponded to the cutting technique when we prepare the samples but their morphology. The smooth variation that we can observed from CMCts and CMC/CMCts/SSS confirm the anisotropy of the sample surface.

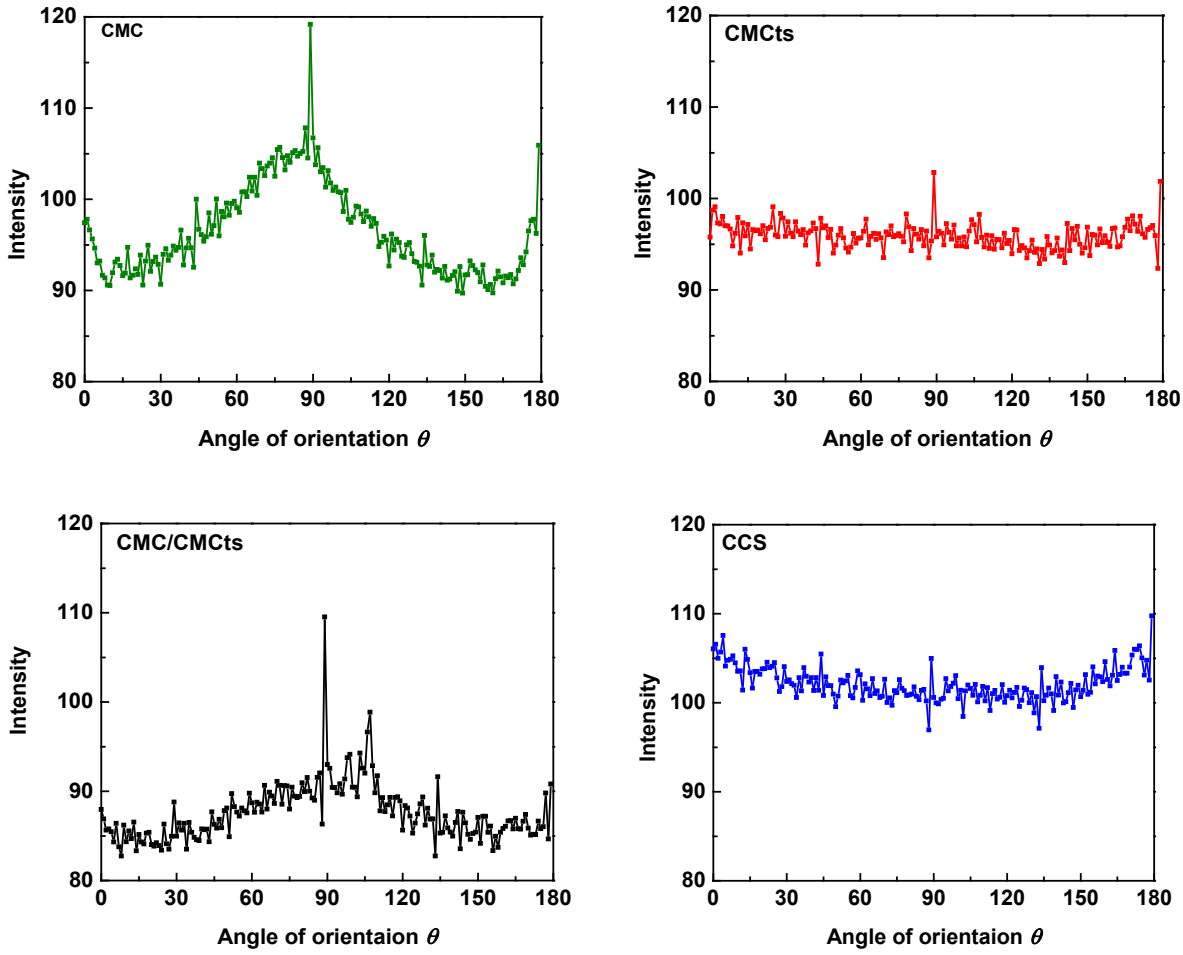

Figure 39. Intensity plots against the angle of acquisition of 2D-FFT power spectra.

The average intensity plots against the angle of orientation θ of hydrogel microstructure are shown in the **Figure 39**. Because each pixel in the grayscale image has only an amount of light, i.e. it carries only intensity information from 0 to 256. The average intensity in this our study varies from black at the weakest intensity (0 value) to white at the strongest (119 value). As can be seen for all 4 cases, there a strong peak at 90°. This is due to the step difference occurring at the edge of the image as mentioned before. Other featured peaks may be caused by cutting lines during sample preparation. Based on the result of intensity, CMCts microstructure is least oriented while the CCS microstructure has 2 main directions. Both CMC and CMC/CMCts angle of orientation graphs present increasing intensity at less than around 73° and 107°, respectively; and then decreasing at higher orientation. It means that CMC and CMC/CMCts might be have main 73 and 107° direction-microstructures, respectively. This different direction among four types of hydrogel is due to difference of components inside hydrogel network.

Second, the radial distribution of 2D-FFT image was also computed. All pixels have the same radius are counted. The average intensity in grayscale depending on the radius in wavenumber (μm^{-1}) is plotted in **Figure 40**. It can be seen in the **Figure 40** that the average intensity of 4 hydrogels present decays with the wavenumber. In the case of CMCts, the red curve shows a plateau at higher wavenumber than 2.78 μm^{-1} with lower intensity while the blue one of CCS displays a plateau from 3.86 μm^{-1} and highest intensity. It reveals the lack of absolutely significant periodicity in the origin microscopic image of CMCts. In other words, there is least periodical structural pattern presented in CMCts and the surface of CCS is the roughest, which agrees well with the visual assessment of the microscopic images. As for CMC, CMC/CMCts (the green and black curves), they present a plateau of intensity at wavenumber higher than 4.07 and 4.27 μm^{-1}, respectively. These curves of two hydrogels display a broad wavenumber range. This corresponds to the diffuse pattern on the power spectrum. Thus, their observed microstructures are actually a combination of some periodical patterns with around 4 μm^{-1}-wavenumbers.

Based on all information from the above **Figure 38**, **Figure 39** and **Figure 40**, we could conclude that the surface morphology of 4 types of hydrogel are different.

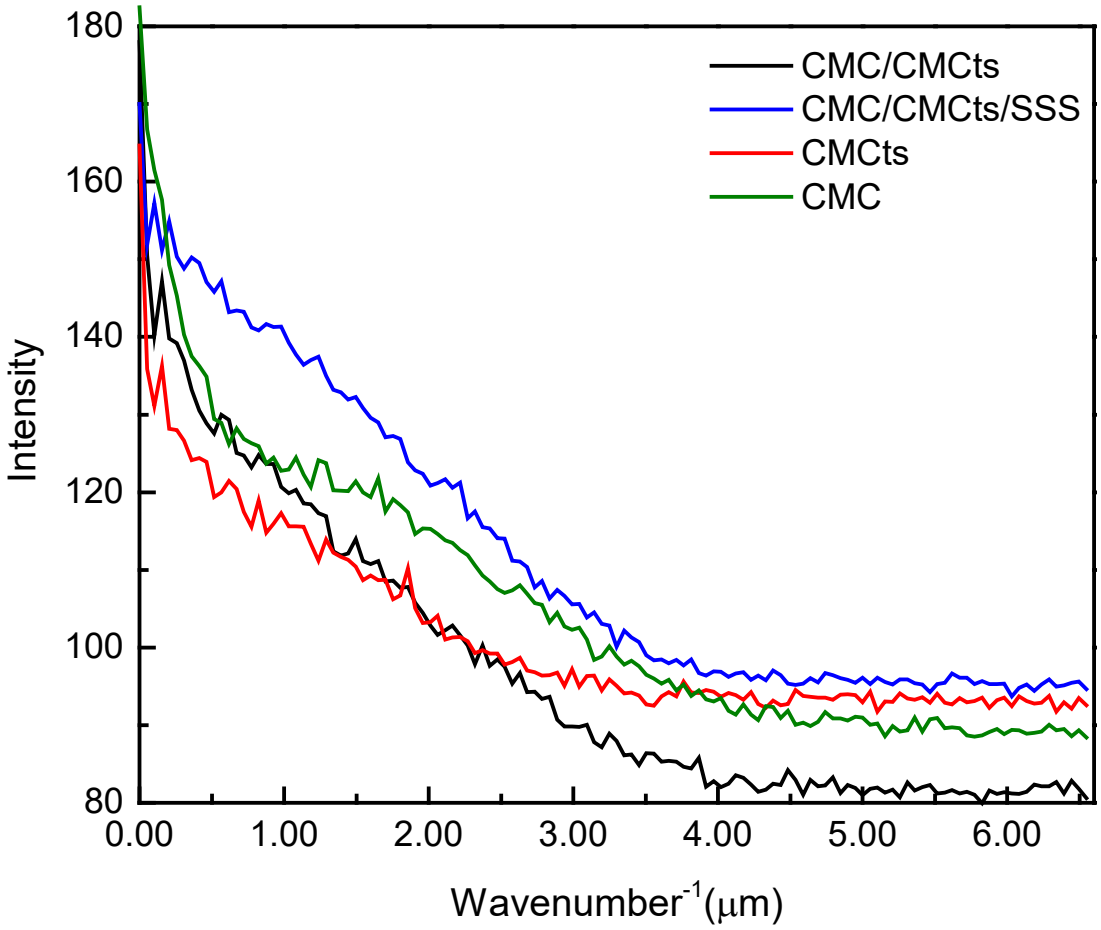

Figure 40. The radial distribution of intensity against wavenumber.

4. Swelling ability

The swelling ability of a hydrogel synthesized by gamma irradiation is always influenced by preparation conditions such as irradiation dose or component content. In the present investigation, observed were the swelling capacities of IPN CCS hydrogels with the different ratios of components at room temperature after immersion in DW for 48hrs. All the data of swelling ratio vs. SSS concentrations is summed in **Figure 41**.

The swelling ratio (g/g) raised significantly from 500 to 2500 (g/g) with SSS concentration from 0.00 to 0.32 M. This phenomenon could be explained by the presence of the $–SO_3^-$ group, which has greater affinity with water molecules compared with $–COO^-$ and $–NH_2$ groups. However, when we continued adding more SSS (> 0.32 mol/L) and simultaneously decreased amount of CMC and CMCts, the swelling capacity of CCS hydrogel reduced immediately; this could be caused by:

(a) the increasing in homo-polymerization of SSS monomers might cause reducing of SSS grafting process. Those SSS polymers are easily dissolved in water later.

(b) the ionic interaction among hydroxyl, sulfonic, carboxylic and amine groups leading decreasing in hydrophilic property of these groups.

The above reasons would make the structure of hydrogel rigid, preventing the diffusion of water molecules into the hydrogel structure network to encounter hydrophilic groups. Similar detection was reported by other researchers [106]. These data indicated the optimal concentration of SSS for CCS preparation was 0.40 M and the CCS hydrogel with the weight ratio of (CMC:CMCts) : SSS = 4:2 was chosen for next studies.

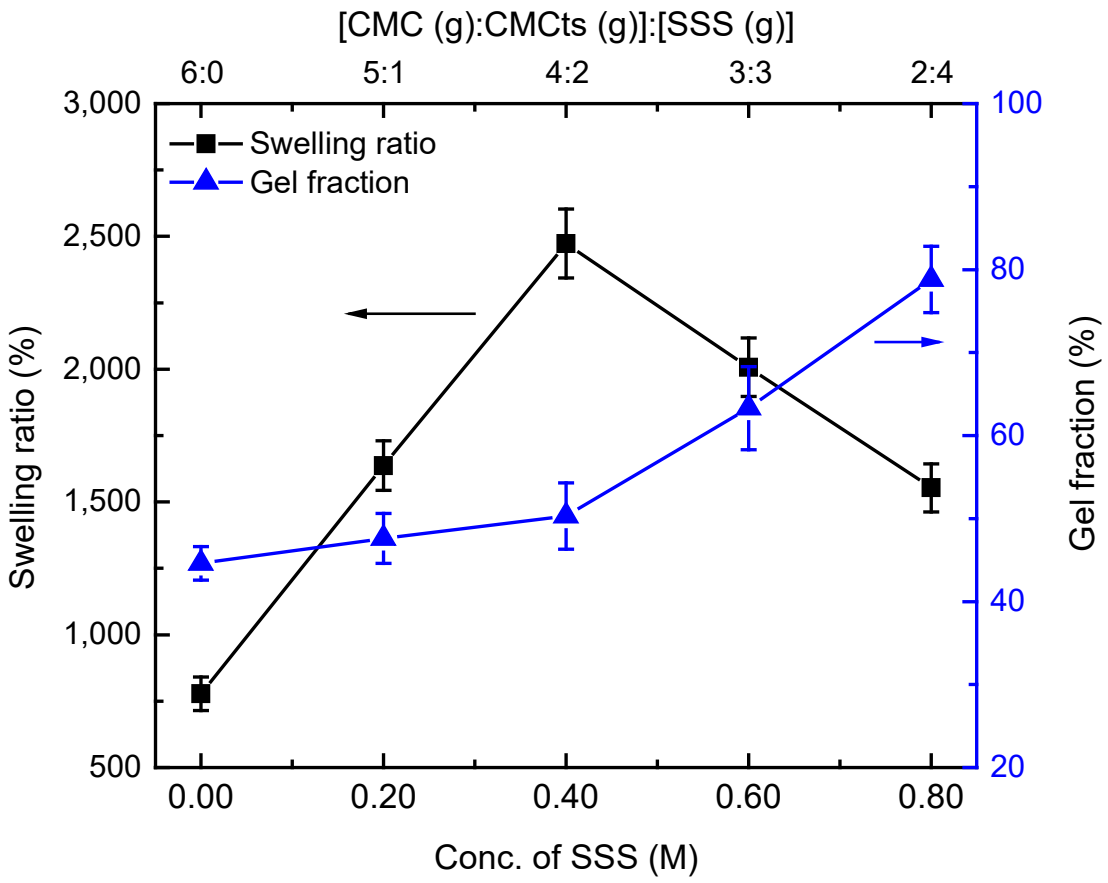

Figure 41. SSS content influence on water-uptake capacity of the CCS (irradiation dose 60 kGy).

III. Metal adsorption behaviors

Batch mode experiments were conducted on the adsorption of heavy metals by adding CCS cubes into 50-mL capped PP tubes that contained 40 mL of metal ion solutions. The experimental conditions to examine metal adsorption capacity of CCS hydrogel adsorbent are shown in **Table 19**. All the experiments were performed in triplicate, and the procured data were analyzed by Origin software 9.0 (OriginLab, Northampton, MA, USA.).

Table 19. Summarized batch mode experimental conditions.

Experiment conditions	Experiment Parameter
Competitive adsorption	Contain multi-elements with initial concentration of 0.10 mg/L; contacting time 24 hrs., pH = 5
Weight of adsorbent	Adsorbent weight of 0.100, 0.200, 0.400 and 0.600 g; initial concentration of 0.10 mg/L; pH = 5
Contacting time	Contacting time of 0.5, 1, 2, 4, 5, 7, 10, 15, 24, 35 and 48 hrs.; initial concentration of 0.100 mg/L; pH = 5
Initial heavy metal ions concentrations	Initial heavy metal ions concentrations of 0.05, 0.10, 0.20, 0.50, 1.00 and 2.00 mg/L; contacting time 24 hrs.; pH = 5
Initial pH values	Initial pH values of 1,2, 3, 4, 5, 6, 7, 8, 9, 10 and 12; initial concentration of 0.100 mg/L; contacting time 24 hrs.

1. *Metal adsorption selectivity*

The first trials of CCS hydrogel's adsorption for Ag^{+}, Cu^{2+}, Cr^{3+} and Ni^{2+} from the respective single-ion solutions are illustrated in **Figure 42**. All the prepared 0.5×0.5×0.5-cm^3-hydrogels (0.200 g) were opalescent and white. After 10 hrs. of adsorption process, all the CCS hydrogel blocks colored indicating adsorption of the metal ions via the strong interaction between CCS hydrogels and metal ions. This result exhibited that the CCS hydrogel could be applied for removing the metal ions out of their aqueous solutions.

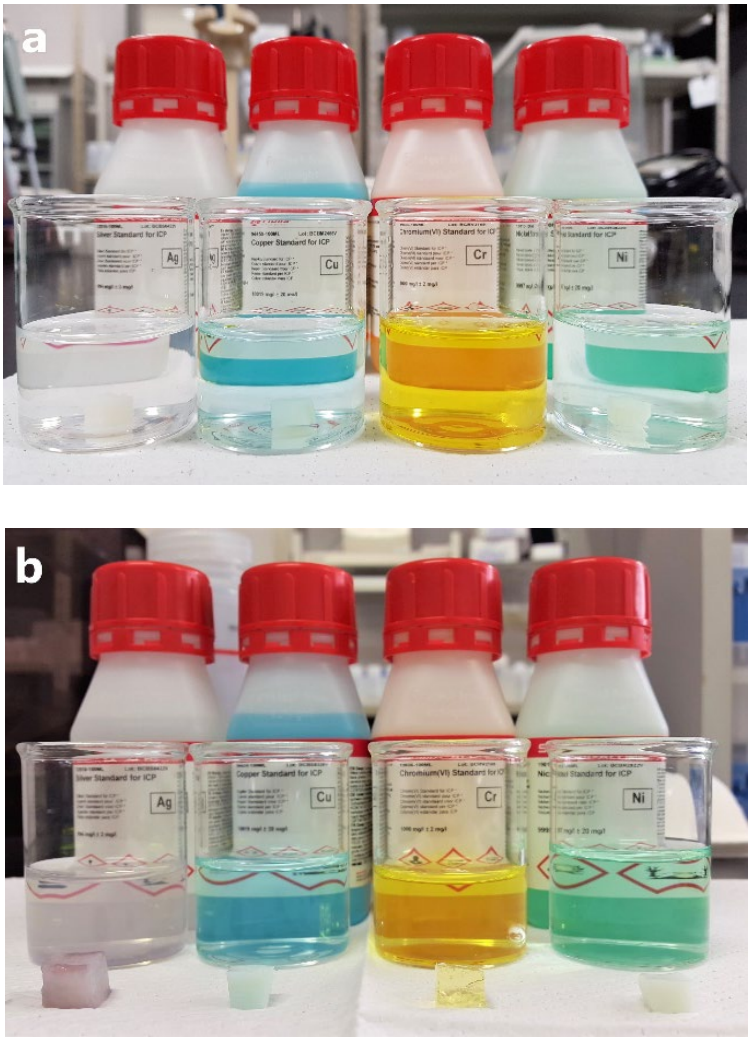

Figure 42. Interaction between metal ion (Ag, Cu, Cr, Ni ions) and CCS hydrogel before (a) and after (b) adsorption.

The selective adsorption of an adsorbent for a metal ion may be influenced by co-existing of other ions in solution. To determine Ag ion uptake selectivity of CCS hydrogel, we used single- (Ag, Cd, Cs, Cr), binary- (Ag + Cd; Ag + Cs and Ag + Cr) and multi- (Ag, Mo, Ni, Cu, Zn, Cd, Co, Cr, Mn, Cs and V) element metal ion solution in polypropylene tube with all metals having initial concentration of 100 µg/L. CCS hydrogel adsorbents of 0.200 g cubic sizes were immersed into 40 ml of this metal ion solution for 48 hrs. All batch adsorption experiments were done at 25 ºC without any stirring. The metal-adsorbed hydrogel was then extracted from the solution and the change in concentration of the residual solution measured using ICP/MS instrument.

The **Figure 43** displays the results measured in the single-, binary- and multi-metal-ion adsorption experiments. Under both of the single or competitive conditions, the functional groups of CCS hydrogel showed a high selective-adsorption capacity to Ag^+. The main reason for the Ag^+ selectivity could be as follows:

(i) Silver is a monovalent metal, so each activated site in CCS hydrogel could bind one Ag^+.

(ii) The amine groups of CCS hydrogel can easily form covalent bonds with Ag^+ ions. According to the HSAB tendency mentioned in Chap. 1-Sec.II.b, the N ligands on amine groups can be considered as soft bases, on the other hand, Ag^+ can be considered as a soft acid. Generally, hard acids coordinate better with hard bases and soft acids with soft bases. Therefore, a strong interaction between Ag^+ and amine group bearing CCS hydrogel are expected.

(iii) Ag^+ has higher electronegativity (1.93 in Pauling scale), compared with other metal ions which refers to relative stabilities of complexes formed by transition metal with ligands [107][108].

With the above explanations, the CCS hydrogel could show a higher selectivity for Ag^+ and the Ag^+ sorption was less influenced by the presence of other ionic species in the solution. From the characteristic property, Ag ion was chosen to investigate the detailed adsorption behaviors of CCS hydrogel.

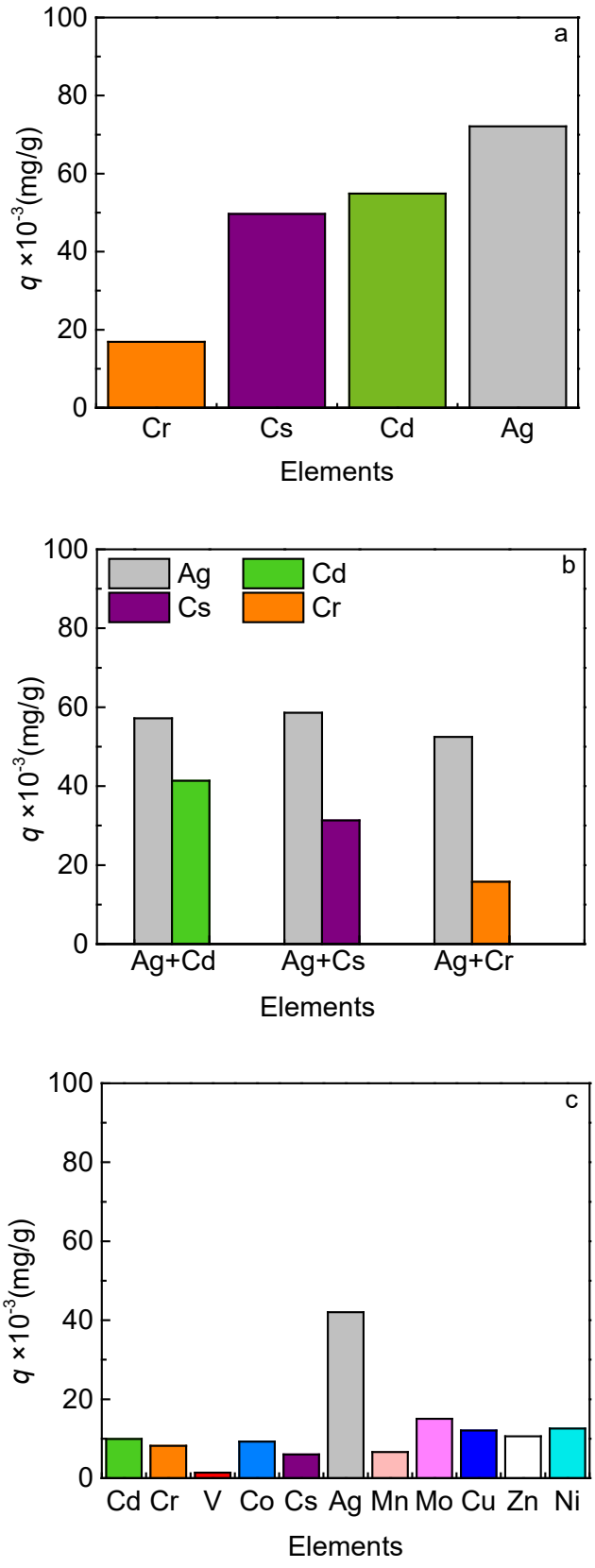

Figure 43. Selective adsorption capacity for Ag^{+} by CCS hydrogels in non-competitive (a) and competitive (b and c) condition.

The selectivity of the CCS adsorbent for Ag ions was calculated from the distribution coefficient K_d (mL/g) and selectivity coefficient α (dimensionless) using **Eq. 1** and **Eq. 2** as mentioned in Chap.1 Sec.II.4.a. The K_d and α in details are all displayed in **Table 20** . It indicates obviously the CCS hydrogel had selectivity for Ag^+ over others in the multi-element solution and the calculated selectivity coefficient for the CCS hydrogel to bind Ag^+ over other species decreased as follows: Ag > Mo > Ni > Cu > Zn > Cd > Co > Cr > Mn > Cs > V. The Ag selectivity sequence for the CCS hydrogel which refers to the relative stabilities of complexes formed by Ag ions and the ligands i.e –COOH, $–SO_3H$ and $–NH_2$ groups.

Table 20. Competitive binding behaviors of CCS hydrogel for Ag^{+} over other ions.

Experimental solution	Metal ion	K_d (mL.g^{-1})	α
Single-component Ag	Ag	0.5536	
Cd	Cd	0.2588	2.1387
Cs	Cs	0.2039	2.7157
Cr	Cr	0.0411	13.4751
Binary-components Ag/Cd	Ag	0.2369	
Ag/Cs	Cd	0.1444	1.6404
Ag/Cr	Cs	0.0916	2.5872
	Cr	0.0375	6.3174
Multi-components Ag/Cd/Cr/V/Co/Cs/Mn/ Mo/Cu/Zn/Ni	Ag	0.1498	
	Cd	0.0221	6.7761
	Cr	0.0180	8.3341
	V	0.0029	52.1125
	Co	0.0204	7.3258
	Cs	0.0128	11.7124
	Mn	0.0143	10.5040
	Mo	0.0357	4.1928
	Cu	0.0276	5.4321
	Zn	0.0238	6.2903
	Ni	0.0289	5.1743

2. *Effect of weight ratios of (CMC+CMCts) to SSS on Ag^+ adsorption*

The molar ratio of SSS monomer to (CMC+CMCts) polymers, i.e., the number ratio of active sites to network-polymer molecules in the CCS hydrogel, influenced considerably on the capacity for adsorbing metal ions.

As shown in **Figure 44**, the hydrogel composed of only CMC and CMCts polymers (weight ratio 6:0, [0.18 + 0.28 mM of CMC+CMCts]:0) exhibited very low adsorption-ability and removal of silver in solution. The adsorption capacity increased with the elevation of SSS ratio (from 0.00 to 0.40 g in M) and became a maximum at {4}:2 of {CMC+CMCts}: SSS weight ratio ([0.12 + 0.18 mM of CMC+CMCts]:0.4 M). Such a difference in the adsorption capacity could be originated from the promotion of Ag^+ adsorption by the presence of sulfonate groups in the CCS hydrogel, which would be superior to those of carboxylate and amine groups [109]. On the other hand, Ag adsorbed amount showed a decrease in the higher region of SSS ratio (from 0.40 to 0..80 g in M) in the similar way reported by Nitayaphat et al. who carried out radiation graft post-polymerization of sodium styrene sulfonate onto polyethylene [100].

Therefore, the factors listed below might affect Ag adsorption process in the present experiments, as explained in Ref. [100]:

(i) the grown radiation induced homo-polymerization of SSS monomer instead of SSS-grafting,

(ii) the overwhelming crosslinking process of CMC and CMCts polymers and

(iii) the ionic interaction among $–NH_2$, –COOH, and $–SO_3H$ groups.

So the ideal weight ratio of (CMC:CMCts) to SSS during CCS hydrogel synthesis to carture Ag^+ in aquatic environment was 4:2.

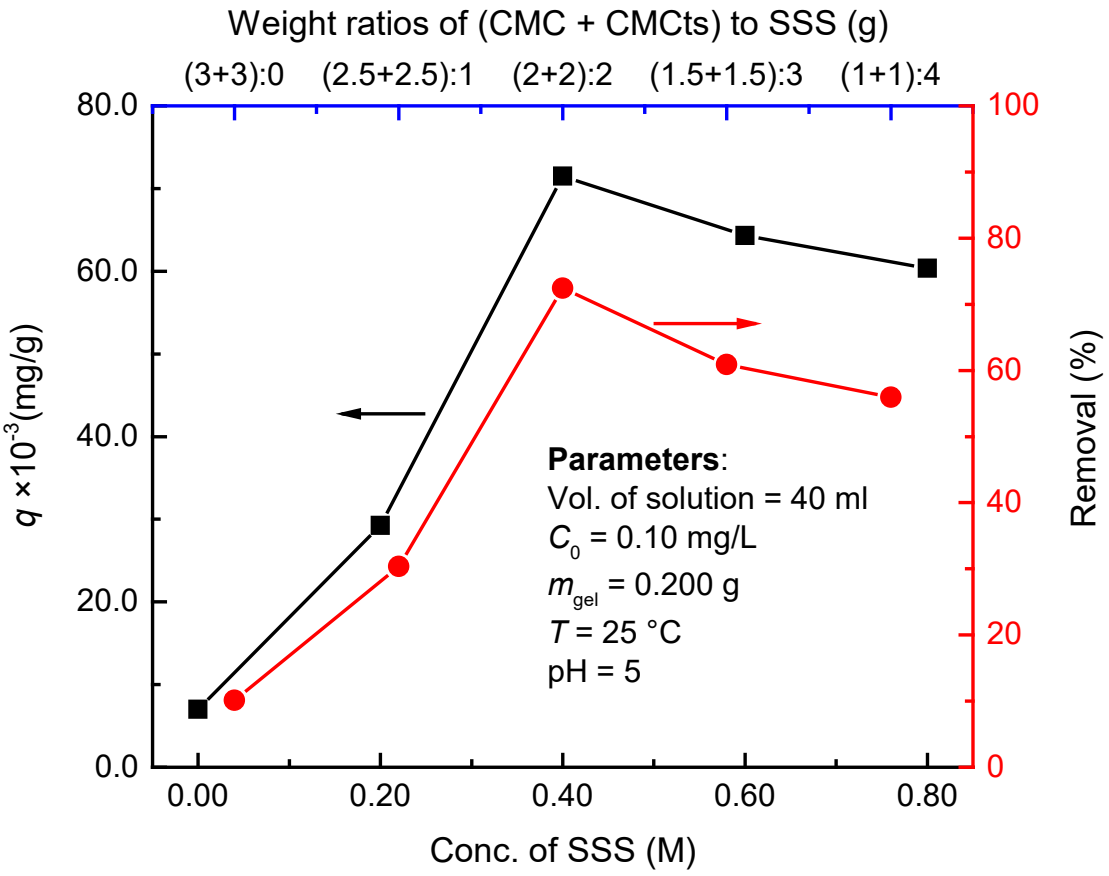

Figure 44. Weight ratio of (CMC/CMCts) to SSS effect on Ag^{+} adsorption performance.

3. *Effect of adsorbent weight*

Evaluation of the effect of adsorbent quantity or size on adsorption process seemed important from a practical viewpoint because apparent adsorption capacity in a limited period would be depend on diffusion velocity of metal ions and on their concentration gradient in the adsorbent. Therefore, in the present investigation, the author carried out the adsorption experiments with different adsorbent size.

According to experimental conditions described in **Table 19**, CCS hydrogel weight was varied from 0.100 to 0.600 g by taking all other parameters constant (solution vol. of 40 ml, pH = 5 and initial Ag concentration of 0.10 mg/L).

Figure 45 shows the results of the experiments. As is seen from the figure, Ag^+ removal was higher for the adsorbents with larger initial-weights: the Ag^+ removal amount change was large for the lighter adsorbents (42 wt% and 71wt% of Ag^+ removal for the adsorbents with 0.100 g and 0.200 g of weight, respectively) compared with those for the heavier ones (0.400 g and 0.600 g). In contrast to the Ag^+ removal, the adsorption capacities became were lower for the heavier adsorbents: the weight dependence of the adsorption capacity was almost a monotonous and showed a negative correlation (85.4 and 27.4 µg/g of adsorption capacity for the adsorbents with 0.100 g and 0.600 g of weight, respectively).

In the present experimental condition with the increase of the sorbent weight from 0.100 – 0.600 g in unchanged volume of solution while the adsorption capacity reduced clearly from 85.4 to 27.4 µg/g. This behavior might be explained that the adsorption capacity is calculated by the amount of absorbed metal ion (in µg) per weight of adsorbent (in g). In the adsorption experiments when the metal-ion diffusion is very slow, the amount of absorbed metal ion increases lightly whereas the used weight of adsorbent increases quickly, leading decreasing in adsorption capacity. However, percentage of removal is not calculated based on adsorbent mass. As the result, the removal percentage increases with increasing adsorbent weight.

Based on obtained data, further study of adsorption equilibrium was analyzed using 0.200 g of CCS hydrogel with adsorption capacity of 71.2 µg/g and removal of ~71 wt%.

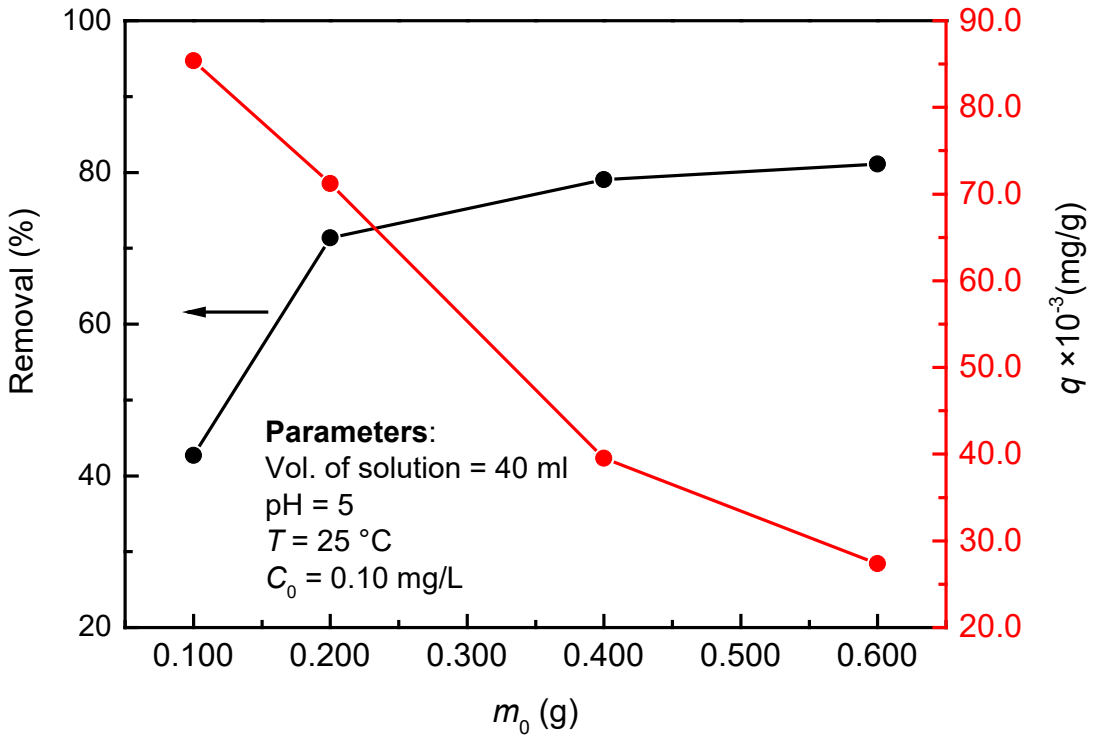

Figure 45. Influence of CCS adsorbent weight on Ag^{+} uptake.

4. *pH solution effect on selective adsorption for Ag^+*

Potential of hydrogen (pH) is one of the most important environmental factors affecting not only the active sites on the adsorbent but also the solubility of metals in solution. Hydroxide formation or complexing caused by redox reaction or precipitation is greatly influenced by the pH of the environmental reaction.

On the other hand, pH has a decisive influence on the formation and available capacity of heavy metal ions on adsorbent materials [110][111]. When pH of environmental reaction changes, it can induce the alterations of the hydrated forms of metal ions which will lead to changes in their natures, charges and sizes. With such a change, the metal ions will be possible to create complex, to be able to be adsorbed and to accumulate on the surface of the materials.

Numerous studies show that the pH value of the solution has a special effect on stemming biological adsorbents. This is because H^+ ions will compete with other adsorbates and because pH of the solution can affect the chemistry of the metal ions, as well as the ionized functional-groups on the adsorbent surface. Therefore, the pH value of the solution will be an important control parameter during biological adsorption; the pH value of the solution in the initial is more influential than that in the final stage.

To assess the effect of pH on Ag^+ adsorption capacity of CCS hydrogel, the experiments conducted were at different initial pH values from 1 to 12 as displayed in **Table 19**. Other experimental conditions such as 40-ml-solution of Ag^+ with initial concentration of 0.10 mg/L and CCS adsorbent weight of 0.200 g were confirmed.

As shown in **Figure 46**, the Ag^+ adsorption performance of the CCS hydrogels depend clearly on pH, of which the range was 1 – 12. It was found that the Ag^+ adsorption was favored at pH's from 4 to 6 (green points), maybe because functional groups like –COOH, $–SO_3H$ and $–NH_2$ in the adsorbents could be de-protonated, namely ionized at these pH values. In addition, silver in solution is known to exist in free Ag^+ ion form rather than hydroxide form in this pH range, which will make easy to form the complex of end groups in the adsorbents and Ag^+ ions.

The optimal pH value for the highest Ag^+ adsorption was ~5, which was chosen for the next experiments.

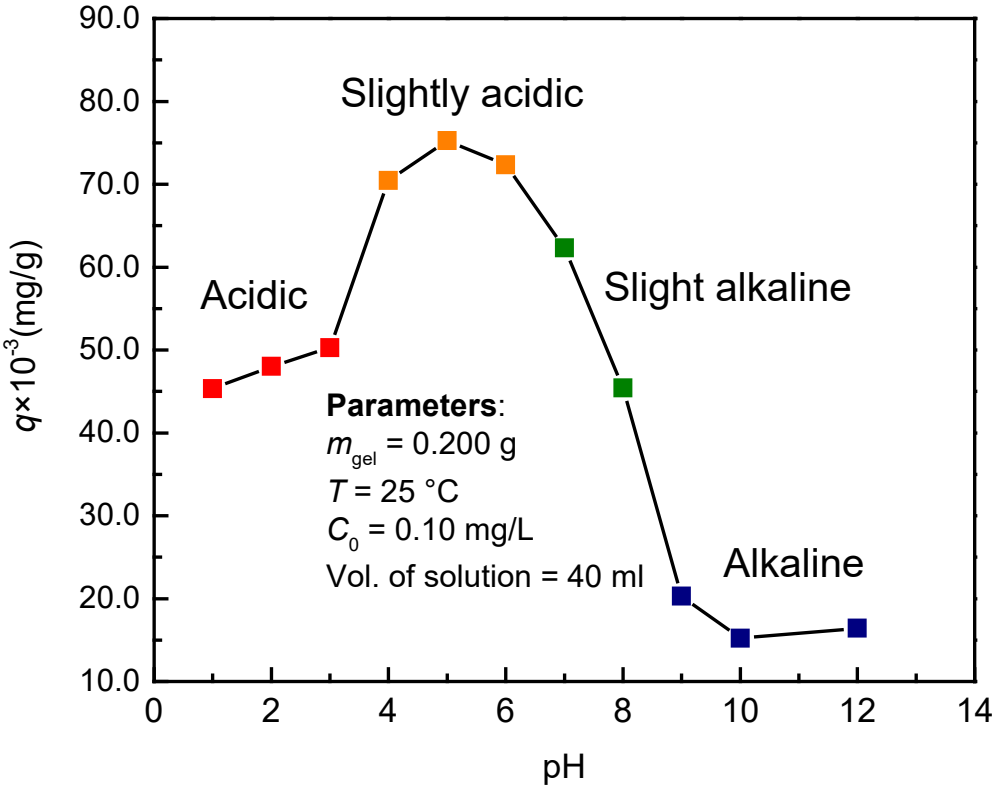

Figure 46. Effect of solution pH on Ag^{+} adsorption capacity of CCS hydrogel.

5. *Adsorption kinetics of Ag^+ metal ion system*

In the present experiment, the time variations of Ag^+ adsorption by a CCS hydrogel partly in order to confirm the period of the adsorption equilibrium, were investigated after having clarified the optimum conditions for Ag^+ ion adsorption by CCS hydrogels on the composition and weight of CCS hydrogel, and pH of the environmental solution, as describe in the preceding sections.

Experimental data obtained in the present investigation is depicted in **Figure 47**. As shown in the figure, Ag^+ adsorption by the CCS hydrogel increased with time exhibiting saturation in the later stage: in a period of 10 hrs. from the beginning of the experiment, adsorbed-Ag^+ amount promptly increased and reached 85 wt% of the amount initially dissolved in the solution, while, after then, the adsorption rate became considerably lower but the adsorption still increased until the end of the experiment (48 hrs.).

The adsorption time-dependence in the present investigation indicated that the diffusion of the metal ions was very slow and, in addition, the Ag-adsorbed parts in the hydrogel might hinder their diffusion into the inside through the network shrinkage and/or the interaction between the adsorbed and migrating Ag's. Such a consideration can be supported by the adsorbent-weight dependence of % removal and adsorption capacity (q) described in Chap.5 Sec.III-3.

In the present investigation, to elucidate the kinetic aspect of Ag^+ adsorption, time variation of the adsorbed Ag amount by CCS hydrogel was fitted by both of the pseudo-1st (**Eq. 6**) and pseudo-2nd (**Eq. 7**) order kinetic models and their suitability were assessed for explaining the kinetic mechanism, as introduced in Chap.1 Sec.II-4-d [45][47].

By comprehensive considerations of three criteria for adsorption capacity (q_{cal}), correlation coefficient (R^2) and chi-squared (χ^2) derived from the pseudo-1st- and pseudo-2nd-order-model fitting, which are shown in **Table 21**, the pseudo-2nd-order kinetic model were estimated to be more suitable than the pseudo-1st order one. Such a feature, which implies the better fitting by pseudo-2nd-order model, can be recognized from **Figure 47**.

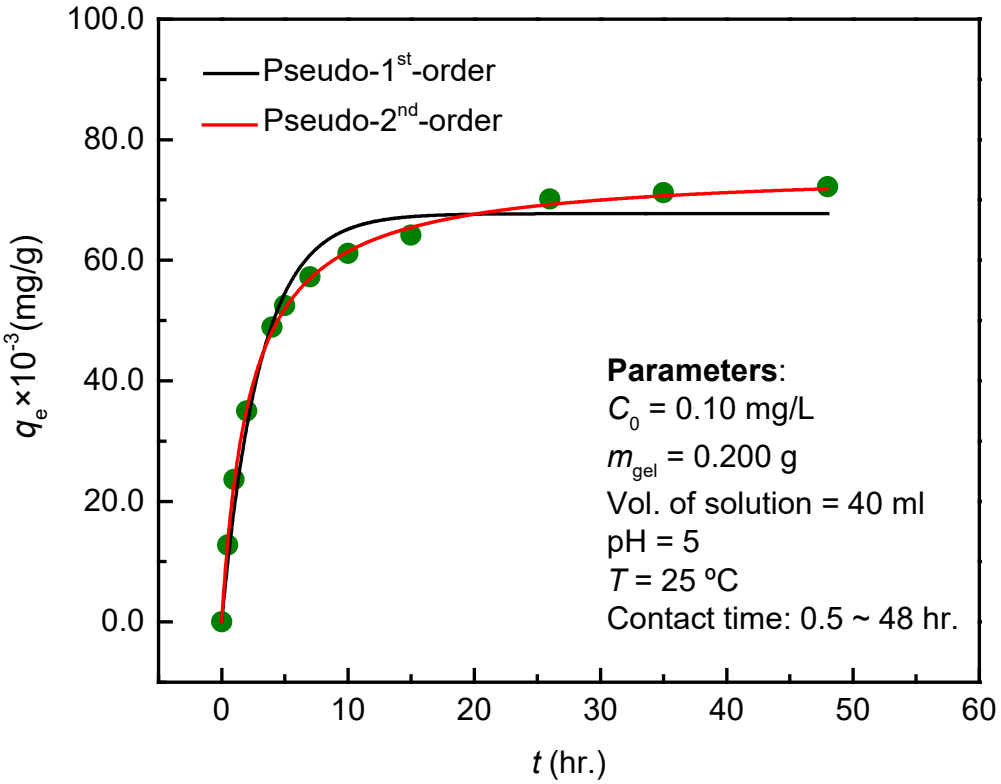

Figure 47. Dependence of Ag^{+} adsorption capacity of CCS hydrogel on contacting time.

Table 21. Calculated kinetic results of Ag^{+} adsorption process by CCS adsorbent.

C_0 (µg/L)	Pseudo-1st-order model				q_{ex} (µg/g)	Pseudo-2nd-order model			
	q_{cal} (µg/g)	k_1 (1/hr)	R^2	χ^2		q_{cal} (µg/g)	k_2 (g/[µg hr])	R^2	χ^2
100	67.7	0.327	0.981	10.9	72.2	75.2	0.0059	0.999	0.544

As can be seen in **Figure 48** and parameters in **Table 22**, the graph of q_t vs. $t^{0.5}$ was composed of three linear-portions which can be explained by the mechanism described in Chap.1-Sec.II-4-d [85]:

(i) Initial phase with fast pace which can correspond to the early stage of adsorption (green line),

(ii) Second phase with slower pace which can be explained by an intra-particle diffusion (black line),

(iii) Last phase reaching equilibrium in which the diffusion begins to reduce and cease (blue line).

These features indicated that Ag^+ adsorption process might include more than one step, similar to those reported by many ealier researches [112][113][114]. However, the third process (green plot) seemed to end in a short period and considered not to play an important role in the adsorption process.

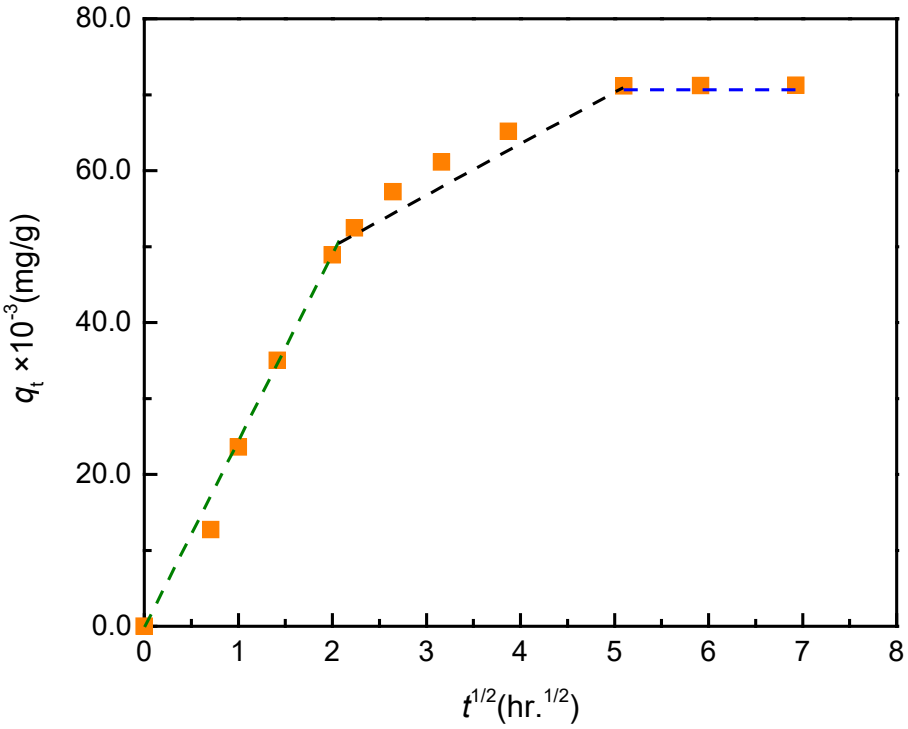

Figure 48. The graphs of q_t vs. $t^{1/2}$ for Ag^+ adsorption.

Table 22. Parameters for intra-particle diffusion.

Step	k_{id} (μg/[g $hr^{1/2}$])	C (μg/g)	R^2
Surface diffusion	25.2	1.73	0.989
Intra-diffusion	7.57	37.9	0.974
Equilibrium phase	0.042	70.9	0.795

6. *Adsorption activate energy*

In the present section, the activation energy E_a (kJ/mol) [Chap.1-Sec.II-4.e] for the Ag^+ adsorption by CCS hydrogel is estimated from the experimental results described in Chap.5 Sec.III-5.

As was described in Chap.5-Sec.III-5, the time variation of the adsorption capacity of the Ag^+ adsorption by CCS hydrogel can be well fitted by the pseudo–2nd–order kinetic model [**Figure 47, Table 21**]. The data necessary for calculating activation energy E_a (kJ/mol) could be obtained from the fitting parameters listed in **Table 21** for the pseudo–2nd–order kinetic model [Chap.1Sec.II-5]:

Adsorption-rate constant k_2 (g/[μg hr]),

Estimated adsorption capacity q_{cal} (μg/g)

Initial adsorption rate $A = k_2 \cdot q_{cal}^2$ (μg/[g hr]).

Because the data estimated from the fitting by the pseudo–2nd–order kinetic model are:

k_2 = 5.9 (g/[μg hr]),

q_{cal} = 75.2 (μg/g),

$A = 33.4\times10^{-3}$ (μg/[g hr]),

the activation energy (E_a) for the Ag^+ adsorption by CCS hydrogel was estimated as 21.4 (kJ/mol) at room temperature (T = 298 K). From the value of derived activation energy (E_a = 21.4 (kJ/mol)), the Ag^+ adsorption by CCS hydrogel could be regarded as a physical adsorption of which the activation energy should be less than 40 kJ/mol.

7. *Adsorption isotherms*

All 0.5×0.5×0.5-cm^3-CCS adsorbent cubes in amount of 0.200 g, were immersed into closed PP tubes containing 40 mL of Ag^+ solution samples. The Ag^+ initial concentration was changed from 0.05 – 2.00 mg/L to examine the interactive behavior between Ag^+ ions and CCS adsorbents. For each run, the batch adsorption proceeded until 24 hrs. under no agitation at room temperature. The Ag-laden adsorbents were later extracted from the solution and the final concentration of the remnant solution was measured using Agilent ICP/MS instrument. This experiment was repeated three times to ascertain consistency of adsorbent performance.

The results of effect of initial Ag^+ concentration on adsorption capacity q_e on CCS hydrogel was shown in **Figure 49**. The figure shows that, in the range of lower Ag^+-concentration from 0.05 – 0.50 mg/L, the adsorption capacity by CCS hydrogel increased linearly with the elevation of the initial Ag^+ concentration in the solution. When the initial Ag^+ amount was in the range of 0.50 – 2.00 mg/L, the adsorption capacity of the material raised with lower rate and reached a constant value. The maximum calculated Ag^+ adsorption capacity q_{max} in the experiment was 368.01×10^{-3}mg/g. Such a saturation could be explained as follows:

In the low metal-ion concentration region, the number of the metal ions might be smaller than that of the adsorbent's active sites capable of capturing metal ions. In this situation, almost all of the metal ions in the aqueous solution could be captured by the active sites without large impeding interaction

between the metal ions sparsely distributed both in the solution and in the adsorbent, therefore the adsorption amount could be simply increase with the concentration of the metal ions in the solution.

On the other hand, in the higher concentration region where the number of metal ions reached or exceeded that of the active sites in the adsorbent, the simple adsorption in the low concentration range could not take place by considerable decrease in the acceptable site in the adsorbent and/or by increase in the repulsive force from the metal ions of the same polarity which had been already adsorbed to the adsorbent, in spite of high osmotic pressure resulted from the interaction between a large number of the metal ions (also with the same polarity) in the solution. Under such circumstances, the increase rate of adsorbed metal-ion amount with the elevation of the metal-ion concentration in the solution could become considerably lower in the higher metal-ion concentration region. The similar results of copper adsorption by soil sample at low equilibrium solution concentrations have discussed by McLaren et al. [115]

Because CCS hydrogel is obtained by the modification of natural-product-derived CMC, there can be complicated structures in CCS hydrogel originated from that of CMC and/or from that generated by the modification; in fact, the surface structure of CCS hydrogel in a micro-meter scale was not uniform as was observed in the SEM photograph (**Figure 37**) given in Chap.5 Sec.II-3-b. Such characteristics were quite different from those of typical pure inorganic materials, therefore there could be various kinds of adsorption mechanisms in the CCS structure.

From this point of view, the author analyzed the experimental results measured in this investigation (initial-Ag^+-concentration (C_0) dependence of adsorption capacity (q_e) for CCS hydrogel (**Figure 49**)) with several adsorption models, Langmuir, Freundlich and Temkin models [Chap.1 Sec.II-4-c], in order to characterize the adsorption measured in this investigation.

The agreement of the models listed in **Table 23** with the experimental data were examined by the values of correlation coefficient (R^2). Because, as shown in **Table 23** and **Figure 49**, the Langmuir model exhibited better agreement with the experimental results than others, the author concluded that the Ag^+-adsorption process by CCS-hydrogel adsorbent could proceed in the condition which the Langmuir model assumed, namely, absorbed Ag's could form a single layer on the surface of the network in CCS hydrogel.

The low value of K_L (L/μg) = 1.90 in this study expressed a weak interaction between Ag^+ ions and CCS adsorbent through ion-exchange process. This phenomenon might come from replacement of H or Na ions on –OH, $–NH_2$, –COOH/ –COONa and $–SO_3H$/ $–SO_3Na$ by Ag^+ ions according to the reaction,

$$R–Na/H + Ag^+ \rightleftharpoons R–Ag + Na^+/H^+ ,$$

where R represents a complicated hydrocarbon group in the CCS hydrogel's structure. The ion exchange process could proceed until no active sites could be available, and then the equilibrium might be established, of which the process a similar feature has been reportedby other authors when they carried out the Ag adsorption by Chitosan/Bamboo charcoal composite beads [116], by Chitosan/Montmorillonite Composite Beads [117] and by Polystyrene-supported trimercaptotriazine resin [118].

Table 23. Isotherm models for analyzing experimental data.

Model	Langmuir	Freundlich	Temkin
Parameters	K_L (L/mg) = 1.90 ×10^{-3} q_{max} (mg/g) = 452 ×10^{-3} R^2 = 0.990	K_F (mg/g) = 13.2 ×10^{-3} 1/n = 0.45 R^2 = 0.857	K_T (L/mg) = 103 ×10^{-3} $B = RT/b$ = 25.9 b (J/mol) = 95.5 R^2 = 0.952

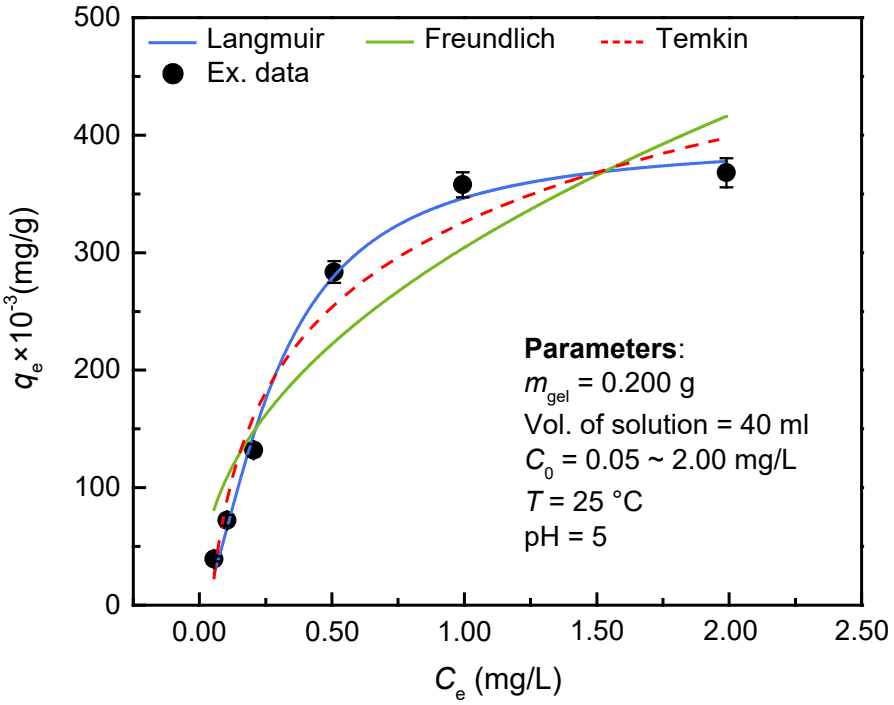

Figure 49. Adsorption isotherms of Ag^+ adsorbed onto CCS hydrogel

8. *Adsorption thermodynamics*

The effect of temperature on Ag^+-ion-adsorption by CCS hydrogel were studied. The adsorption experiments were done at 298, 323 and 343 K for 24 hrs. after the operation of changing the temperature setting in order to make sure to reach the experimental system's thermal equilibrium. The quantity of each CCS hydrogel was 0.200 g. The volume of the Ag^+ solutions was 40 mL with concentration of Ag^+ in a range 0.05 – 2.00 mg/L.

As shown in **Figure 50**, noticed was an increase from 72.2×10^{-3} to 88.5×10^{-3} (mg/g) in adsorption capacity with increasing temperature from 298 to 343 (K) in the condition with 0.1 mg/L (100 ppb) of the initial Ag^+ concentration.

These results could be resulted from increase in the mobility of Ag^+ in the solution, in the permeability of the solution into the hydrogel and in the Ag^+s' binding ability to the functional groups in CCS hydrogel. In addition, the deprotonation degree of the functional groups could also increase at higher temperatures. However, the increasing rate of the Ag^+ adsorption capacity would be lowered at further higher temperature because of the elevation of thermal vibration.

Temperature dependence of the adsorption capacity of adsorbent is related to a nature of the adsorption process, whether endothermic or exothermic, based on thermodynamics. The equation related to this aspect can be formulated as bellow:

$$\Delta G = -RT\ln K \qquad \text{and} \qquad \Delta G = \Delta H - T\Delta S\,, \qquad \textbf{Eq. 17}$$

where

ΔS (kJ/mol K): entropy change,

ΔH (kJ/mol): enthalpy change,

ΔG (kJ/mol): change in Gibbs free energy,

T (K): temperature,

R = 8.314 ($J.mol^{-1}.K^{-1}$): gas constant,

K: thermodynamic equilibrium constant.

K can be derived from an isotherm equilibrium model in non-liner form which fits the experimental data best [119][120][121]. In our current research, the value of K was derived from the Langmuir isotherm equation because the model gave the best-fit data. By using the present experimental data gotten from the Ag^+ adsorption experiments performed at 298, 323 and 343K, ΔH and ΔS were determined from the slope and intercept of the ΔG vs. T plot, respectively (**Figure 50** and **Figure 51**).

The obtained Langmuir constant values K_L had a dimension described with the unit of L/mg, while thermodynamic equilibrium constant K should be dimensionless. For treating this problem on the dimension, the values of K_L expressed in L/mg was first multiplied by 1000 to convert the unit in L/g and then was multiplied by the molecular weight of the adsorbate (M_w; g/mol) for transforming to K_L in L/mol. Then, considering the activity coefficient of the adsorbate 1 and also regarding that the unitary

activity of pure adsorbate is 1 mol/L by definition, the equilibrium constant becomes dimensionless, according to the **Eq. 18** [39].

$$K = K_L \times 1000 \times M_w \ , \qquad \textbf{Eq. 18}$$

where

K: thermodynamic equilibrium constant.

K_L (L/mg): Langmuir constant

M_w = 108 (g/mol)*:* Molecular weight of Ag

Because the Langmuir isotherm model could fit also well the experimental data at 298, 323 and 343K, K_L could be obtained at these temperatures, as can be seen in **Figure 50**. Calculated K values are displayed in **Table 24**.

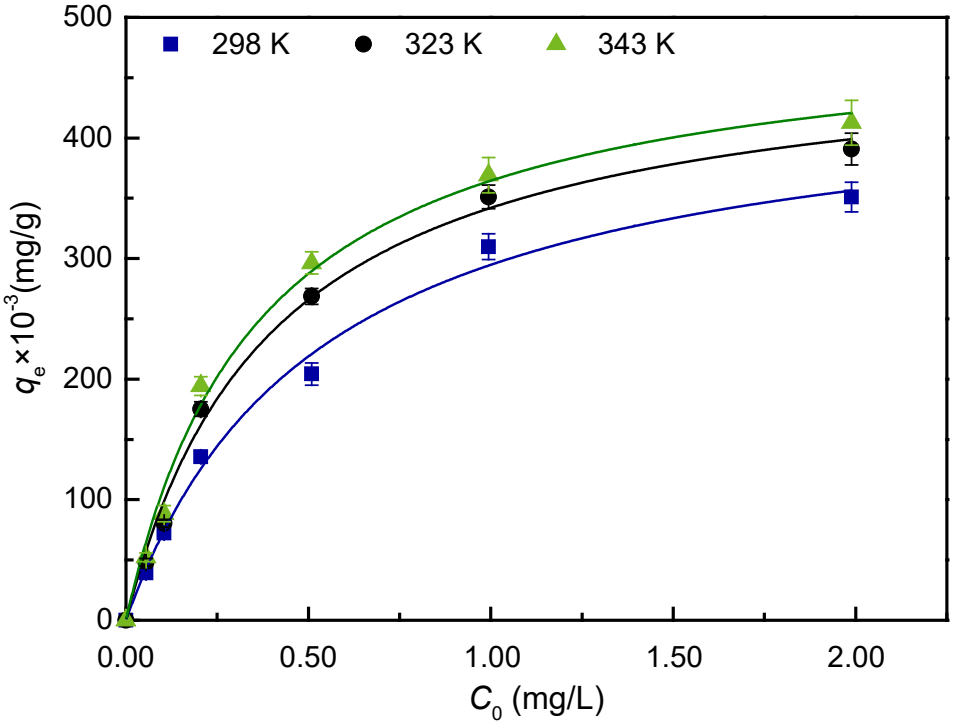

Model	Langmuir		
Equation	————		
Reduced Chi-Sqr			
Adj.			
		Value	Standard Error
■			
			2.73625E-4
●			
			3.24328E-4
▲			
			3.82431E-4

Figure 50. Langmuir fitting curves for Ag adsorption on CCS hydrogel at 298, 323 and 343 K.

The free energy ΔG is the basic standard for determining whether an adsorption process occurs spontaneously or not. At a given temperature, the process is spontaneous when ΔG is negative. From data shown in **Figure 51** and **Table 24**, the negative ΔG values confirm the adsorption reaction was able to happen by itself. It proved that the Ag^+ adsorption onto CCS hydrogel surface was a process of self-development with no need to provide additional energy. Under the standard conditions, the spontaneous adsorption becomes faster when the temperature increased.

Regardless of chemical or physical reaction, heat energy can either be absorbed or be released to its environment. If the pressure does not change in the process, the exchange energy (namely the amount of heat transfer to the environment) is equal to the enthalpy change ΔH in the process, however, enthalpy H itself cannot be directly measured. In the present analysis, the degree of reaction over time is used to calculate the variation of enthalpy over time. By knowing ΔH in a reaction, it can be distinguished whether the reaction is endothermic (heat transfer occurs from the environment to the reacting system) or exothermic (heat transfer from the reacting system to the environment).

The positive ΔH in the present experiment meant that the Ag capturing was endothermic process, which indicates that the elevation of environmental temperature caused the heat transfer from the environment to the reacting system, which promoted the endothermic adsorption reaction. As for the entropy change, positive ΔS in the adsorption process indicated increase in disorder at the solid–solution interface of the adsorption system with elevating temperature and promoted the affinity of the adsorbent material to Ag^+.

Eventually, an adsorption process is thermodynamically favorable or not is determined by the change of ΔG and K in the process. In the present experiment, the ΔG reduced with the increase of temperature and the thermodynamic equilibrium constant was >1, which means that endothermic reaction could proceed at higher temperature and the adsorption of Ag^+ was favorable process.

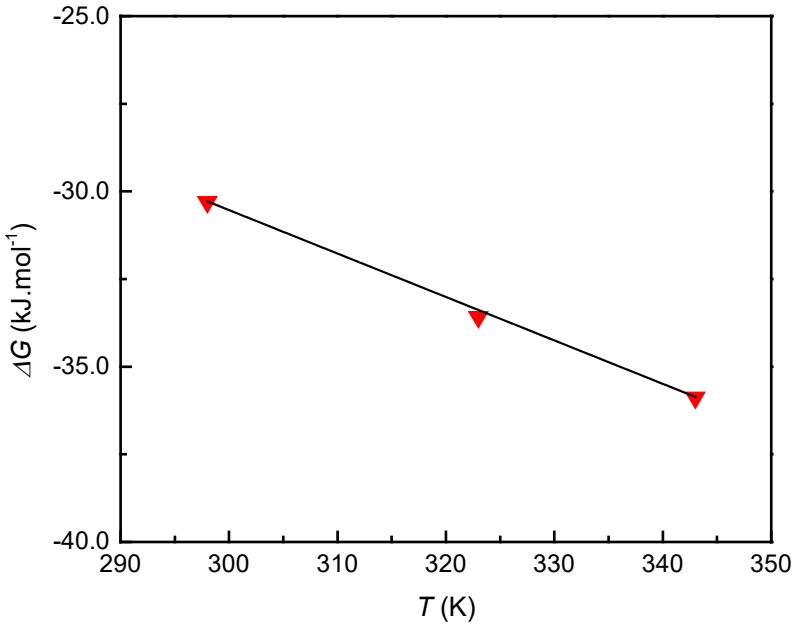

Equation	ΔG		
Weight	No Weighting		
Residual Sum of Squares	0.001		
Pearson's r	-0.999		
Adj. R	0.999		
		Value	Standard Error
G	Intercept	6.64	0.411
	Slope	-0.12	0.001

Figure 51. Graph for ΔG vs. T of the Ag adsorption by CCS hydrogel.

Table 24. Calculation of thermos-dynamic data for Ag^+ adsorption of Ag^+ by CCS hydrogel.

T (K)	*K*	Δ*G* (kJ/mol)	Δ*S* (kJ/mol K)	Δ*H* (kJ/mol)
298	205	–30.3	0.12	6.64
323	270	–33.6		
343	291	–35.9		

9. *Desorption and reusability of CCS hydrogel*

Desorbing agent solution of 0.05 M HNO_3 was used to separate Ag^+ ions out of CCS hydrogel structure. Each the hydrogel block adsorbing its maximum amount of Ag had been immersed in 40 mL of the solution containing the desorbing agent for 24 hrs., and then the Ag concentration in the desorbed solution was measured by ICP-MS. Four adsorption–desorption repetitions were done in order to find the persistence of the CCS hydrogel's Ag^+-ion-removal capacity. The aqueous solution at 100 μg/L of Ag^+ concentration was used for the adsorption procedure in the repetitive experiments at 25 ºC.

The adsorption efficiency and Ag^+-desorption ratio of the CCS hydrogel during the repetitive adsorption–desorption cycles is shown in **Figure 52**. Though, after 4th iteration, the Ag^+ adsorption capacity of CCS hydrogel somewhat decreased compared with the first time, the Ag^+-removing capacity remained still high: Ag^+-desorption wt%'s from the Ag^+-adsorbed hydrogel were 91 wt% in the 1st experiment and 82 wt% in the 4th one, which indicated that CCS hydrogel was a relatively good polymeric absorbent and reusable many times. The reduce in the adsorption capacity after the iteration can be from the damage caused by HNO_3 used in the desorption process.

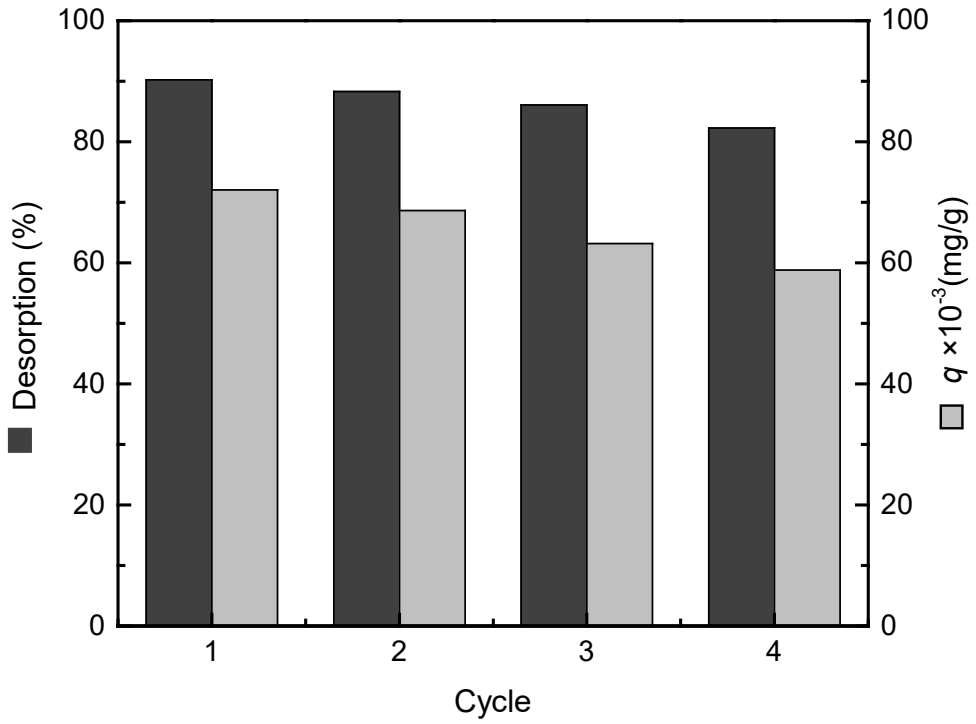

Figure 52. Adsorption and desorption recycles.

IV. Conclusion

Silver is a white, soft transition metal with high thermal and electrical conductivity, which is naturally present in pure form such as native silver and in alloy with gold, copper, and also occurs in minerals like argentite and chlorargyrite. One of the characteristic property of Silver is its highest conductivity in metals (followed by copper, gold, aluminum, sodium and wolfram), however due to its expensiveness, Silver is not widely used as an electrical conductor like copper but often used as a standard to compare the electrical conductivity of metals. Other than such an electronic property, Silver also has wonderful features: malleability, reflectivity of any metal and antimicrobial, etc., by which it has been widely used in industrial and pharmaceutical activities for hundred years. As a result of the usage of a much amount of Ag in the industrial process, large flow of the Ag-containing waste-fluid has occurred and has been discharged into rivers and/or sea, causing serious damage to aquatic organisms [86].

The most significant findings in the present investigation was that the CCS hydrogel newly developed in the present study showed very strict selectivity for Ag^+ ion in the competitive condition among many kinds of coexisting metal ions. The selective adsorption is one of important criterions for evaluating the performance of absorbents because almost of the wastewater and industrial effluents contain plural metal ions; and the selectivity can be more important than the level of capturing perforemance in some cases such as extracting a targeted pollutant without affecting the other conditions during mining process.

From the results reported in the present chapter, the author identified and demonstrated the optimum conditions for the Ag^+ adsorption by CCS hydrogel newly developed in the present study: pH, temperature and the minimum immersion-period in the solution by performing the experiments for getting the equilibrium isotherms (Langmuir, Freundlich and Temkin models). The derived adsorption capabilities of the CCS hydrogel seemed useful in the industrial applications, especially for Ag^+ ion recovery from the low-concentration industrial wastewater and effluents.

In addition, in the present investigation, the repetitive and recycled use of the CCS hydrogels has been also proposed as one of the most economical way of the adsorbent usage in the case of removing wastes and of collecting resources; such features have been ignored and/or have not been addressed in many publications. One or more of the newly developed CCS hydrogels in the present study demonstrated >90 % of desorption of the adsorbed metal ions, which was reproductive with only 15 % of decrease in capturing efficiency after the fourth cycle.

CHAPTER 6

SUMMARY

Recently, there are huge series of research about hydrogel and its applications. Especially, it has been convinced to be one of the best candidates for removing metal ions from water during two last decades. In the present author's study, prepared were three new types of hydrogel derived from carboxymethyl cellulose (CMC), which could be regrded as potential metal adsorbents with promising performance:

1) The CMC-hydrogels grafted with an active monomer, sodium styrene sulfonate(SSS), (CS hydrogel). In sipte of high adsorption capacity, it could not be recycled which is essential for the practical application.

2) The SSS-grafted CMC-hydrogels reinforced by a co-polymeric agent, Bis[2-(Methacryloyloxy) Ethyl] Phosphate (BMEP), (CSB hydrogel), which showed both of the high adsorption performance and reusability.

3) The SSS-grafted CMC-based hydrogel with an additional interpenetrating network of carboxymethyl chitosan (CMCts) polymer (CCS hydrogel), which showed enhanced capturing capacity and strict selectivity for Ag^+ ion.

It was also concluded that these CMC-based hydrogels can be satisfactorily prepared by utilizing ^{60}Co gamma radiation. By designing experimental methods and by performing statistical analyses, the optimal adsorbent preparation processes were succefully revealed.

I. Research achievement

1. The first highlight was the performance of CS hydrogel. This hydrogel was able to absorb efficiently multi elements in the aquatic environment due to simultaneous presence of $–SO_3H$ and –COOH active groups on the polymer networks. The FT-IR and C-NMR spectrum were applied to confirm these groups involved in binding of metal ions. To maintain the adsorption performance efficiently, CS hydrogel should be prepared from CMC and monomer SSS with the ratio of 1:2 and the pH for adsorption experiments needs to keep around 5 value. Between the pseudo-first-order and second-order kinetic model, the latter can be used to interpret the kinetics of adsorption data and indicated rapid binding of metal ions to the adsorbents during 10 hours, followed by a slow increase until equilibrium state was reached after 26h and unchanged in equilibrium time up to 48h.

2. Secondly, based on the previous obtained results from CS material, the CSB hydrogel was modified to enhance reusability. The Poisson's ratio and compressive modulus of the CS hydrogel were only 0.47 and 2.76 kPa, respectively while those value of CSB with 2.6 mM of BMEP were 0.45 and 3.40 kPa. It means that the hydrogel matrix became more compact and strong. Besides, the CSB hydrogel performed well with varying elements, especially Ni under non- and competitive conditions. Although the adsorption rate reached equilibrium after 24 hours, the re-usability did not change clearly after the 4th cycle of adsorption-desorption of Ni and was maintained up to 81%.

3. Lastly, the hydrogel derived from CMC with CMCts and SSS has an interpenetrating polymeric network. This helps hydrogel possess an impressive swelling capacity of ×2500 its initial dry weight

and become a potential adsorbent for metal ions. The experimental results indicated the CCS hydrogel was able to achieve superb selectivity towards Ag^+ metal ion from an integrated solution of multi metal ions. The maximum uptake of Ag^+ ion under competitive condition is more than 40.00×10^{-3} mg/g. The pseudo-second-order rate equations are able to describe the sorption process and the adsorption process was controlled by more than one rate-determining step. The Langmuir isotherm equation provides good description of the adsorption process of Ag^+ ion with calculated maximum adsorption capacity of 452.0 µg/g. The CCS hydrogel containing various functional groups i.e. hydroxyl, amine, sulfonate and carboxylate groups has strong interaction with of Ag^+ ion at solution pH from 4.0 to 6.0. The reusability of the CCS hydrogel was also investigated, and proved to be very good.

As conclusion, this laboratory scale study of improving of CMC hydrogel has resulted in a number of above interesting conclusions as well as leads for the further development of products and of utilization. Depending on different adsorption purpose, each method preparation of CMC-based hydrogels will be chosen. Although a certain overlap between the chapters is inevitable, the author think this division not only brings in some structure but most importantly, it will make the information more easily accessible.

II. Limitations of current work and corresponding recommendations for future work

Although the synthesized hydrogels have good adsorption performance for heavy metal ions, only batch experiments have been conducted in the present study. Furthermore, adsorption experiments were done without stirring are not a probably predictor for the best adsorption capacity. Deionized water was used to prepare hydrogels and all solutions as well as wash glassware to eliminate contaminants. However, for industrial applications, it is impossible to remove all unwanted components before adsorption. As a result, the evaluation of adsorbent performance should be carried out in solutions prepared with natural water. It is certainly needed to further exploit the potential of promising applications as well as methods to produce modified CMC hydrogels at a larger scale and test these absorbents against actual industrial solutions.

REFERENCES

[1] Heavy Metal Toxicity and the Environment,
P. B. Tchounwou, C. G. Yedjou, A. K. Patlolla, and D. J. Sutton,
Experientia Supplementum, vol. 101, pp. 133–64, 2012.

[2] Review of Heavy Metals in Drinking Water and Their Effect on Human Health,
C. V Mohod and J. Dhote
International Journal of Innovative Research in Science, Engineering and Technolog, vol. 2, Issue 7, pp. 2992–2996, 2013.

[3] The ATSDR 2017 Substance Priority List [Online]:
http://www.atsdr.cdc.gov/SPL/index.html. [Accessed: 30-Dec-2019].

[4] New trends in removing heavy metals from industrial wastewater,
M. A. Barakat,
Arabian Journal of Chemistry, vol. 4, Issue 4, pp. 361–377, 2011.

[5] Methods of Removing Heavy Metals from Industrial Wastewater
S. K. Gunatilake,
Journal of Multidisciplinary Engineering Science Studies, vol. 1, Issue 1, Nov. 2015.

[6] Recent developments in polysaccharide-based materials used as adsorbents in wastewater treatment,
G. Crini,
Progress in Polymer Science, vol. 30, Issue 1, pp. 38–70, 2005.

[7] Industrial wastes as low-cost potential adsorbents for the treatment of wastewater laden with heavy metals,
M. Ahmaruzzaman,
Advances in Colloid and Interface Science, vol. 166, Issues 1–2, pp. 36–59, Aug. 2011.

[8] Low cost adsorbents for the removal of organic pollutants from wastewater,
I. Ali, M. Asim, and T. A. Khan,
Journal of Environmental Management, vol. 113, pp. 170–183, Dec. 2012.

[9] Comparisons of low-cost adsorbents for treating wastewaters laden with heavy metals,
T. A. Kurniawan, G. Y. S. Chan, W. Lo, and S. Babel,
Science of The Total Environment, vol. 366, Issues 2–3, pp. 409–426, Aug. 2006.

[10] Agricultural waste material as potential adsorbent for sequestering heavy metal ions from aqueous solutions – A review,
D. Sud, G. Mahajan, and M. P. Kaur,
Bioresource Technology, vol. 99, Issue 14, pp. 6017–6027, Sep. 2008.

[11] Development of polymeric and polymer-based hybrid adsorbents for pollutants removal from waters,
B. Pan, B. Pan, W. Zhang, L. Lv, Q. Zhang, and S. Zheng,
Chemical Engineering Journal, vol. 151, Issues 1–3, pp. 19–29, Aug. 2009.

[12] *Industrial water pollution control*,
W. Wesley Eckenfelder, Jr.,
McGraw-Hill, 1989.

[13] History and Applications of Hydrogels,
Naziha Chirani, L'Hocine Yahia, Lukas Gritsch, Federico Leonardo Motta, SoumiaChirani, Silvia Faré,
Journal of Biomedical Sciences, vol. 4, no. 2:13, 2015.

[14] Adsorption characteristics of lead(II) ions onto the clay/poly(methoxyethyl)acrylamide (PMEA) composite from aqueous solutions,

M. Şölener, S. Tunali, A. S. Özcan, A. Özcan, and T. Gedikbey,
Desalination, vol. 223, Issues 1–3, pp. 308–322, March 2008.

[15] Synthesis and metal ion adsorption properties of poly(4-sodium styrene sulfonate-co-acrylic acid),
B. L. Rivas and C. Muñoz,
Journal of Applied Polymer Science, vol. 114, Issue 3, pp. 1587–1592, Nov. 2009.

[16] Removal of Co(II), Cu(II) and Pb(II) ions by polymer based 2-hydroxyethyl methacrylate: thermodynamics and desorption studies.,
O. Moradi, B. Mirza, M. Norouzi, and A. Fakhri,
Iranian Journal of Environmental Health Science & Engineering, vol. 9, Article number: 31, Dec. 2012.

[17] Adsorption isotherms, kinetic, and desorption studies on removal of toxic metal ions from aqueous solutions by polymeric adsorbent,
N. Samadi, R. Hasanzadeh, and M. Rasad,
Journal of Applied Polymer Science, vol. 132, Issue 11, Article number 41642, Nov. 2014, DOI:10.1002/app.41642.

[18] Environmental remediation of heavy metal ions from aqueous solution through hydrogel adsorption: A critical review,
F. N. Muya, M. Ward, C. E. Sunday, P. Baker, and E. Iwuoha,
Water Science & Technology, vol. 73, Issue 5, pp. 983–992, Nov. 2015.

[19] Classification, processing and application of hydrogels: A review,
F. Ullah, M. B. H. Othman, F. Javed, Z. Ahmad, and H. M. Akil,
Materials Science and Engineering: *C*, vol. 57, pp. 414–433, Dec. 2015.

[20] Radiation-grafted copolymers for separation and purification purposes: Status, challenges and future directions,
M. M. Nasef and O. Güven,
Progress in Polymer Science, vol. 37, Issue 12, pp. 1597–1656, Dec. 2012.

[21] *Gums and Stabilisers for the Food Industry* 14 (*Special Publications*),
Ed. by P. A. Williams and G. O. Phillips,
RSC Publishing (Royal Society of Chemistry), May 2008.

[22] Characterisation of carboxymethyl cellulose and polyacrylamide graft copolymer,
D. R. Biswal and R. P. Singh,
Carbohydrate polymers, vol. 57, Issue 4, pp. 379–387, 2004.

[23] *Encyclopedia of Polymer Science and Technology, Concise*,
H. F. Mark,
John Wiley & Sons, 2013.

[24] Optimization of reaction conditions for preparing carboxymethyl cellulose from sago waste,
V. Pushpamalar, S. J. Langford, M. Ahmad, and Y. Y. Lim,
Carbohydrate polymers, vol. 64, Issue 2, pp. 312–318, May 2006.

[25] Synthesis , Characterisation and Flocculation Properties of Carboxymethyl Cellulose-g Acrylamide,
D. E. Ogbeifun and F. E. Okieimen,
Journal of Sciences, Islamic Republic of Iran, vol. 15, Issue 1, pp. 53–57, 2004.

[26] Investigation of metal ion adsorption of carboxymethyl cellulose gel beads,
T. Heinze, K. Helbig, and D. Klemm,
Acta Polymerica, vol. 44, Issue 2, pp. 108–109, Apr. 1993.

[27] Metal ion absorption of carboxymethylcellulose gel formed by gamma-ray irradiation for the environmental purification,
K. Hara, M. Iida, K. Yano, and T. Nishida,

Colloids and Surfaces B: *Biointerfaces*, vol. 38, Issues 3–4, pp. 227–30, Nov. 2004.

[28] Adsorption properties of crosslinking carboxymethyl cellulose grafting dimethyldiallylammonium chloride for cationic and anionic dyes,
Q. Lin, M. Gao, J. Chang, and H. Ma,
Carbohydrate Polymers, vol. 151, pp. 283–294, Oct. 2016.

[29] Adsorption of Heavy Metal Ion from Aqueous Solution by Using Cellulose Based Hydrogel Composite,
N. Astrini, L. Anah, and H. R. Haryadi,
Macromolecular Symposia, vol. 353, Issue 1, pp. 191–197, July 2015.

[30] Dyes adsorption using a synthetic carboxymethyl cellulose-acrylic acid adsorbent,
G. Zhang, L. Yi, H. Deng, and P. Sun,
Journal of Environmental Sciences, vol. 26, Issue 5, pp. 1203–1211, May 2014.

[31] Novel carboxymethyl cellulose based nanocomposite membrane: Synthesis, characterization and application in water treatment,
S. Saber-Samandari, S. Saber-Samandari, S. Heydaripour, and M. Abdouss,
Journal of Environmental Management, vol. 166, pp. 457–465, Jan. 2016.

[32] Adsorption of lead ions from aqueous solution by using carboxymethyl cellulose-g-poly (acrylic acid)/attapulgite hydrogel composites,
Y. Liu, W. Wang, and A. Wang,
Desalination, vol. 259, no. 1–3, pp. 258–264, Sep. 2010.

[33] Metal adsorption of gamma-irradiated carboxymethyl cellulose/polyethylene oxide blend films,
A. A. El-Naggar, M. M. Magida, and S. M. Ibrahim,
Radiation Effects and Defects in Solids, Incorporating Plasma Science and Plasma Technology, vol. 171, Issue 3–4, May 2016,
http://dx.doi.org/10.1080/10420150.2016.1179308, 2016.

[34] Metal adsorption of carboxymethyl cellulose/carboxymethyl chitosan blend hydrogels prepared by Gamma irradiation,
A. Hiroki, H. T. Tran, N. Nagasawa, T. Yagi, and M. Tamada,
Radiation Physics and Chemistry, vol. 78, Issue 12, pp. 1076–1080, Dec. 2009.

[35] Adsorption of Metal Ions from Aqueous and Ethanol Solutions by Silica Gel Functionalized with Pyridinium Ions,
M. S. Iamamoto and Y. Gushikem,
Journal of Colloid and Interface Science, vol. 129, Issue 1, pp. 162–165, Apr. 1989.

[36] Hard and soft acids and bases,
S. Ritter,
Chemical & Engineering News Archives, vol. 81, no. 7, p. 50, Feb. 2003.

[37] A Comparison of the Langmuir, Freundlich and Temkin Equations to Describe Phosphate Adsorption Properties of Soils,
J. A. Mead,
Australian Journal of Soil Research, vol. 19, No. 3, pp. 333–342, 1981.

[38] The Adsorption of Gases on Plane Surfaces of Glass, Mica And Platinum,
B. Irvinq Langmuir,
Journal of the American Chemical Society, vol. 40, Issue 9, pp. 1361–1403, Sep. 1918.

[39] Mistakes and inconsistencies regarding adsorption of contaminants from aqueous solutions: A critical review,
H. N. Tran, S.-J. You, A. Hosseini-Bandegharaei, and H.-P. Chao,
Water Research, vol. 120, pp. 88–116, Sep. 2017.

[40] Über die Adsorption in Lösungen,

H. Freundlich,
Zeitschrift für Physikalische Chemie, vol. 57U, Issue 1, pp. 385–470, Oct. 1907 (in print).

[41] Heavy metals in the environment
Ed. by L. K. Wang, J. P. Chen, Y.-T. Hung, and N. K. Shammas,
CRC Press, May 2009.

[42] Adsorption of gold(III), platinum(IV) and palladium(II) onto glycine modified crosslinked chitosan resin,
A. Ramesh, H. Hasegawa, W. Sugimoto, T. Maki, and K. Ueda,
Bioresource Technology, vol. 99, Issue 9, pp. 3801–3809, June 2008.

[43] Temkin-Type Model for the Description of Induced Heterogeneity: CO Adsorption on Group 4 Transition Metal Dioxides,
V. Bolis, C. Morterra, B. Fubini, P. Ugliengo, and E. Garrone,
Langmuir, vol. 9, pp. 1521–1528, June 1993.

[44] Biosorption of nickel(II) ions onto Sargassum wightii: Application of two-parameter and three-parameter isotherm models,
K. Vijayaraghavan, T. V. N. Padmesh, K. Palanivelu, and M. Velan,
Journal of Hazardous Materials, vol. 133, Issues 1–3, pp. 304–308, May 2006.

[45] Review of second-order models for adsorption systems,
Y. S. Ho,
Journal of Hazardous Materials, vol. 136, Issue 3, pp. 681–689, Aug. 2006.

[46] Kinetic and equilibrium models of adsorption,
É. C. Lima, M. A. Adebayo, and F. M. Machado,
Carbon Nanomaterials as Adsorbents for Environmental and Biological Applications,
Springer, Chapter 3, pp. 33–69, June 2015.

[47] Removal of copper from aqueous solution by aminated and protonated mesoporous aluminas: Kinetics and equilibrium,
S. Rengaraj, Y. Kim, C. K. Joo, and J. Yi,
Journal of Colloid and Interface Science, vol. 273, Issue 1, pp. 14–21, May 2004.

[48] The removal of colour from effluent using various adsorbents – III. Silica: Rate processs,
G. McKay, M. S. Oyrwsurn, and A. G. Swe,
Water Research, vol. 14, Issue 1, pp. 15–20, 1980.

[49] Application of the Arrhenius equation to solid state kinetics: can this be justified?,
A. K. Galwey and M. E. Brown,
Thermochimica Acta, vol. 386, Issue 1, pp. 91–98, Apr. 2002.

[50] Heat of adsorption, adsorption energy and activation energy in adsorption and ion exchange systems,
V. J. Inglezakis and A. A. Zorpas,
Desalination and Water Treatment, vol. 39, Issue 1–3, pp. 149–157, Feb. 2012.

[51] Role of Radiation Processing in Production of Hydrogels For Medical Applications,
D. Darwis,
Atom Indonesia, vol. 35, No. 2, pp. 85–104, 2009.

[52] Radiation induced polymerization and crosslinking behavior of N-hydroxy methyl acrylamide in aqueous solutions,
A. Acharya, H. Mohan, and S. Sabharwal,
Radiation Physics and Chemistry, vol. 65, Issue 3, pp. 225–232, Oct. 2002.

[53] *Fundamentals of Fourier Transform Infrared Spectroscopy*,
B. C. Smith,
CRC Press, Mar. 2011.

[54] Determining Functional Groups of Commercially Available Ink-Jet Printing Reactive Dyes Using Infrared Spectroscopy,
C. W. M. Yuen, S. K. A. Ku, P. S. R. Choi, C. W. Kan, and S. Y. Tsang,
Research Journal of Textile and Apparel, vol. 9, Issue 2, pp. 26 –38, May 2005.

[55] Interpretation of Infrared Spectra, A Practical Approach,
J. Coates,
Infrared Spectroscopy, Encyclopedia of Analytical Chemistry: *Applications*, *Theory and Instrumentation*, Wiley, Sep. 2006.

[56] *Thermal and Rheological Measurement Techniques for Nanomaterials Characterization Volume* 3,
Ed. by S. Thomas, R. Thomas, A. Zachariah, R. Kumar,
Elsevier, May 2017..

[57] Scanning Electron Microscope as a Tool in Geology and Biology,
Kimoto, Sizuo; Honjo, Susumu,
Journal of the Faculty of Science, Hokkaido University. Series 4*, Geology and mineralogy, 14*(*1*), pp. 57–69, 1962.

[58] The Latest Analytical Electron Microscope and its Application to Ceramics,
Y. Harada and Y. Ikuhara,
Handbook of Advanced Ceramics: Materials, Applications, Processing, and Properties: Second Edition, Elsevier Inc., 2013, pp. 3–21.

[59] Comb-type grafted hydrogels of PNIPAM and PDMAEMA with reversed network-graft architectures from controlled radical polymerizations,
S. Q. Chen, J. M. Li, T. T. Pan, P. Y. Li, and W. D. He,
Polymers, vol. 8, Article number 38, Feb. 2016.

[60] Rapid temperature/pH response of porous alginate-g-poly(N-isopropylacrylamide) hydrogels,
J. H. Kim, S. B. Lee, S. J. Kim, and Y. M. Lee,
Polymer, vol. 43, Issue 26, pp. 7549–7558, Dec. 2002.

[61] pH/temperature-responsive behaviors of semi-IPN and comb-type graft hydrogels composed of alginate and poly(*N*-isopropylacrylamide),
H. K. Ju, S. Y. Kim, and Y. M. Lee,
Polymer, vol. 42, Issue 16, pp. 6851–6857, Jul. 2001.

[62] Acid-synergized grafting of sodium styrene sulfonate onto electron beam irradiated-poly(vinylidene fluoride) films for preparation of fuel cell membrane,
M. M. Nasef, H. Saidi, and K. Z. M. Dahlan,
Journal of Applied Polymer Science, vol. 118, Issue 5, pp. 2801–2809, Dec. 2010.

[63] Preparation of comb-type grafted hydrogels composed of polyacrylamide and chitosan and their use for DNA adsorption,
B. Başer, G. B. Demirel, L. Açık, and T. Çaykara,
Journal of Applied Polymer Science, vol. 111, Issue 4, pp. 1862–1868, Feb. 2009.

[64] Heavy metals complexes of poly (sodium 4-styrenesulfonate) — thermogravimetric studies,
I. Korus,
Polymery, vol. 57, no. 4, pp. 290–295, Apr. 2012.

[65] Graft copolymerization of Carboxymethylcellulose : An Overview,
V. Mishra and R. Kumar,
Trends in Carbohydrate Research, vol. 4, no. 3, pp. 1–, Jan. 2012,
https://www.researchgate.net/profile/Dr_Vivek_Mishra/publication/232041783_Graft_copolymerization_of_Carboxymethylcellulose_An_overview/links/0912f507390b99624d000000.pdf.

[66] An Introduction to Hydrogels and Some Recent Applications,
M. Bahram, N. Mohseni, and M. Moghtader,

Emerging Concepts in Analysis and Applications of Hydrogels, InTech, Aug. 2016, pp. 9–38

[67] Advances in cellulose-based superabsorbent hydrogels,
J. Ma, X. Li, and Y. Bao,
RSC Advances, vol. 5, Issue 73, pp. 59745–59757, Jul. 2015.

[68] Poly (Acrylamide-co-styrene sodiumsulfonate) and poly (2-acrylamide-2-methyl-1-propanesulfonic acid-co-acrylic acid) resins with removal properties for Hg(II), Pb(II), Cd(II), and Zn(II),
D. V Morales and B. L. Rivas,
Journal of the Chilean Chemical Society, vol. 59, no. 2, pp. 2420–2426, 2014.

[69] *Remington*: *The Science and Practice of Pharmacy*,
J. P. Remington and P. Beringer,
Lippincott Williams & Wilkins, 2006.

[70] Adsorption of copper (II), chromium (III), nickel (II) and lead (II) ions from aqueous solutions by meranti sawdust,
M. Rafatullah, O. Sulaiman, R. Hashim, and A. Ahmad,
Journal of Hazardous Materials, vol. 170, Issues 2–3, pp. 969–977, 2009.

[71] Pseudo-second order model for sorption processes,
Y. S. Ho and G. McKay,
Process Biochemistry, vol. 34, Issue 5, pp. 451–465, July 1999.

[72] Isotherms for the sorption of lead onto peat: Comparison of linear and non-linear methods,
Y. S. Ho,
Polish Journal of Environmental Studies, vol. 15, no. 1, pp. 81–86, Jan. 2006.

[73] Spherical Chitosan/Gelatin Hydrogel Particles for Removal of Multiple Heavy Metal Ions from Wastewater,
S. Perumal, R. Atchudan, D. H. Yoon, J. Joo, and I. W. Cheong,
Industrial & Engineering Chemistry Research, vol. 58, Issue 23, pp. 9900–9907, May 2019.

[74] A possibility of heavy-metal recycling by utilizing hydrogels,
K. Hara, S. Yoshioka, and T. Nishida,
Transactions of the Materials Research Society of Japan, vol. 20thAnniversary, pp. 23–28, 2010.

[75] Hydrogel of biodegradable cellulose derivatives. I. Radiation-Induced Crosslinking of CMC,
B. Fei, R. A. Wach, H. Mitomo, F. Yoshii, and T. Kume,
Journal of Applied Polymer Science, vol. 78, Issue 2, pp. 278–283, July 2000.

[76] Preparation of poly (bis[2-(methacryloyloxy)ethyl] phosphate) crosslinked polymer brushes on Poly(vinylidene fluoride) nanofibers,
B. Oktay, M. H. Uğur, and N. K. Apohan,
Materials Chemistry and Physics, vol. 217, pp. 168–174, Sep. 2018.

[77] Bis[2-(methacryloyloxy)ethyl] phosphate radiografted into track-etched PVDF for uranium (VI) determination by means of cathodic stripping voltammetry,
U. Pinaeva, T. C. Dietz, M. Al Sheikhly, E. Balanzat, M. Castellino, T. L. Wade, and M. C. Clochard,
Reactive and Functional Polymers, vol. 142, pp. 77–86, Sep. 2019.

[78] Bioactive polymethylmethacrylate bone cement modified with combinations of phosphate group-containing monomers and calcium acetate,
J. Liu, Y. Shirosaki, and T. Miyazaki,
Journal of Biomaterials Applications, vol. 29, Issue 9, pp. 1296–303, Jan. 2015.

[79] Preparation of biocompatible magnetite-carboxymethyl cellulose nanocomposite: Characterization of nanocomposite by FTIR, XRD, FESEM and TEM,
N. Habibi,

Spectrochimica Acta Part A: Molecular and Biomolecular Spectroscopy, vol. 131, pp. 55–58, Oct. 2014.

[80] Scientific Opinion on the risks to public health related to the presence of nickel in food and drinking water,
EFSA Panel on Contaminants in the Food Chain (CONTAM),
EFSA Journal, vol. 13, Issue 2, Article number 4002, Feb. 2016.

[81] *The Rodiochemistry of Molybdenum*,
E. M. Scadden and N. E. Ballou,
NAS-NS 3009, Nuclear Science Series, National Academy of Sciences (National Research Council, U. S. Atomic Energy Commision), 1960.

[82] Recovery of Silver from X-Ray Film Processing Effluents Using Trimercapto-*s*-triazine (TMT),
E. Y. Yazici, H. Deveci, and R. Yazici,
Separation Science and Technology, vol. 46, Issue 14, pp. 2231–2238, Sep. 2011.

[83] Nickel Nanoparticles Exposure and Reproductive Toxicity in Healthy Adult Rats,
L. Kong, M. Tang, T. Zhang, D. Wang, K. Hu, and W. Lu,
International Journal of Molecular Sciences, vol. 15, Issue 11, pp. 21253–21269, 2014.

[84] Scientific Opinion on the risks to animal and public health and the environment related to the presence of nickel in feed,
EFSA Panel on Contaminants in the Food Chain (CONTAM),
EFSA Journal, vol. 13, Issue 4, Article number 4074, Apr. 2015.

[85] Adsorption and Desorption of Nickel(II) Ions from Aqueous Solution by a Lignocellulose/Montmorillonite Nanocomposite,
X. Zhang and X. Wang,
PLoS One, vol. 10, Issue 2, Article number e0117077, Feb. 2015.

[86] Mechanism of acute silver toxicity in the euryhaline copepod Acartia tonsa,
M. S. Pedroso, G. L. L. Pinho, S. C. Rodrigues, and A. Bianchini,
Aquatic Toxicology, vol. 82, Issue 3, pp. 173–80, May 2007.

[87] Bioaccumulation and toxicity of silver compounds: A review,
H. T. Ratte,
Environmental Toxicology and Chemistry, vol. 18, Issue 1, pp. 89–108, Jan. 1999.

[88] Behavioural effects on marine amphipods exposed to silver ions and silver nanoparticles,
M. Vannuci-Silva, S. Kohler, G. de A. Umbuzeiro, and A. T. Ford,
Environmental Pollution, vol. 252, Part B, pp. 1051–1058, Sep. 2019.

[89] *Ambient water quality criteria for silver*
Office of Water Regulations and Standards,
Criteria and Standards Division, United States Environmental Protection Agency,
EPA 440/5-80-071, Oct. 1980.

[90] *Handbook on the Toxicology of Metals – 4th Edition*,
G. Nordberg, B. Fowler, and M. Nordberg,
Academic Press, Aug. 2014.

[91] Silver recovery from waste radiographic films by cementation and reduction,
S. Aktas, M. H. Morcali, and O. Yucel,
Canadian Metallurgical Quarterly, The Canadian Journal of Metallurgy and Materials Science, vol. 49, Issue 2, pp. 147–154, July 2013.

[92] Hydrated metal ions in aqueous solution: How regular are their structures?
I. Persson,
Pure and Applied Chemistry, The Scientific Journal of IUPAC, vol. 82, No. 10, pp. 1901–1917, Aug. 2010.

[93] Separation and Recovery of Silver(I) Ions from Base Metal Ions by Thiourea- or Urea-Formaldehyde Chelating Resin,
S. Kirci, M. Gülfen, and A. O. Aydin,
Separation Science and Technology, vol. 44, Issue 8, pp. 1869–1883, June 2009.

[94] Comparative study of the recovery of silver(I) from aqueous solutions with different chelating resins derived from glycidyl methacrylate,
A. A. Atia, A. M. Donia, and A. M. Yousif,
Journal of Applied Polymer Science, vol. 97, Issue 3, pp. 806–812, May 2005.

[95] Selective adsorption of silver ions from aqueous solution using polystyrene-supported trimercaptotriazine resin,
S. Wang, H. Li, X. Chen, M. Yang, and Y. Qi,
Journal of Environmental Sciences, vol. 24, Issue 12, pp. 2166–2172, Dec. 2012.

[96] Definitions of terms relating to the structure and processing of sols, gels, networks, and inorganic-organic hybrid materials (IUPAC Recommendations 2007),
V. Alemán, A. V. Chadwick, J. He, M. Hess, K. Horie, R. G. Jones, P. Kratochvíl, I. Meisel, I. Mita, G. Moad, S. Penczek, and R. F. T. Stepto,
Pure and Applied Chemistry, The Scientific Journal of IUPAC, vol. 79, Issue 10, pp. 1801–1829, Jan. 2007.

[97] Design and applications of interpenetrating polymer network hydrogels. A review,
E. S. Dragan
Chemical Engineering Journal, vol. 243, pp. 572–590, May 2014.

[98] Semi-interpenetrating polymer network microspheres of gelatin and sodium carboxymethyl cellulose for controlled release of ketorolac tromethamine,
A. P. Rokhade, S. A. Agnihotri, S. A. Patil, N. N. Mallikarjuna, P. V. Kulkarni, and T. M. Aminabhavi,
Carbohydrate Polymers, vol. 65, Issue 3, pp. 243–252, Aug. 2006.

[99] Novel interpenetrating polymer network microspheres of chitosan and methylcellulose for controlled release of theophylline,
A. P. Rokhade, N. B. Shelke, S. A. Patil, and T. M. Aminabhavi,
Carbohydrate Polymers, vol. 69, Issue 4, pp. 678–687, Jul. 2007.

[100] Radiation graft post-polymerization of sodium styrene sulfonate onto polyethylene,
N. K. Kitaeva, V. R. Duflot, and N. S. Ilicheva,
Journal of Radioanalytical and Nuclear Chemistry, vol. 298, pp. 1041–1047, Aug. 2013.

[101] Synthesis and swelling behaviors of sodium carboxymethyl cellulose-g-poly(AA-co-AM-co-AMPS)/MMT superabsorbent hydrogel,
N. Li, J. Ma, and Y. Bao,
Carbohydrate Polymers, vol. 84, Issue 1, pp. 76–82, Feb. 2011.

[102] Synthesis and Characterization of Carboxymethyl Cellulose from Sugarcane Bagasse,
M. Mousavi, S. A. Asl, and M. Labbafi,
Journal of Food, Processing & Technology, vol. 8, Issue 8, Article number 1000687, Jan. 2017.

[103] Copolymerization characteristics of sodium styrenesulfonate,
C. E. Grabiel and D. L. Decker,
Journal of Polymer Science, vol. 59, Issue 168, pp. 425–431, June 1962.

[104] Carboxylic Acid Structure and Chemistry: Part 2,
J. DeRuiter,
Principles of Drug Action 1*, Spring* 2005*, Carboxylic Acids Part* 2, pp. 1–10,
http://webhome.auburn.edu/~deruija/pda1_acids2.pdf, 2005.

[105] Development and characterization of a new hydrogel based on galactomannan and κ-

carrageenan,
P. A. G.Soares, J. R. P. C de Seixas, P. B. S. Albuquerque, G. R. C. Santos, P. A. S. Mourão, Wilson Barros Jr., M. T. S. Correia, M. G. Carneiro-da-Cunha,
Carbohydrate Polymers, vol. 134, pp. 673–679, Dec. 2015.

[106] Equilibrium swelling properties of poly(N-vinylimidazole-co-sodium styrenesulfonate) hydrogels,
J. Valencia and I. F. Piérola,
European Polymer Journal, vol. 37, Issue 12, pp. 2345–2352, Dec. 2001.

[107] The stability of transition-metal complexes,
H. Irving and R. J. P. Williams,
Journal of the Chemical Society, pp. 3192–3210, 1953.

[108] Critical Stability Constants,
R. Bruce Martin,
Plenum Press, 1953.

[109] Kinetics and Thermodynamics of Lead Adsorption from Aqueous Solutions Onto Iranian Sepiolite and Zeolite,
F. Sharifipour, S. Hojati, A. Landi, and F. Cano,
International Journal of Environmental Research, vol. 9, Issue 3, pp. 1001–1010, Summer 2015.

[110] pH-Effect on Heavy-Metal Adsorption and Desorption of Sodium acrylate/Acrylamide and *p*-Styrenesulfonicacidsodiumsalt/Acrylamide Gels
N. Kawamura, D. Yamada, T. Nishida, S. Yoshioka, and K. Hara,
Transactions of the Materials Research Society of Japan, vol. 34, no. 3, pp. 493–496, Jan. 2009.

[111] Biosorption of heavy metals by Sphaerotilus natans: An equilibrium study at different pH and biomass concentrations,
A. Esposito, F. Pagnanelli, A. Lodi, C. Solisio, and F. Vegliò,
Hydrometallurgy, vol. 60, Issue 2, pp. 129–141, Apr. 2001.

[112] Evaluation of pyrene sorption e desorption on tropical soils,
B. I. Olu-owolabi, P. N. Diagboya, and K. O. Adebowale,
Journal of Environmental Management, vol. 137, pp. 1–9, May 2014.

[113] A review of the kinetics adsorption models and their application to the adsorption of lead by an activated carbon,
L. Largitte and R. Pasquier,
Chemical Engineering Research and Design, vol. 109, pp. 495–504, May 2016.

[114] Highly efficient removal of uranium(VI) from wastewater by polyacrylic acid hydrogels,
X, Yi, Z. Xu, Y. Liu, X. Guo, M. Ou, and X. Xu
RSC Advances, Issue 7, pp. 6278–6287, Jan. 2017.

[115] The adsorption of copper by soil samples from scotland at low equilibrium solution concentrations,
R. G. McLaren, J. G. Williams, and R. S. Swift,
Geoderma, vol. 31, Issue 2, pp. 97–106, Sep. 1983.

[116] Removal of silver(I) from aqueous solutions by chitosan/bamboo charcoal composite beads,
W. Nitayaphat and T. Jintakosol,
Journal of Cleaner Production, vol. 87, pp. 850–855, Jan. 2015.

[117] Adsorption of Silver (I) From Aqueous Solution Using Chitosan/Montmorillonite Composite Beads,
T. Jintakosol and W. Nitayaphat,
Materials Research, vol. 19, no. 5, pp. 1114–1121, Aug. 2016.

[118] Selective adsorption of silver ions from aqueous solution using polystyrene-supported trimercaptotriazine resin,
Y. Qi,
Journal of Environmental Sciences, vol. 24, Issue 12, pp. 2166–2172, Dec. 2012.

[119] Kinetic and Equilibrium Models of Adsorption,
É. C. Lima, M. A. Adebayo, and F. M. Machado,
Carbon Nanomaterials as Adsorbents for Environmental and Biological Applications,
Springer, pp. 33–69, 2015.

[120] Biosorption isotherms, kinetics and thermodynamics,
Y. Liu and Y.-J. Liu,
Separation and Purification Technology, vol. 61, Issue 3, pp. 229–242, July 2008.

[121] Is the Free Energy Change of Adsorption Correctly Calculated?,
Y. Liu,
Journal of Chemical & Engineering Data, vol. 54, Issue 7, pp. 1981–1985, July 2009.